

Universität
Rostock



Traditio et Innovatio

**Binding of Chlorinated Environmentally Active
Chemicals to Soil Surfaces:
Chromatographic Measurements and Quantum
Chemical Simulations**

Dissertation

zur

Erlangung des akademischen Grades

Doctor rerum naturalium (Dr. rer. Nat.)

der Mathematisch-Naturwissenschaftlichen Fakultät

der Universität Rostock

vorgelegt von

Ashour Abdelaal Mahmoud Ahmed

geb. am 14 November 1983 in Souhag

aus Kairo, Ägypten

Gutachter:

1. Gutachter:

Prof. Dr. Oliver Kühn
Institut für Physik, Universität Rostock

2. Gutachter:

Prof. Dr. Peter Leinweber
Professur Bodenkunde, Universität Rostock

3. Gutachter:

Prof. Dr. Ralf Ludwig
Institut für Chemie, Universität Rostock

4. Gutachter:

Prof. Dr. Sören Thiele-Bruhn
Institut für Bodenkunde, Universität Trier

Datum der Einreichung: 28. May 2013

Datum der Verteidigung: 05. November 2013

**With All Love I Would Like
To Dedicate My Thesis To
My Parents & My Wife**

CONTENTS

CONTENTS	I
ABBREVIATIONS	III
LIST OF FIGURES	V
LIST OF TABLES	VIII
ABSTRACT	IX
ZUSAMMENFASSUNG	XI
1. INTRODUCTION	1
1.1. MOTIVATION.....	1
1.2. SOIL COMPOSITION	2
1.3. SOIL ORGANIC MATTER CHARACTERIZATION	8
1.4. SOIL POLLUTION.....	8
1.5. PERSISTENT ORGANIC POLLUTANTS.....	9
1.6. POLLUTANT-SOIL ORGANIC MATTER INTERACTION	12
1.7. OBJECTIVE AND STRATEGY OF THE CURRENT WORK.....	14
2. THEORETICAL BACKGROUND	16
2.1. SCHRÖDINGER EQUATION AND BORN-OPPENHEIMER SEPARATION.....	16
2.1.1. Molecular Orbital Theory.....	18
2.1.2. Variational Method and Hartree-Fock Theory.....	20
2.1.3. Electron Correlation Methods	21
2.1.3.1. Møller-Plesset Perturbation Method.....	22
2.1.3.2. Coupled Cluster Method.....	23
2.1.4. Density Functional Theory	24
2.2. SOLVATION EFFECT	26
2.2.1. Conductor-Like Screening Model	27
2.2.2. Force Field Molecular Dynamics Simulations	27
2.3. QUANTITATIVE STRUCTURE–ACTIVITY RELATIONSHIP.....	28
3. MATERIALS AND METHODS	30
3.1. SOIL SITE AND SAMPLING.....	30
3.2. SYSTEMATIC MODIFICATION OF THE SOIL ORGANIC MATTER	30
3.2.1. Hot Water Extraction.....	31
3.2.2. Off-Line Pyrolysis.....	32
3.3. ANALYTICAL METHODS.....	32
3.3.1. C, N, S Elemental Analysis	32
3.3.2. Pyrolysis-Field Ionization Mass Spectrometry (Py-FIMS).....	32
3.3.3. Carbon and Nitrogen K-edge XANES.....	33

3.4.	HEXACHLOROBENZENE	34
3.5.	ADSORPTION KINETICS OF HCB	34
3.6.	ADSORPTION ISOTHERMS OF HCB.....	35
3.7.	SOIL ORGANIC MATTER MODELLING AND QUANTUM CHEMICAL CALCULATIONS	36
3.8.	MOLECULAR DYNAMICS SIMULATIONS.....	38
3.9.	QUANTITATIVE STRUCTURE-ACTIVITY RELATIONSHIP	39
4.	EXPERIMENTAL RESULTS AND DISCUSSION.....	40
4.1.	GENERAL CHARACTERIZATION OF SAMPLES	40
4.2.	PYROLYSIS-FIELD IONIZATION MASS SPECTROMETRY	41
4.3.	CARBON K-EDGE XANES SPECTROSCOPY	46
4.4.	NITROGEN K-EDGE XANES SPECTROSCOPY.....	48
4.5.	HCB ADSORPTION KINETICS.....	50
4.6.	HCB ADSORPTION ISOTHERMS.....	50
4.7.	SUMMARIZING DISCUSSION	57
5.	THEORETICAL RESULTS AND DISCUSSION.....	60
5.1.	TEST SET SYSTEMS CLASSIFICATION	60
5.2.	GEOMETRY OPTIMIZATION.....	62
5.3.	EFFECT OF DISPERSION CORRECTION.....	63
5.4.	EFFECT OF BASIS SETS	65
5.5.	EFFECT OF DFT-FUNCTIONALS.....	67
5.6.	BENCHMARK CALCULATIONS.....	69
5.7.	GAS PHASE HCB-SOM INTERACTION AND EFFECT OF SOLVENT.....	70
5.8.	CORRELATION WITH THE EXPERIMENTAL RESULTS.....	74
5.9.	MOLECULAR DYNAMICS SIMULATIONS.....	76
5.10.	QUANTITATIVE ACTIVITY-STRUCTURE RELATIONSHIP.....	82
6.	SUMMARY AND OUTLOOK.....	89
	REFERENCES	94
	APPENDICES.....	104
	ACKNOWLEDGEMENTS.....	105
	PUBLISHED PAPERS.....	106
	TALKS AND POSTERS.....	107
	CURRICULUM VITAE.....	108
	ERKLÄRUNG.....	109

ABBREVIATIONS

AI: absolute ion intensity

ALKY: alkyl aromatics

B3LYP: Becke, three-parameter, Lee-Yang-Parr hybrid functional

BLYP: Becke, Lee-Yang-Parr hybrid functional

BSSE: basis set superposition error

CCSD: coupled cluster single and double excitations

CHYDR: carbohydrates with pentose and hexose subunits

COSMO: conductor-like screening model

CSM: continuum solvation model

DDT: dichlorodiphenyltrichloroethane

DFT: density functional theory

E_B: total binding energy

FA: fulvic acids

FATTY: free fatty acids

GC-ECD: gas chromatograph equipped with electron capture detector

GTO: Gaussian type orbital

H: Henry's law constant

HA: humic acids

HCB: hexachlorobenzene

HF: Hartree-Fock

HWE: hot-water extract

ICP-AES: inductively coupled plasma atomic emission spectroscopy

K_{OC}: organic carbon water partition coefficient

K_{OW}: octanol-water partition coefficient

LCAO: linear combination of atomic orbitals

LDIM: lignin dimers

LIPID: lipids, alkanes, alkenes, bound fatty acids, and alkyl monoesters

MD: molecular dynamics

MP2: 2nd order Moller-Plesset perturbation theory

NCOMP: non-peptidic N-containing compounds

PCBs: polychlorinated biphenyls

PCCDs: polychlorinated dibenzo-p-dioxins

PCDFs: polychlorinated dibenzofurans

PEPTI: peptides

PES: potential energy surface

PHLM: phenols and lignin monomers

POPs: persistent organic pollutants

Py-FIMS: pyrolysis-field ionization mass spectrometry

QSAR: quantitative structure-activity relationship

RMSD: root mean square deviation

SCF: self-consistent-field

SD: Slater determinant

SGM: spherical grating monochromator

SOM: soil organic matter

STEROL: sterols

STO: Slater type orbital

SUBER: suberin

TII: total ion intensity

XANES: X-ray absorption near-edge structure spectroscopy

LIST OF FIGURES

Figure 1. Organic pollutants reach the soil by different ways. ⁽³⁾	1
Figure 2. A: The main soil horizons (O, A, E, B, C, and R) ⁽²²⁾ and B: The different soil types based on clay, silt, and sand composition. ⁽²³⁾	5
Figure 3. Some examples of SOM compound classes such as carbohydrates, protein, lignin ⁽²⁴⁾ , waxes, and fats.5	
Figure 4. A proposed structure of a humic acid molecule by Schulten ⁽²¹⁾ showing a wide range of functional groups (e.g. phenolic, carboxylic, salicylic, phthalate, nitrogen-bearing groups).	7
Figure 5. The chemical structures of the different POPs.....	10
Figure 6. The three dimensional structure of SOM model developed by R.-H. Schulten. ⁽⁷⁹⁾	14
Figure 7. Scheme is showing how remove/addition HWE from/to original soil was performed.....	31
Figure 8. The optical layout of the Canadian spherical grating monochromator beam line. ⁽¹³²⁾	34
Figure 9. The chemical as well as the three-dimensional structure of HCB	34
Figure 10. The developed test set for studying the interaction of HCB with different SOM functional groups including PHLM, ALKY, CHYDR, PEPTI, NCOMP, LIPID, O- and N-functional groups, and special cases such coronene, and silicon hydroxide.	38
Figure 11. Thermograms of ion intensity in 10^6 counts mg^{-1} (inserts), and summed and averaged pyrolysis-field ionization mass spectra in % of total ion intensity (TII) of HWE (a), soil+6 HWE(b), soil+3 HWE (c), original soil (d), soil residue (e), and pyrolyzed soil (f).....	44
Figure 12. The 20 times magnified thermogram of the pyrolyzed soil sample.....	45
Figure 13. Normalized stacked Carbon K-edge XANES spectra of pyrolyzed soil, soil residue, original soil, soil+3 HWE, soil+6 HWE, and HWE.....	47
Figure 14. Normalized stacked Nitrogen K-edge XANES spectra of pyrolyzed soil, soil residue, original soil, soil+3 HWE, soil+6 HWE, and HWE.	49
Figure 15. Sorption kinetics of HCB on the original rye soil sample.....	52
Figure 16. The adsorption isotherms of HCB on the soil samples in which amount of adsorbed HCB normalized to the total soil mass, in $\mu\text{g HCB/g soil}$, (A) and the total carbon content, in $\mu\text{g HCB/g } C_{\text{tot}}$ (B) were plotted versus the corresponding initial HCB concentrations (C_0). The lines were, obtained from an exponential correlation, plotted as guide for eye.....	54
Figure 17. The Freundlich fitted adsorption isotherms of HCB on the soil samples normalized to the total soil mass, in $\mu\text{g HCB/g soil}$, (A) and the total carbon content, in $\mu\text{g HCB/g } C_{\text{tot}}$ (B).	55
Figure 18. The Langmuir fitted adsorption isotherms of HCB on the soil samples normalized to the total soil mass, in $\mu\text{g HCB/g soil}$, (A) and the total carbon content, in $\mu\text{g HCB/g } C_{\text{tot}}$ (B).	56
Figure 19. The gas phase equilibrium geometries of the test set complexes with HCB optimized at B3LYP-D3/6-311++G(d,p).....	61
Figure 20. The binding energies of HCB with the SOM representative systems (upper-left panel), dipole moments of HCB-SOM complexes (upper-right panel) at 6-31G, 6-31++G, and 6-311++G(d,p) basis sets, and structure RMSD of each HCB-SOM complex (lower panel) at 6-31G and 6-311++G(d,p) basis sets with respect to structures at 6-31++G basis set.	63

Figure 21. The binding energies of HCB with the SOM representative systems at 6-311++G(2d,2p) using HF, B3LYP, B3LYP-D2, and B3LYP-D3.	64
Figure 22. The binding energies of HCB with the SOM representative systems using B3LYP-D3 at 6-31G, 6-31++G, 6-311++G(d,p), 6-311++G(2d,2p), and aug-cc-pvdz basis sets.	65
Figure 23. The binding energy differences of HCB with the SOM representative systems, dipole moment differences of the HCB-SOM complexes using B3LYP-D3 at 6-31G, 6-31++G, 6-311++G(d,p), 6-311++G(2d,2p) basis sets with respect to aug-cc-pvdz basis set.	66
Figure 24. The binding energies of HCB with the SOM representative systems using BLYP-D3, B3LYP-D3, B3LYP5-D3, and CAMB3LYP-D3 at 6-311++G(2d,2p) basis set.	67
Figure 25. The binding energy differences of HCB with the SOM representative systems, dipole moment differences of the HCB-SOM complexes at 6-311++G(2d,2p) basis set using BLYP-D3, B3LYP5-D3, and CAMB3LYP-D3 with respect to B3LYP-D3.	68
Figure 26. The binding energies of HCB with the SOM representative systems using B3LYP-D3, the corrected BSSE MP2, and CCSD at aug-cc-pvdz basis set.	70
Figure 27. The binding energy differences of HCB with the SOM representative systems at MP2/aug-cc-pvdz (raw data) and B3LYP-D3/aug-cc-pvdz (raw data) with respect to the corrected BSSE MP2/aug-cc-pvdz.	70
Figure 28. The binding energies for HCB with the test set given in Fig. 19 calculated at the B3LYP-D3/6-311++G(d,p) level of theory in gas phase and using the COSMO model. (I), (II), and (III) mark complexes which are most strongly affected by solvation (21, 27, and 32).	73
Figure 29. The root-mean square deviation, in Å, between the optimized conformers in the gas phase and solution at B3LYP/D3/6-311++G(d,p).	73
Figure 30. Correlation of the binding free energies for HCB-test set complexes with the dispersion energies at the B3LYP-D3/6-311++G(d,p) level of theory using COSMO model.	74
Figure 31. The dispersion binding energy of HCB with the representative systems in gas phase and in solution by using COSMO model.	74
Figure 32. The total binding energies between HCB and the different SOM systems calculated using GROMOS force-field by single point calculations as well as MD simulations, and binding free energies at B3LYP/D3/6-311++G(d,p) using COSMO model.	78
Figure 33. The binding energies due to the dispersion energy of the HCB-SOM complexes calculated using GROMOS force-field by single point calculations as well as MD simulations, and binding free energies at B3LYP/D3/6-311++G(d,p) using COSMO model.	78
Figure 34. Average number of HCB atoms surrounding the SOM systems in different spheres with radii 4, 6, and 8 Å along 100 ps trajectory.	81
Figure 35. Average number of water atoms surrounding the SOM systems in different spheres with radii 4, 6, and 8 Å along 100 ps trajectory.	81
Figure 36. The total binding energies between HCB and acetic acid (red), HCB and water (green), and acetic acid and water (blue) along 100 ps trajectory.	82

Figure 37. The total binding energies between HCB and methylbenzene (red), HCB and water (green), and methylbenzene and water (blue) along 100 ps trajectory.....	82
Figure 38. The predicted binding free energies of HCB with the SOM representative systems versus the calculated (actual) binding free energies at B3LYP/D3/6-311++G(d,p) and the red line is a linear correlation plotted as guide for eye.....	83
Figure 39. Correlation of the binding free energies for HCB-test set complexes with the polarizability of the test molecule at the B3LYP-D3/6-311++G(d,p) level of theory using COSMO model.	85
Figure 40. The predicted binding energies of HCB with the SOM representative systems versus the calculated (actual) binding energies from MD simulations and the red line is a linear correlation plotted as guide for eye.	86
Figure 41. Binding energy differences of HCB with the SOM representative systems, dipole moment differences of the HCB-SOM complexes using BLYP-D3 at 6-31G, 6-31++G, 6-311++G(d,p) basis sets with respect to 6-311++G(2d,2p) basis set.....	104

LIST OF TABLES

Table 1. Concentrations of total carbon (C_t), nitrogen (N_t), sulfur (S_t) and the C_t/N_t ratio for the samples pyrolyzed soil, soil residue, original soil, soil+3 HWE, soil+6 HWE, and HWE.....	40
Table 2. Concentrations of total Al, Ca, Fe, K, Mg, Mn, Na, and P in both original soil and HWE samples in addition to concentrations of the pedogenic oxides in the original soil sample.....	41
Table 3. Volatile matter (VM), average molecular weight by number (M_n) and weight (M_w), polydispersity (M_w/M_n), total ion intensity (TII) and relative proportions of ion intensity of different compound classes: carbohydrates = CHYDR, phenols + lignin m monomers = PHLM, lignin dimers = LDIM, lipids = LIPID, alkyl aromatics = ALKY, heterocyclic nitrogen containing compounds = NCOMP, sterols = STEROL, peptides = PEPTI, suberin = SUBER, free fatty acids = FATTY for pyrolyzed soil, soil residue, original soil, soil + 3 HWE, soil + 6 HWE and HWE	45
Table 4. Fitted parameters with respect to Freundlich and Langmuir equations which are normalized to the total soil mass as well as the total carbon mass for the original soil, soil+3 HWE, soil+6 HWE, and the pyrolyzed soil samples.	53
Table 5. The absolute ion intensity in 10^4 counts mg^{-1} of original soil (AII_1), soil+3 HWE (AII_2), soil+3 HWE (AII_3); the absolute ion intensity difference between original soil and soil+3 HWE (ΔAII_1), and between soil+3 HWE and soil+6 HWE (ΔAII_2).....	53
Table 6. The average binding free energy (E_B) in kcal/mol for the different SOM compound classes and the absolute ion intensity difference in 10^4 counts mg^{-1} ΔAII_1 , and ΔAII_2 which are taken from Table 5.....	76
Table 7. The fitted parameters, correlation of the binding energy with the relevant descriptors, and the most mutual correlated descriptors obtained using QSAR analysis (taking into account that +1.0 and -1.0 indicates to perfect positive and negative correlations, respectively, and 0.0 means that there is no any correlation) in case of COSMO calculations and MD simulations.....	88

ABSTRACT

The binding of hazardous persistent organic pollutants (POPs) to soil continues to pose a significant environmental problem. POPs can reach the soil and interact with soil constituents, especially soil organic matter (SOM). Understanding of this interaction is important for choosing effective remediation procedures. This interaction has been studied experimentally and theoretically. Experimentally, adsorption of hexachlorobenzene (HCB) on different soil samples has been achieved. Establishing of a set of different, well-characterized soil samples is a precursor step to the adsorption study. Since SOM is the most effective soil component for adsorption of hydrophobic systems, systematic modifications of SOM content and molecular composition in soil have been performed. Modifications were done by off-line pyrolysis and removal/addition of hot-water extracted (HWE) organic fraction from/to the original soil sample. Both pyrolysis-field ionization mass spectrometry (Py-FIMS) and synchrotron-based C- and N- X-ray absorption near-edge structure spectroscopy (XANES) have been applied to investigate the composition of SOM. These complementary analytical methods in addition to elemental analysis agreed in showing the following order of organic matter contents: pyrolyzed soil < soil residue < original soil < soil+3 HWE < soil+6 HWE < HWE. Regarding the SOM composition, addition of HWE to the soil sample increased the relative proportions of carbohydrates, N-containing heterocyclic compounds and peptides. Pyrolysis enriched the aromatics, unsaturated, N-heterocyclic compounds in addition to charcoal production. Regarding the total soil, percentage of each compound class increased in the order: original soil < soil+3 HWE < soil+6 HWE. Adsorption of HCB on the pyrolyzed soil, original soil, soil+3 HWE, and soil+6 HWE samples was done and the data were fitted to both Langmuir and Freundlich equations. The adsorption of HCB increased upon addition of HWE in the order: original soil < soil+3 HWE < soil+6 HWE. Adsorption of HCB on the pyrolyzed soil sample exceeded that of soil+6 HWE at low initial concentrations. By increasing of HCB concentration, the adsorption of HCB on the pyrolyzed soil sample became smaller. The same is valid over a larger range of HCB concentrations when the adsorbed HCB concentrations are normalized to the total C content in the soil sample. The differences in the chemical composition between the soil samples combined with the adsorption behaviour suggested that alkylated aromatic, phenol, and lignin monomer compounds dominate the adsorption process. To obtain a molecular-level understanding, a test set has been developed which comprises 32

representative soil constituents. Complexes of these test set systems with HCB were constructed by selecting the most favorable three dimensional configurations for each complex. Great computational effort has been spent for studying of this interaction including both quantum-mechanical calculations and molecular dynamics simulations in addition to quantitative structure activity relationship (QSAR). This interaction was studied by calculating the binding energy which is the most important parameter quantifying the interaction. Binding energy of HCB to each representative system in the complex has been calculated at different levels of theory. Effects of dispersion corrections, DFT-functionals, and basis sets have been studied. Moreover, benchmark calculations (MP2 and CCSD) have been performed. Effect of solvation on the individual SOM representative systems and their complexes with HCB as well as binding energies of these complexes has been established. These calculated binding energies at different levels of theory agreed in showing that HCB binds to SOM stronger than to soil mineral. Within SOM, HCB binds to alkylated aromatic, phenols, lignin monomers, and hydrophobic aliphatic compounds stronger than to polar aliphatic compounds. Moreover, it was found that the most vital physical properties controlling this interaction are polarizability, quadrupole moment of the representative system as well as charges and percentage of the C atoms in that system. The obtained results can be summarized in two points: 1- This combination of analytical techniques can be recommended for similar problems that require characterizing the bulk, non-extracted SOM instead of pre-selected compounds or compound classes. 2- Since the computational results substantiate the experimental conclusion, the developed test set should have a broader applicability.

ZUSAMMENFASSUNG

Die Bindung von gefährlichen Langlebigen organischen Schadstoffen (*POPs*) wird in den Böden weiterhin ein signifikantes Umweltproblem darstellen. *POPs* können in die Böden gelangen und wechselwirken dort mit den Bestandteilen des Erdreichs, insbesondere den organischen Bodensubstanzen (*SOM*). Das Verständnis dieser Interaktion ist für die Wahl eines effektiven Sanierungsverfahrens wichtig. Diese Wechselwirkung wurde experimentell und theoretisch untersucht. Experimentell wurde die Adsorption von Hexachlorbenzol (*HCB*) auf verschiedene Bodenproben untersucht, nachdem zuvor eine Satz von verschiedenen, gut charakterisierten Bodenproben festgelegt worden ist. Da die *SOM* die Bodenbestandteile mit der effektivsten Adsorption von hydrophoben Systemen sind, wurden systematische Modifikationen ihrer Zusammensetzung durchgeführt. Geändert wurden durch die off-line Pyrolyse und Hinzugabe/Entfernung von heißwasserextrahierten (*HWE*) organische Anteilen zu/von der ursprünglichen Bodenprobe. Sowohl Pyrolyse-feld-Ionisation-Massenspektrometrie (*Py-FIMS*) als auch synchrotronbasierte Kohlenstoff und Stickstoff Röntgen-Nahkanten-Absorptions-Spektroskopie (*XANES*) wurden angewendet, um die Zusammensetzung zu untersuchen *SOM*. Diese ergänzenden analytischen Methoden stimmten in der Reihenfolge der Gehalte an organischer Substanz überein: pyrolysiertes Boden < Bodenrückstände < ursprünglicher Boden < Boden+3 *HWE* < Boden+6 *HWE* < *HWE*. Bezüglich der *SOM* Zusammensetzung, erhöht eine Zugabe von *HWE* zur Bodenprobe die relativen Proportionen von Kohlenhydraten, von N-haltigen heterozyklischen Verbindungen und von Peptide. Pyrolyse bereichert die aromaten, ungesättigten, N-heterozyklischen Verbindungen zusätzlich zu Bildung von Holzkohle. Bezüglich des gesamten Bodens steigt der prozentuale Anteil jeder Stoffklasse in der Reihenfolge: ursprünglicher Boden < Boden+3 *HWE* < Boden+6 *HWE*. Adsorption von *HCB* auf Proben von pyrolysiertem Boden, ursprünglichem Boden, Boden+3 *HWE* und Boden+6 *HWE* wurde durchgeführt und die Daten sowohl an Langmuir- als auch Freundlichgleichungen angepasst. Die Adsorption von *HCB* erhöht sich durch Zugabe von *HWE* in der folgenden Reihenfolge: ursprünglicher Boden < Boden+3 *HWE* < Boden+6 *HWE*. Die Adsorption von *HCB* auf dem pyrolysierten Bodenproben überschreitet die Adsorption auf Böden mit 6 *HWE* bei niedrigen anfänglichen Konzentrationen. Durch die Erhöhung der Konzentration an *HCB*, wird die Adsorption von *HCB* auf der pyrolysierten Bodenprobe kleiner. Das gleiche gilt über einen größeren Bereich der *HCB*-Konzentrationen, wenn die adsorbierten

HCB-Konzentrationen auf den gesamten Kohlenstoffgehalt in der Bodenprobe normiert sind. Die Unterschiede in der chemischen Zusammensetzung zwischen den Bodenproben in Kombination mit dem Adsorptionsverhalten legen nahe, dass alkylierte Aromaten, Phenol und Monomerverbindungen von Lignin den Adsorptionsprozess dominieren. Um ein Verständnis auf molekularer Ebene zu erhalten, wurde ein Test-Set entwickelt, welches 32 repräsentative Bodenbestandteile umfasst. Komplexe dieser Test-Set-Systeme mit *HCB* werden durch die Auswahl der günstigsten dreidimensionalen Konfigurationen konstruiert. Großer Rechenaufwand wurde für das Studium dieser Wechselwirkung betrieben, quantenmechanischer Berechnungen und Molekulardynamiksimulationen, in Ergänzung zu quantitativen Struktur-Aktivitäts-Beziehung (*QSAR*). Diese Wechselwirkung wurde durch die Berechnung der Bindungsenergie, die der wichtigste Parameter zur Quantifizierung der Wechselwirkung ist, untersucht. Die Bindungsenergie von *HCB* zu jedem repräsentativen System im Komplex wurde auf unterschiedlichen Niveaus der Theorie berechnet. Die Effekte der Dispersionkorrekturen, der *DFT*-Funktionale und der Basissätze wurden untersucht. Darüber hinaus wurden Benchmark-Berechnungen (*MP2* und *CCSD*) durchgeführt. Der Effect Solvatisierung auf die einzelnen *SOM* repräsentativen Systeme und ihrer Komplexe mit *HCB* sowie Bindungsenergien dieser Komplexe wurde bestimmt. Diese auf verschiedenen Ebenen der Theorie berechneten Bindungsenergien zeigen übereinstimmend, dass *HCB* sich stärker mit den *SOMs* als mit den mineralischen Bestandteilen bindet. Innerhalb der *SOM* bindet sich *HCB* stärker an alkylierte Aromaten, Phenole, Lignin-Monomeren und hydrophoben aliphatische Verbindungen als an polare aliphatischen Verbindungen. Darüber hinaus kann gezeigt werden, dass die wichtigsten physikalischen Eigenschaften, die diese Wechselwirkung bestimmen, die Polarisierbarkeit, das Quadrupolmoment des repräsentativen Systems, sowie Ladung und Anteil der C-Atome in diesem System sind. Die auf diese Weise erhaltenen Ergebnisse können zu zwei Punkten zusammengefasst werden: 1 - Diese Kombination von analytischen Techniken können für ähnliche Probleme empfohlen werden, die Charakterisierung der Masse, nicht-extrahierten *SOM* statt vorgewählten Verbindungen oder Verbindungsklassen erfordern. & 2 - Da die berechneten Ergebnisse die experimentellen Schlussfolgerungen untermauern, sollte der entwickelte Test-Set eine breitere Anwendung haben.

1. INTRODUCTION

1.1. Motivation

Persistent organic pollutants (POPs) comprise an environmentally hazardous compound class that is resistant to environmental degradation through chemical, biological, and photolytic processes and tend to accumulate in soil, ground water and waste water.⁽¹⁾ They are ubiquitously distributed in the environment having long life times, which can be several days in the atmosphere and years or decades in the soil.⁽²⁾ In aqueous systems and soil, POPs preferentially move into the solid fraction because of their hydrophobicity. POPs can reach the soil either by purpose, such as pesticides and other agricultural chemicals, or incidentally through manufacture of industrial chemicals.⁽³⁾ In soil, POPs can be taken up by plant roots, adsorbed on soil constituents, especially on soil organic matter (SOM) and/or leached through the unsaturated zone eventually reaching the groundwater.⁽⁴⁾ So there are many possibilities that these pollutants reach humans through food. Exposure of humans to POPs can cause death and illnesses including disruption of the endocrine, reproductive, and immune systems, neurobehavioral disorders and cancers.⁽¹⁾ POPs don't only affect human and animals health but also decrease the fertility of the soil.

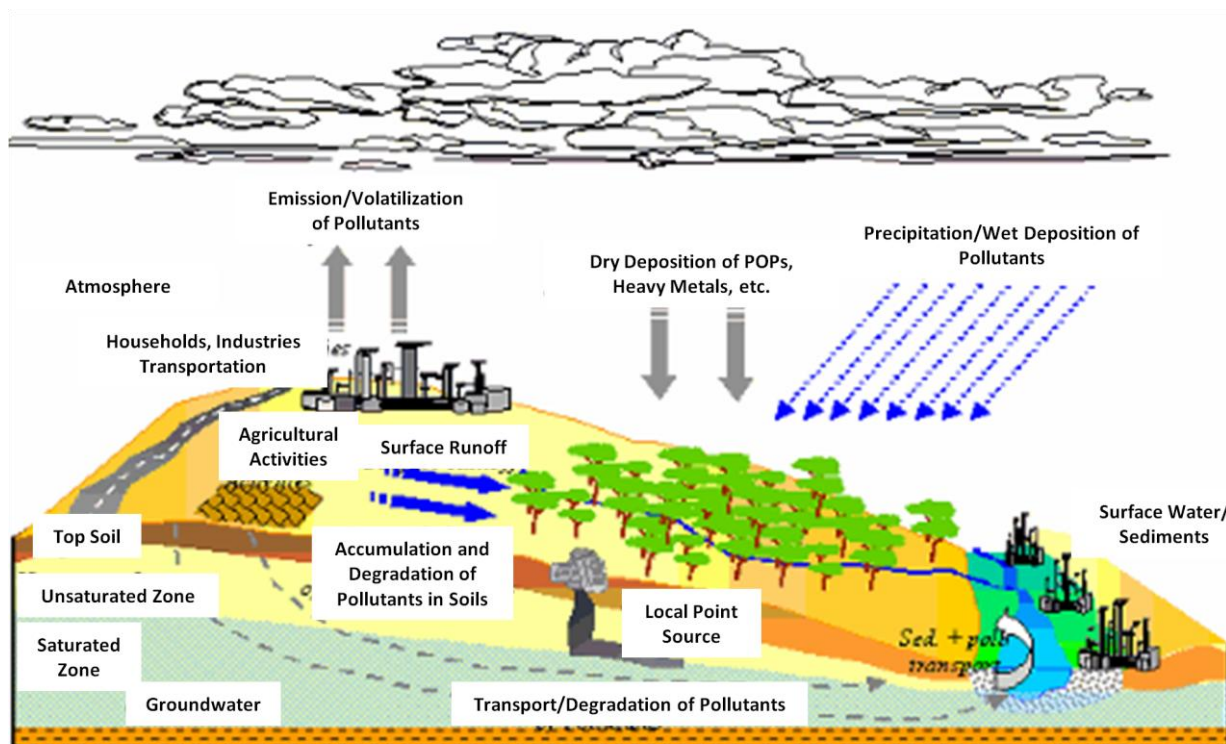


Figure 1. Organic pollutants reach the soil by different ways.⁽³⁾

This pollution can be reduced by applying bio-fertilizers and manures instead of chemical fertilizer and pesticide use⁽⁵⁾ as well as by physical, chemical and biological treatment of the industrial wastes. Once pollution occurred, there are various decontamination methods involving large scale excavation or long-term treatment, but they may be prohibitively costly and/or ineffective.⁽⁶⁾ Although there is the risk of binding of most pollutants to SOM, this binding can be a promising approach for reduction of this problem for some pollutants as well.⁽⁶⁾ These pollutants can be incorporated into SOM during process of humic acid formation. For these pollutants, process acts as neutralizing agent of toxic compounds.⁽⁶⁾ Thus binding of organic pollutants to SOM is considered as double-edged sword which can be a problem or a fantastic solution. The final decision in this issue should be preceded by a detailed study about nature of pollutants-SOM interaction.

Binding of POPs to SOM is influenced by several factors, including physical and chemical properties of the pollutant, moisture and chemical composition of soil, and the type and strength of the interactions between the pollutant and the reactive soil surfaces.⁽⁴⁾ These interactions of hydrophobic pollutants with soil can be studied experimentally and theoretically. Adsorption experiments described these interactions by an initial rapid and a following slower stage.^(7,8) This rapid stage is a surface phenomenon resulting from the hydrophobic behaviour of these pollutants. During this fast step, the vacant sites in the soil are filled up rapidly following linear variation. This stage contributes to the total adsorption more than the slow step. The most common mechanism for the slow step is diffusion into the organic matter.⁽⁹⁾ Since adsorption experiments yield only information, which can be correlated statistically to soil properties, computational chemistry is a complementary promising approach to develop an atomistic understanding of the binding of POPs to soil.^(10,11) In the next sections, the physical and chemical properties of soils as well as POPs and their interactions will be discussed.

1.2. Soil Composition

In the following, some basics of soil composition are introduced with information taken from different textbooks, literature, and websites.⁽¹²⁻²⁴⁾ Soil provides ecosystem services critical for life. It is the basis of our nation's agro-ecosystems which provides us with fiber, food and fuel. It acts as a water filter and a growing medium, provides habitat for billions of organisms, and supplies most of the antibiotics used to fight diseases. Soil is a complex natural body, multi-component system of interacting materials, and its properties result

from the net effect of all these interactions. Soil is composed of particles of broken rock which have been altered by physical, chemical and biological processes that include weathering with associated erosion. Soil is altered from its parent material by the interactions between the lithosphere “the rigid outermost shell of a rocky planet”, hydrosphere “the combined mass of water found on, under, and over the surface of a planet”, atmosphere, and biosphere “all ecosystems including plants, animals and microbes”.

Regarding the chemical composition, soil is a mixture of mineral and organic materials in the form of solids, gases and liquids. A good quality soil contains about 25% water, 25% air, 45% minerals (sand, silt, clay) , and 5% organic material. Soil water “soil moisture” is very important for soil formation “soil pedogenesis”, plant growth, soil temperature regulation, metabolic activities of microorganisms, and chemical and biological activities of soil. Between soil water and colloids, cation and anion exchanges take place which alter soil structure, and purify percolating water. The negative charges on colloid particles lead to attraction of cations to colloid surfaces. Presence of these cations preserves the fertility of soils in areas of moderate rainfall and low temperatures. In high rainfall areas, water washes the basic cations (nutrients) out which leads to acidic (low pH) and sterile soils. In low rainfall areas, unleached calcium pushes pH to 8.5 and soils may reach pH 10 by the addition of exchangeable sodium which leads to reduction of the plant growth. Most of agricultural crops do best with mineral soils of pH 6.5 and organic soils of pH 5.5. With respect to soil gases, soils include in their pores air, water vapour and the pollutants that might be picked up from the soil underneath. Soil air contains oxygen (20.6%) which is important for respiration of plant roots and soil organisms, nitrogen (79.2%), and carbon dioxide (0.25%).

Soil minerals play a vital role in soil fertility since mineral surfaces serve as potential sites for nutrient storage. Soil minerals “parent materials” and all plant nutrients with the exceptions of nitrogen, hydrogen and carbon are originally produced from rocks. As the parent material is chemically and physically weathered, transported, deposited and precipitated, it is transformed into a soil. The main soil minerals are quartz (SiO_2), calcite (CaCO_3), feldspar (KAlSi_3O_8), and mica ($\text{K}(\text{MgFe})_3\text{AlSi}_3\text{O}_{10}(\text{OH})_2$). Parent materials are classified into residual materials which have weathered in place from primary bedrock,

transported materials which have been deposited by water, wind, ice or gravity, and cumulose materials which are organic matters that have grown and accumulate in place.

Soil contains different layers “horizons” parallel to the soil surface and have different physical characteristics. The main distinct layers can be summarized as follows from top to bottom which can be shown in Figure 2 A. These horizons consist of horizon “O” containing organic matter, horizon “A” containing mineral soil with organic matter, horizon “E” which is similar to horizon “A” but with lighter color, horizon “B” which accumulates iron, clay, aluminum and organic compounds, horizon “C” containing large unbroken rocks, and horizon “R” containing continuous masses of hard rock.

The most important physical properties of soils used for the differentiation among the different horizons are texture, structure, density, porosity, consistency, temperature, color and resistivity. Soil texture is determined by the relative proportion of sand, silt, and clay particles. Sand and silt are the products of physical and chemical weathering, while clay is a product of chemical weathering. The terms sand, silt, and clay refer to relative sizes of soil particles which have the order: the sand particles ($0.063 \text{ mm} < \text{particle diameter} < 2.0 \text{ mm}$) > the silt particles ($0.002 \text{ mm} < \text{particle diameter} < 0.063 \text{ mm}$) > the clay particles (particle diameter $< 0.002 \text{ mm}$). The different types of the soils based on their texture are shown in Figure 2 B. The clumping of the sand, silt and clay forms aggregates and the further association of those aggregates into larger units forms soil structures called “peds”. Soil density is a measure of soil compaction. Soil porosity consists of the part of the soil volume occupied by air and water. Consistency is the ability of soil to stick together. Resistivity refers to the resistance to conduction of electric currents and affects the rate of corrosion of metal and concrete structures. The properties may vary through the depth of a soil profile.

Although SOM represents only a few percent of most soils, it has a great influence on soil properties and agricultural productivity. SOM is a key indicator of soil health which plays a role in a number of key functions. It serves as a reservoir of nutrients and water in the soil. It behaves as a sponge which has the ability to absorb and hold up to 90 percent of its weight in water. Therefore, it releases most of this water to plants. It is important for soil aggregates formation which improves soil structure. SOM is composed of plant and animal residues in different stages of decomposition, cells of soil microorganisms, and substances that are so well-decomposed. Also the living organisms are considered to be part of SOM.

Various organic compounds are made up of complex carbohydrates including pectins and gums, proteins, mucilages (polarglycoproteins and exopolysaccharides), lignins, fats, oils, waxes, resins, alcohols, organic acids, phenols etc. Plant roots and various soil animals provide organic materials to the soil that eventually become part of the SOM cycle. There are four main processes in that cycle, and all of them rely on soil microbes: decomposition of organic residues, release of nutrients (mineralization), release of carbon dioxide (respiration), and transfer of carbon from one SOM “pool” to another.

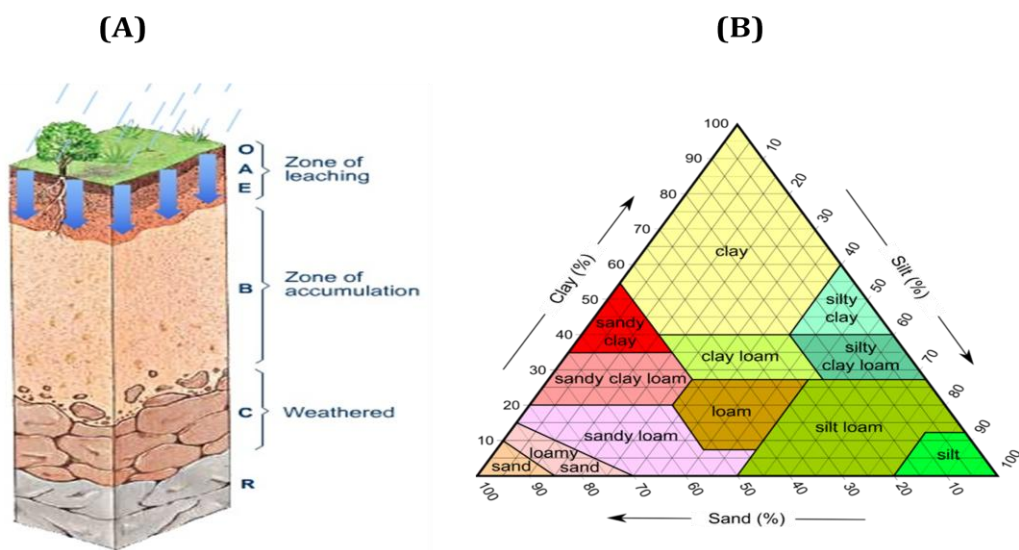


Figure 2. A: The main soil horizons (O, A, E, B, C, and R)⁽²²⁾ and B: The different soil types based on clay, silt, and sand composition.⁽²³⁾

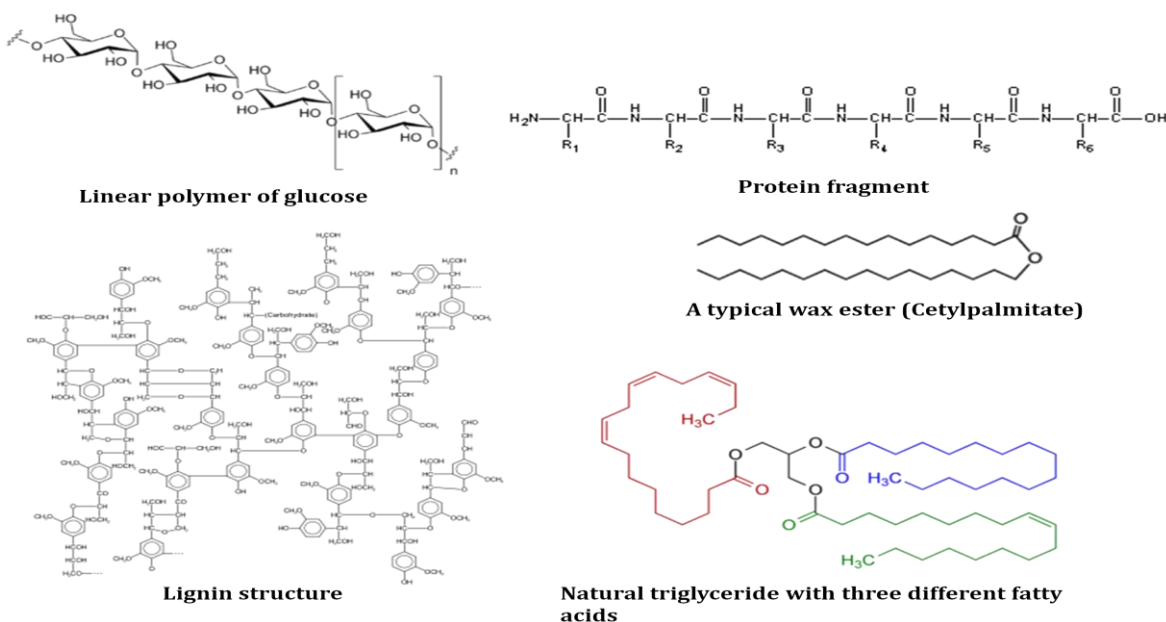


Figure 3. Some examples of SOM compound classes such as carbohydrates, protein, lignin⁽²⁴⁾, waxes, and fats.

In addition to the living organic matter, there are three dead SOM types which are active, slow, and passive. These are determined by the required time for complete decomposition. Active SOM, which have a lot of biological activity, is primarily made up of fresh plant and animal residues that break down in a very short time, from a few weeks to a few years. It is easily digested and decomposed by soil organisms. It stabilizes soil aggregates, releases nutrients by mineralization, and provides food for microbial activity. Passive SOM or humus, which is not biologically active, provides very little food for soil organisms. It may take hundreds or even thousands of years to fully decompose. Slow SOM consists primarily of detritus, partially broken down cells and tissues that are only gradually decomposing. It is somewhat resistant to decay and may take a few years to a few decades to completely break down.

Passive fraction of SOM "Humus" is a dark, complex mixture of organic substances that have been significantly modified from their original form over time. It also contains other substances that have been synthesized by soil organisms. It represents the majority of total SOM, and it is relatively stable over time. It supplies organic chemicals to the soil solution that can serve as chelates, which can hang onto trace elements and increase their availability to plants. Humus can be classified into humic substances and non-humic substances.

Non-humic substances are all those materials that can be placed in one category of discrete compounds such as carbohydrates, lipids, amino acids, and so on. Carbohydrates constitute 5 to 25% of the organic matter in most soils. Plant contributes carbohydrates in the form of simple sugars, hemicellulose, and cellulose. They have the ability to bind inorganic soil particles and metal ions into stable aggregates and complexes. They can be divided into 3 subclasses: Monosaccharides which are aldehyde and ketone derivatives of the higher polyhydric alcohols; Oligosaccharides which are polymeric structure of few monosaccharide units; and Polysaccharides which contain many monomeric units 8 or more. Carbohydrates can be found in soils as free sugars, complex polysaccharides, and polymeric molecules of various sizes and shapes which are so strongly attached to clay and/or humic colloids. Lipids represent a diverse group of materials ranging from relatively simple compounds such as fatty acids to more complex substances such as the sterols, terpens, polynuclear hydrocarbons, chlorophyll, fats, waxes, and resins. Lipids constitute 2 to 6% of the organic matter in most soils as fats, waxes, resins. Amino acids exist in soil in

several different forms such as: free amino acids; amino acids, peptides, or proteins bound to clay minerals on both external and internal surfaces; amino acids, peptides or proteins bound to humic colloids via H-bonding and van der Waals forces and covalent linkage.

Humic substances are unidentifiable natural bio-polymers components with relatively high-molecular weights that are involved as mediators in numerous life processes. They are a result of humification process which is accumulation and natural polymerization of by-products yielded by the biodegradation of organic matter. They enhance the absorption of both supplemented fertilizers as well as nutrients. They are divided into three fractions based on their color or water solubility, humic acids (HA), fulvic acids (FA), and humins. Fulvic acids are highly reactive young molecules of low molecular weights with random structure which are water soluble at all pH values. They are highly oxygenated aliphatic and aromatic biopolymers having color range from a light yellow to yellow-brown depending on the concentration. Humic acids are highly reactive old molecules of high molecular weights with random structure which are water insoluble under acidic conditions ($\text{pH} < 2$) but water soluble at higher pH values. They are mostly poly-phenolic aromatic biopolymers having dark brown to black color. Humins are not soluble in water at any pH value and has black color.

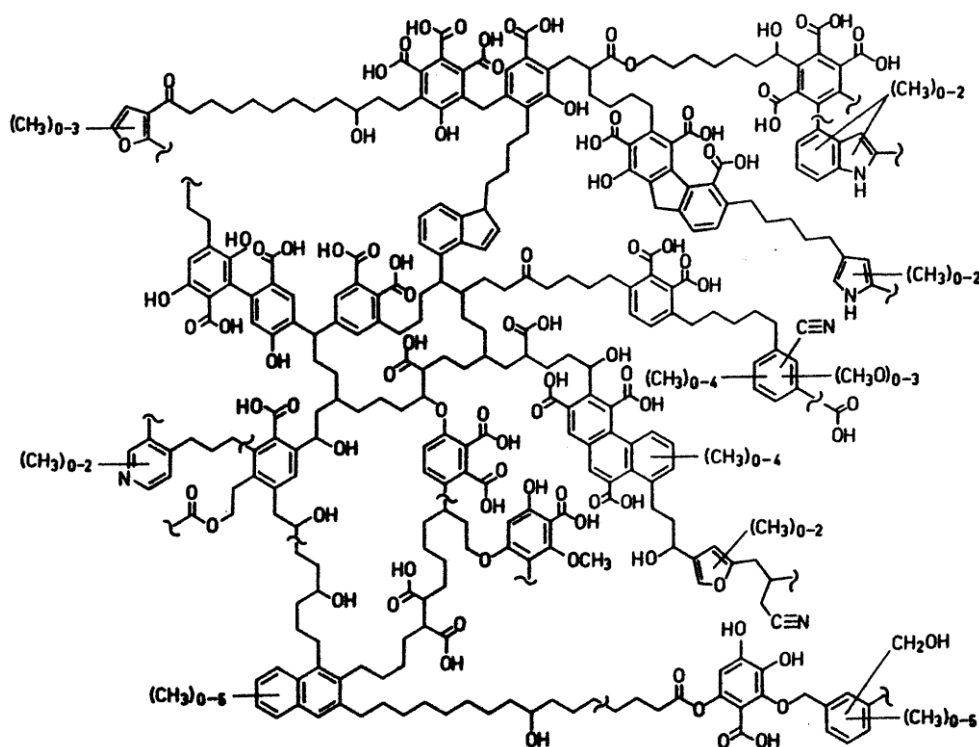


Figure 4. A proposed structure of a humic acid molecule by Schulten⁽²¹⁾ showing a wide range of functional groups (e.g. phenolic, carboxylic, salicylic, phthalate, nitrogen-bearing groups).

1.3. Soil Organic Matter Characterization

SOM is important for life on earth as it affects almost all physical, chemical and biological soil properties, and consequently, plant growth.⁽²⁰⁾ Therefore, disclosing of the chemical structure of SOM is the aim of a fast growing, interdisciplinary, scientific community. A variety of analytical methods were applied to develop structural concepts for SOM⁽²¹⁾ among which combinations of pyrolysis and mass spectrometry were useful for obtaining structural information on the molecular building blocks of SOM.⁽²⁵⁻²⁷⁾ Pyrolysis-field ionization mass spectrometry (Py-FIMS) uses soft electric field ionization to minimize fragmentation of the pyrolyzed molecules and to produce the molecular masses of the decomposition products from humic substances,⁽²⁸⁾ dissolved organic matter,^(29,30) organo-mineral particle size and aggregate fractions,^(31,32) and whole soil samples.^(26,27,33)

Recently, synchrotron-based C- and N-X-ray absorption near edge structure spectroscopy (XANES) analysis has been used to investigate the different species and functional groups of C and N in environmental samples.^(34,35) XANES is a nondestructive technique⁽³⁶⁾ that targets individual elements based on their core electron binding energies, and it is able to differentiate specific substance classes in a mixture. The C K-edge XANES has been applied to identify C-functional groups in soil.⁽³⁷⁻³⁹⁾ Applications of N K-edge XANES were reported as well.⁽⁴⁰⁻⁴³⁾ Although XANES in combination with mass spectrometry was applied to investigate SOM and its alterations, these methods were not yet explored to test how a controlled experimental modification of SOM alters the functional groups distribution and structure. Our interest is in the combination of elemental analysis, Py-FIMS, and C- and N-XANES methods to explore the molecular-level composition of SOM in a soil sample.

1.4. Soil Pollution

Soil pollution is one of the most serious environmental problems which have adverse effects on plant growth, animal health and thus human health. It is associated with indiscriminate use of fertilizers, pesticides, insecticides and herbicides; dumping of large quantities of solid waste; deforestation and soil erosion. It possibly happens as a result of accumulation of persistent toxic compounds, chemicals, salts, radioactive materials, or disease causing agents. The most common chemicals causing soil pollution are petroleum hydrocarbons, heavy metals, pesticides, and solvents. These pollutants can deteriorate the quality, texture and mineral content of the soil or disturb the biological balance of the organisms in the soil. Soil pollution damages the clay ionic structure and soil stability,

creates toxic dusts, releases vapors and hydrocarbon into buildings and cellars, runs off into rivers and kills the fish, plants and other aquatic life, and so on. Soil pollution changes the makeup of the soil and the types of organisms living therein, and reduces nitrogen fixation, nutrients, soil fertility, and crop yield. The contaminated soil should no longer be used to grow food, because the chemicals can leech into the food chain.

Most of pesticides have been associated with the soil over long time. Soil plays a major role in determination of the fate of chemical pollutants. In the soil, pesticides may be transformed by biotic or abiotic processes. Ideally, pesticides are mineralized to release carbon dioxide, water, and mineral elements. Pesticides and their metabolites can be transported through the soil by the processes of leaching, bioconcentration and volatilization. Xenobiotics directly interact with soil through the processes of adsorption and possibly subsequent covalent bond formation. Adsorption occurs via several mechanisms including Van der Waals forces, ion exchange, hydrogen bonding, charge transfer complexation, and hydrophobic interactions.^(44,45) The nature and strength of adsorption depend on the chemical and structural characteristics of the xenobiotic and this interaction is particularly sensitive to changes in the environment. It was found that the adsorbed residues become more stable and more resistant to extraction and microbial degradation with time.⁽⁴⁶⁾ This may be due to a redistribution of the xenobiotic from a weaker to a stronger site and/or to covalent bond formation between xenobiotics and soil.

The most persistent complexes result from the direct covalent binding of xenobiotics to soil humic matter or clay. The pesticides which are most likely to bind covalently to soil have chemical functionalities similar to the humus components. These molecules are polymeric and consist of an aromatic core containing mono-, di- and polyphenolic subunits. In fact, phenolic compounds account for up to 30% by weight of the humic polymer. Thus, pesticides that structurally resemble phenolic compounds can covalently bind to humus and these complexes can be found in all of the above environments. Covalently bound residues are extremely stable and are characterized by their resistance to acid or base hydrolysis, thermal treatment and microbial degradation.⁽⁴⁷⁻⁵⁰⁾

1.5. Persistent Organic Pollutants

The following information about persistent organic pollutants (POPs) is mainly taken from a report by Ritter et al.⁽¹⁾ POPs comprise an environmentally hazardous compound class that

is resistant to environmental degradation through chemical, biological, and photolytic processes. Exposure of humans to POPs can cause death and illnesses including disruption of the endocrine, reproductive, and immune systems, neurobehavioral disorders and cancers. The chemical structures of POPs are shown in Figure 5. They include aldrin, chlordane, dichlorodiphenyltrichloroethane (DDT), dieldrin, endrin, heptachlor, hexachlorobenzene (HCB), mirex, polychlorinated biphenyls (PCBs), polychlorinated dibenzo-p-dioxins (PCDDs), polychlorinated dibenzofurans (PCDFs), and toxaphene. POPs are ubiquitously distributed in the environment and have been measured at sites representing every major climatic zone and geographic sector. These include the open oceans, the deserts, the arctic and the Antarctic. There is no significant local sources and the only reasonable explanation for their presence is long-range transport from other parts of the globe. They have long life times, which can be several days in the atmosphere and years or decades in soil/sediment.⁽²⁾ They are originating from industry, agriculture and disease vector control. Some of them were used as pesticides in agricultural crops. By the late 1970s, most of POPs had been either banned or subjected to severe use restrictions in many countries. Some of POPs are still used in parts of the world.

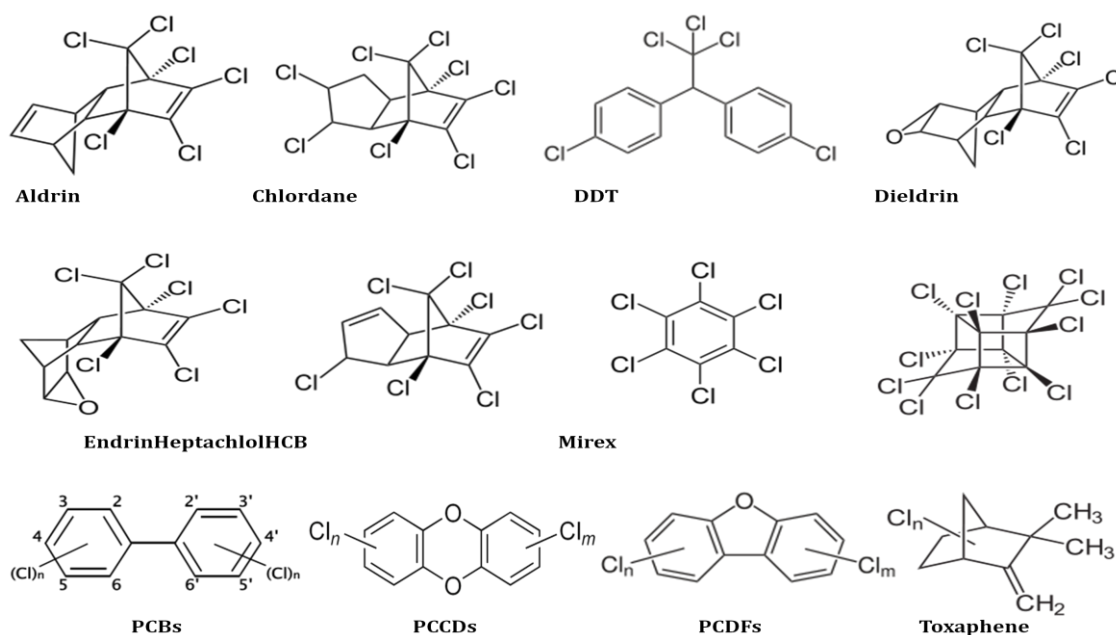


Figure 5. The chemical structures of the different POPs.

The most important physical properties of POPs are water solubility, vapor pressure, Henry's law constant (H), octanol-water partition coefficient (K_{OW}), and the organic carbon-water partition coefficient (K_{OC}). POPs are often chlorinated having low water

solubility and high lipid solubility (lipophilicity), leading to a tendency to preferentially dissolve in fats and lipids rather than water. Due to their high lipophilicity, bioconcentration from the surrounding medium into the organism takes place. Combined with environmental persistence and a resistance to biological degradation, lipophilicity also results in biomagnification through the food chain.

The carbon-chlorine bond is very stable towards hydrolysis. Chlorine attached to an aromatic ring is more stable than chlorine in aliphatic structures. Therefore, the more highly chlorinated organic compounds are more resistant to degradation and tend to accumulate in fat deposits. Additionally, POPs with molecular masses lower than 236 g/mol are less toxic, less persistent in the environment, and have more reversible effects than those with higher molecular masses.⁽²⁵⁾ Semi-volatility of POPs permits them to occur either in the vapor phase or adsorbed on atmospheric particles, thereby facilitating their long range transport through the atmosphere.

Humans can be exposed to POPs through diet, occupational accidents and the environment. Exposure of humans to POPs can be associated with a wide range of adverse health effects including illness (e.g. endocrine disruption, reproductive and immune dysfunction, neurobehavioural disorders, and cancer), and death. Recently some POPs have been implicated in reduced immunity in infants and children, and the concomitant increase in infection, also with developmental abnormalities, neurobehavioural impairment and cancer and tumor induction or promotion. Some POPs are also being considered as a potentially important risk factor in the etiology of human breast cancer. Both environmental behaviour and exposure are strongly correlated. Thus, the risk of exposure to a substance will be much lower if the substance is not persistent and the risk will be localized.

In the current study, our central focus is on HCB which is widely spread in the environment and has side effects on the human health. HCB is a white monoclinic crystalline solid, highly insoluble in water (water solubility: 40 µg/L at 20 °C), soluble in organic solvents (logK_{oc}: 2.56-4.54 at 20 °C), and quite volatile. It is very resistant to breakdown and has a high partition coefficient (logK_{ow}: 3.03-6.42), and as a result is known to bioconcentrate in the fat of living organisms. HCB was introduced as a fungicide for the first time in 1945 for seed treatment, especially for control of bunt of wheat. HCB is also a byproduct of the manufacture of industrial chemicals including carbon tetrachloride, perchlorethylene,

trichloroethylene and pentachlorobenzene. It is known as an impurity in several pesticide formulations, including pentachlorophenol and dieldrin (2,6-dichloro-4-nitrobenzamide) and others. HCB was detected in Spain (in meat and meat products), United States (in pasteurized milk), India (in foods, oils, milk, fish, and prawns; and the estimated daily intake is $0.13 \mu\text{g}/\text{person}$), and Vietnam (in some foods such as pulses and caviar with an estimated daily intake of $0.10 \mu\text{g}/\text{person}$). The most notable episode involving the effects of HCB on humans involves the ingestion of HCB-treated seed grain in eastern Turkey between 1954 and 1959. The patients who ingested the treated seed experienced a range of symptoms including photosensitive skin lesions, hyperpigmentation, hirsutism, colic, severe weakness, porphyria, and debilitation. Approximately 3,000-4,000 people developed porphyria cutanea tarda, a disorder of haem biosynthesis. Mortality was up to 14%. Mothers who ingested the seeds passed the HCB to their children by placental transfer and through maternal milk. Children born to these women developed "pembeyara" or pink sore, with a reported mortality rate of approximately 95%. A study of 32 individuals twenty years after the outbreak showed that porphyria can persist years after the ingestion of HCB. A small cross-sectional study of workers exposed to HCB did not find any evidence of cutaneous porphyria or any other adverse effects associated with exposure of 1 to 4 years.

1.6. Pollutant-Soil Organic Matter Interaction

Interaction of such hydrophobic pollutants with SOM was described to be non-covalent or dispersion like.⁽⁵¹⁾ This interaction is the dominant interaction type between supermolecules⁽⁵²⁾ and is critical in maintaining the three-dimensional structure of large molecules and is involved in many biological processes. The pervasiveness of the dispersion interaction has motivated persistent efforts⁽⁵³⁻⁵⁵⁾ to develop reliable computational methodologies for non-covalent interactions. Extensive work has established the importance of high levels of electron correlation⁽⁵⁶⁾ as embodied by coupled-cluster through perturbative triples CCSD(T)⁽⁵⁷⁾ for the proper characterization of dispersion interactions. The introduction of the density functional theory (DFT)+dispersion, like DFT-D2⁽⁵⁸⁾ and DFT-D3,⁽⁵⁹⁾ method and the crafting of several improved functionals are among the promising approaches of low computational cost to improve description of the dispersion interaction.

Due to the complexity and heterogeneity of the SOM chemical composition, its modelling is still a very tough problem. There are different opinions about the principal structural

organization of humic substances and SOM, i.e. macromolecular vs. supramolecular.⁽⁶⁰⁻⁶²⁾ Kubicki and coworkers, and Lischka and coworkers modelled SOM by few or several compounds containing the predominant functional groups of humic acid. Kubicki, Sparks and coworkers performed an atomistic simulation such as the binding of polycyclic aromatic hydrocarbons to soot⁽⁶³⁾ and the dynamics of phenol-water⁽⁶⁴⁾ or salt⁽⁶⁵⁾ solutions at clay surfaces. Also they modelled processes at mineral surfaces such as surface complexation with a variety of compounds.⁽⁶⁶⁻⁷⁰⁾ Lischka and coworkers studied the effect of protonation, deprotonation, and dehydroxylation of different reactive sites on a goethite model surface⁽⁷¹⁾ as well as adsorption of polycyclic aromatic hydrocarbons on such a surface.^(72,73) Furthermore, they investigated interactions between a 2,4-dichlorophenoxy acetic acid herbicide and various functional groups⁽⁷⁴⁾ and the role of hydrogen bonds in stabilizing poly acrylic acid oligomer structures mimicking humic acid.^(75,76) Another approach for SOM modelling can be arisen from construction of only one segment of polymeric complex containing all or most of the SOM functional groups in. The perhaps most complex polymeric-type, effective atomistic model of SOM has been developed by Schulten and coworkers on the basis of extensive investigations containing geochemical, wet-chemical, biochemical, spectroscopic, spectrometric, agricultural, and ecological data with analytical pyrolysis (see Figure 6).⁽⁷⁷⁻⁸⁰⁾

Polymer-like modelling of SOM is critical because of the huge number of possibilities for combining all of SOM compounds and functional groups together into a single macromolecule. In the same context, deficiency in description of SOM can be arisen from modelling of SOM by few numbers of functional groups. Therefore, to overcome these two problems, recently⁽⁸¹⁾ we developed a new approach for SOM modelling. We modelled the SOM by separate representative systems covering almost all functional groups as well as analytically determined compound classes which appear most promising. A test set of representative SOM systems was developed⁽⁸¹⁾ to study interaction of one of the most important POPs,⁽²⁾ hexachlorobenzene (HCB), to SOM by computational chemistry. The calculated binding energies of HCB with these representative SOM systems had been correlated to adsorption data of HCB on different well-characterized soil samples.⁽⁸²⁾

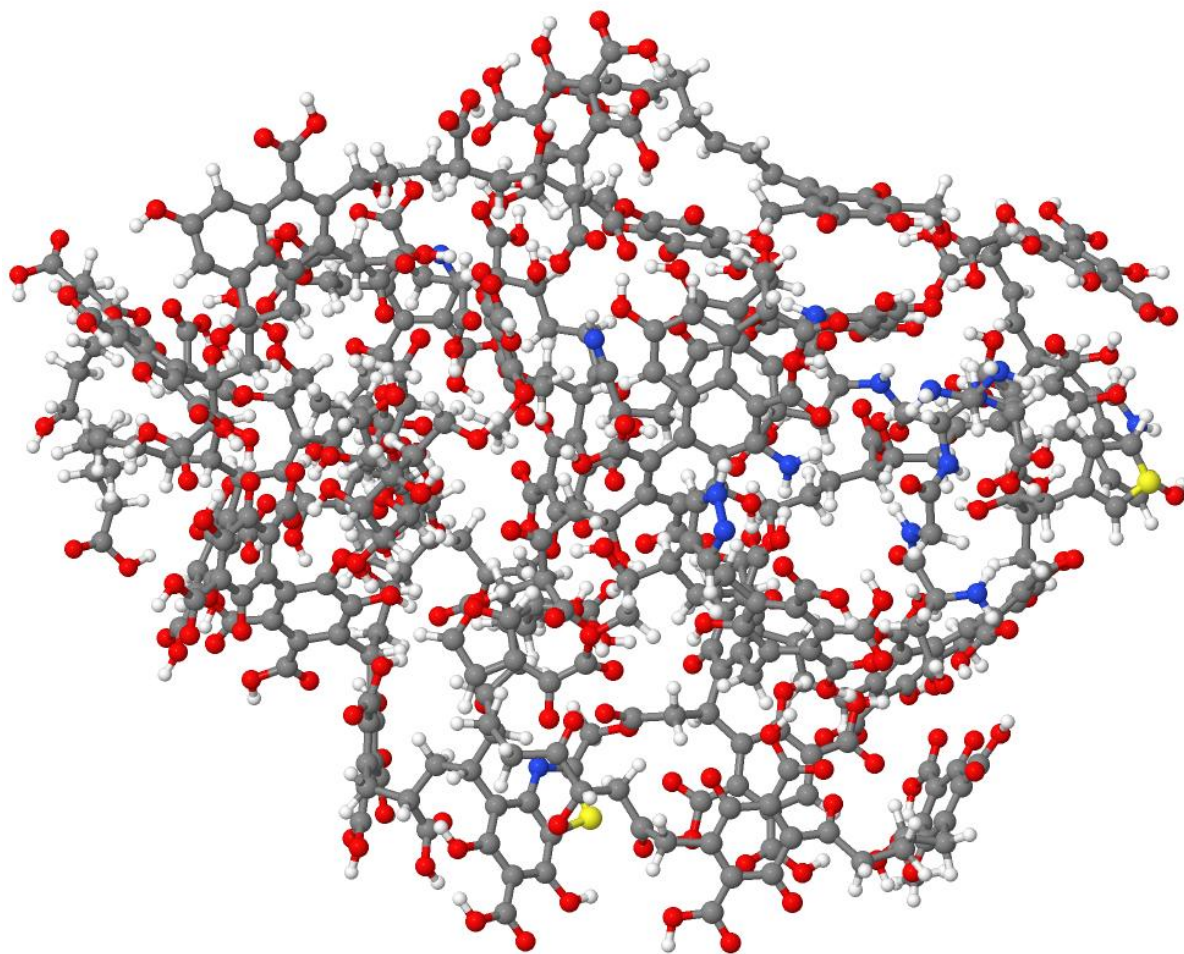


Figure 6. The three dimensional structure of SOM model developed by R.-H. Schulten.⁽⁷⁹⁾

1.7. Objective and Strategy of the Current Work

We are aiming to understand the interaction of HCB with soil constituents especially SOM. Experimental and theoretical efforts have been done to achieve this goal. This interaction has been studied experimentally via adsorption of HCB on soil samples with different chemical composition. The differences in the chemical composition have a significant effect on the adsorption behaviour. So it is important to change or modify in the chemical composition of soil. Theoretically, the interaction has been studied via building a model for SOM based on characterization of the different soil samples. Then study interaction of HCB with the modelled systems by calculating their binding energies. Hence, to achieve purpose of this study we are keeping track of the following strategy:

1. Establishing a set of well-characterized soil samples with altering the SOM composition by changing the polarity character of SOM in different ways.

- a. The first way is by removing a hot-water extracted organic fraction from the original soil sample and adding it in increasing amounts to the original soil sample.
 - b. The second way is thermal heating by off-line pyrolysis of the soil sample.
 2. Investigation to what extent these modifications have altered the SOM molecular composition by a combination of Py-FIMS, and C and N K-edge XANES.
 3. Study of the interaction of HCB with SOM experimentally by adsorption of HCB on some of these different well-characterized soil samples.
 4. In order to link the experimentally observed HCB adsorption by samples with systematically changed SOM composition a test set of 32 representative systems is developed for a comparative theoretical study.
 5. Study of the interaction of HCB with SOM model by means of computational chemistry.
 - a. Study this interaction by calculating binding energies of HCB with the SOM constituents within the HCB-SOM complexes at different levels of theory.
 - b. Study effects of dispersion (without and with D2⁽⁵⁸⁾ and D3⁽⁵⁹⁾ dispersion corrections), DFT-functionals (BLYP,⁽⁸³⁾ B3LYP,⁽⁸⁴⁾ B3LYP5,⁽⁸⁵⁾ and CAMB3LYP⁽⁸⁶⁾), and basis sets (6-31G,⁽⁸⁷⁻⁸⁹⁾ 6-31++G,^(89,90) 6-311++G(d,p),⁽⁸⁹⁻⁹¹⁾ 6-311++G(2d,2p),⁽⁸⁹⁻⁹¹⁾ and aug-cc-pvdz⁽⁹²⁾).
 - c. Performing of benchmark calculations using MP2 and CCSD.^(57,93)
 - d. Study effect of solvation on the individual SOM representative systems and their complexes with HCB as well as binding energies of these complexes by the COSMO model as well as the classical molecular dynamics simulations.
 - e. Obtaining an atomistic understanding of HCB-SOM-interaction through correlation of the binding energy with the molecular properties the representative systems by quantitative structure-activity relationship (QSAR).⁽⁹⁴⁾
-

2. THEORETICAL BACKGROUND

The theory behind the current work has been divided into three main sections and presented below. The different quantum mechanical models for solution of the electronic Schrödinger equation are outlined in section (2.1). Generally these models are classified into two directions including the size of the used basis set expansion and the level of treatment of electron correlation. Approximation of the wave-function by a single Slater determinant and expansion of the spatial part of the wave-function in terms of basis functions are shown in section (2.1.1). The variational principle and the Hartree-Fock theory are reviewed in section (2.1.2). In section (2.1.3), Improvement of the Hartree-Fock method by introducing electron correlation is presented for the cases of 2nd order perturbation theory (MP2) and coupled cluster theory. Effectively, the problem of dispersion interactions has been treated by these two levels of theory. Promising approaches of low computational cost to improve description of the dispersion interaction can be introduced by adding dispersion corrections to, the most widely used method, density functional theory (DFT). This alternative economical method, DFT, is presented in section (2.1.4) which also considers the electron correlation. Section (2.2) shows how solvent effect can be incorporated via implicit treatment through the conductor-like screening model (COSMO) or explicit treatment using of force-field molecular dynamics simulation. At each level of theory the binding energies between HCB and the SOM representative systems are calculated. These binding energies are correlated to some physical parameters of SOM representative systems. This type of correlation is known as “quantitative structure–activity relationship” (QSAR) and is given in section (2.3).

2.1. Schrödinger Equation and Born-Oppenheimer Separation

Generally, it is impossible to solve exactly the time-independent Schrödinger equation (2.1) for polyatomic systems. Therefore, approximations must be made such as the Born-Oppenheimer approximation.⁽⁹⁵⁾ It arises from the fact that the mass of the electrons is much smaller than that of the nuclei. Then, one can treat the motion of the electrons and motion of the nuclei separately. The kinetic energy of the nuclei can be neglected since it is smaller than that of the electrons by a factor of M_1/m_{el} (where, M_1 and m_{el} are masses of nuclei and electron respectively). The electrons can be considered as moving in the field of fixed nuclei, where the nuclear-nuclear repulsion is constant.

$$\hat{H}\Psi_{el,nuc}(\vec{r}, \vec{R}) = E\Psi_{el,nuc}(\vec{r}, \vec{R}) \quad (2.1)$$

where, \hat{H} is the molecular Hamiltonian operator, $\Psi_{el,nuc}(\vec{r}, \vec{R})$ is the time independent wave-function, \vec{r} and \vec{R} are coordinates of all electrons and nuclei respectively, and E is the electronic energy of the system. \hat{H} takes the form: $\hat{H} = \hat{T} + \hat{V}$ where, \hat{T} and \hat{V} are the kinetic and potential energy operators respectively which are represented below:

$$\hat{T} = -\frac{\hbar^2}{2} \sum_{i=1}^N \frac{1}{m_{el}} \nabla_i^2 - \frac{\hbar^2}{2} \sum_{I=1}^M \frac{1}{M_I} \nabla_I^2 \quad (2.2)$$

$$\hat{V} = \sum_{i=1}^N \sum_{i<j}^N \frac{e^2}{4\pi\epsilon_0 r_{ij}} - \sum_{i=1}^N \sum_{I=1}^M \frac{Z_I e^2}{4\pi\epsilon_0 r_{iI}} + \sum_{I=1}^M \sum_{I<J}^M \frac{Z_I Z_J e^2}{4\pi\epsilon_0 R_{IJ}} \quad (2.3)$$

Where, the sums run over electrons i and nuclei I , the Laplacian operators ∇_i^2 and ∇_I^2 involve differentiation with respect to the coordinates of the i^{th} electron and the I^{th} nucleus, where, $r_{ij} = |\vec{r}_i - \vec{r}_j|$, $r_{iI} = |\vec{r}_i - \vec{R}_I|$, $R_{IJ} = |\vec{R}_I - \vec{R}_J|$, and the double sum is over distinct pairs of particles (electrons or nuclei). The electronic Schrödinger equation is represented in equation (2.4):

$$\hat{H}_{el}\Psi_{el}(\vec{r}; \vec{R}) = E_{el}(\vec{R})\Psi_{el}(\vec{r}; \vec{R}) \quad (2.4)$$

$$\hat{H}_{el} = -\frac{\hbar^2}{2} \sum_{i=1}^N \frac{1}{m_{el}} \nabla_i^2 + \sum_{i=1}^N \sum_{i<j}^N \frac{e^2}{4\pi\epsilon_0 r_{ij}} - \sum_{i=1}^N \sum_{I=1}^M \frac{Z_I e^2}{4\pi\epsilon_0 r_{iI}} \quad (2.5)$$

Solution of equation (2.4) is the electronic wave-function $\Psi_{el}(\vec{r}; \vec{R})$ which describes the motion of the electrons and explicitly depends on the electronic coordinates but parametrically (indicated by semicolon) on the nuclear coordinates, as does the electronic energy $E_{el}(\vec{R})$. One can write the nuclear Schrödinger equation as

$$\hat{H}_{el,nuc}\Psi_{el,nuc}(\vec{R}) = E_{el,nuc}\Psi_{el,nuc}(\vec{R}) \quad (2.6)$$

where,

$$\hat{H}_{el,nuc} = -\frac{\hbar^2}{2} \sum_{I=1}^M \frac{1}{M_I} \nabla_I^2 + V_{el}(\vec{R}) \quad \& \quad V_{el}(\vec{R}) = E_{el}(\vec{R}) + \sum_{I=1}^M \sum_{I<J}^M \frac{Z_I Z_J e^2}{4\pi\epsilon_0 R_{IJ}} \quad (2.7)$$

where, $V_{el}(\vec{R})$ represents the potential energy surface (PES) which is a potential for the nuclear motion depending on the electronic state el .

This approximation ignores the possibility of having non-radiative transitions between different electronic eigen states. Transitions can only arise through coupling with an external field.

2.1.1. Molecular Orbital Theory

Since the electronic wave-function, $\Psi_{el}(\vec{r}; \vec{R})$, depends parametrically on (\vec{R}) , we will suppress (\vec{R}) in our notation from now on. A new coordinate \vec{x} representing the set of all coordinates associated with an electron (spatial coordinates \vec{r} and spin coordinate ω , i.e., $\vec{x} = \{\vec{r}, \omega\}$) should be defined. Also a spin orbital $\chi(\vec{x})$ which is a function of the space and spin coordinates of a single electron is presented as a product of a spatial orbital $\psi(\vec{r})$ and one of the two spin functions $\alpha(\omega)$ and $\beta(\omega)$.

$$\chi(\vec{x}) = \psi(\vec{r}) \begin{cases} \alpha(\omega) \\ \beta(\omega) \end{cases} \quad (2.8)$$

For a given spatial orbital $\psi(\vec{r})$, two possible spin orbitals, one with α spin and one with β spin can be introduced. Construction of N-electron wave-function Ψ_{el} from spin orbitals is explained by the molecular orbital theory and usually formed from a single Slater determinant (SD) (2.9):

$$\psi^{SD} = \frac{1}{\sqrt{N!}} \begin{vmatrix} \chi_1(\vec{x}_1) & \chi_2(\vec{x}_1) & \dots & \chi_N(\vec{x}_1) \\ \chi_1(\vec{x}_2) & \chi_2(\vec{x}_2) & \dots & \chi_N(\vec{x}_2) \\ \vdots & \vdots & \ddots & \vdots \\ \chi_1(\vec{x}_N) & \chi_2(\vec{x}_N) & \dots & \chi_N(\vec{x}_N) \end{vmatrix} \quad (2.9)$$

where, $\frac{1}{\sqrt{N!}}$ is a normalization factor. An interchange of two electrons will interchange two rows of the SD, which changes the sign of the SD. Besides this exchange, the single SD doesn't take into account of correlation of two opposite spin electrons.⁽⁹⁶⁾

Basis Set Expansion

The individual molecular spatial orbital $\psi_i(r_i)$ (for simplicity we used r instead of \vec{r}) is expressed in (2.10) as a linear combination of a finite set of prescribed one-electron functions known as basis functions ϕ_μ . This treatment is known as linear combination of atomic orbitals (LCAO) theory.

$$\psi_i(r_i) = \sum_{\mu} C_{\mu i} \Phi_{\mu}(r_i) \quad (2.10)$$

where, $C_{\mu i}$ are the molecular orbital expansion coefficients.

Basis sets were developed for first time by J.C. Slater.⁽⁹⁷⁾ Two atomic basis function types are represented by (2.11a) and (2.11b) which are referred to the Slater type orbital (STO) and the Gaussian type orbital (GTO).

$$STO = \frac{\zeta^3}{\pi^{0.5}} e^{-\zeta r} \quad (2.11a)$$

$$GTO = \frac{2\alpha}{\pi^{0.75}} e^{-\alpha r^2} \quad (2.11b)$$

where, ζ (zeta) is the Slater orbital exponent and α is the Gaussian orbital exponent.

GTOs are less satisfactory to represent the atomic orbitals than STOs but they have low computational cost. A compromise is to use linear combinations of Gaussian functions as basis functions to mimic the Slater-type behavior. The contracted Gaussian basis function $\Phi_{\mu}(r_i)$ is represented in (2.12) by the primitive Gaussian basis functions g_s . Many contraction schemes exist and the employed ones in this work are introduced below.

$$\Phi_{\mu}(r_i) = \sum_s d_{\mu s} g_s(\alpha, r_i) \quad (2.12)$$

Split-Valence Basis Sets

Since the inner-shell electrons are not vital to the calculation, only the valence orbitals are split into two parts: an inner compact function and more diffuse outer function. During the construction of the molecular orbitals, the coefficients of these two types of functions can be varied independently as well as those of the core orbitals. Here we are using a 6-31G basis set: the inner shell orbitals are described by six contracted Gaussian functions while the inner and outer valence orbitals consist of three and one Gaussian functions, respectively.

Polarized Basis Sets

The previous basis set can be improved by adding polarization functions, which are functions of higher angular momentum number. This provides the non spherical symmetric displacement of electronic density away from the nuclear center upon molecule formation (charge polarization). For instance, 6-31G(d,p) is constructed by the addition of a set

of gaussian d-type and p-type primitives to the split-valence 6-31G basis set for the description of each heavy (non-hydrogen) atom and hydrogen atom, respectively.

Diffuse Basis Sets

One can add highly diffuse functions to the basis set for a proper description of the electron density at large distances from the nuclei. This is done by adding a "+" such as 6-31+G(d,p), which indicates that one adds to the 6-31G(d,p) basis set four highly diffuse functions (s, p_x , p_y , p_z) on each non-hydrogen atom of the second row in the periodic table.

Correlation Consistent Basis Sets

They are developed by Dunning and coworkers⁵⁰ to converge systematically to the complete basis set limit using empirical extrapolation techniques. They have the symbol cc-pVNZ where N=D,T,Q,5,6,... (D=double, T=triples, etc.). The 'cc-p' stands for correlation-consistent polarized and the 'V' indicates they are valence-only basis sets. They include successively larger shells of polarization functions (d, f, g, etc.). Addition of diffuse functions for them produces the augmented versions which have the symbol aug-cc-pVNZ.

2.1.2. Variational Method and Hartree-Fock Theory

One can use Hartree-Fock (HF) theory⁽⁹⁶⁾ to fix the coefficients of equation (2.10). It is based on the variational principle of quantum mechanics. The basic idea is to guess a trial wave-function for the problem, which contains of some adjustable parameters "variational parameters". These parameters are adjusted until the energy of the wave-function is minimized. The resulting optimized wave-function and its corresponding energy are variational method approximations to the exact wave-function and energy, respectively. The HF method is applied to determine the optimum orbitals in single-determinant wave-functions. The optimum spin orbitals must satisfy the following HF equations:⁽⁹⁸⁾

$$\hat{F}(\vec{x}_i)\chi_i(\vec{x}_i) = \varepsilon_i\chi_i(\vec{x}_i) \quad (2.13)$$

$$\hat{F}(\vec{x}_i) = \hat{h}(\vec{x}_i) + v^{HF}(\vec{x}_i) = \hat{h}(\vec{x}_i) + \sum_{j=1}^N \hat{J}_j(\vec{x}_i) - \hat{K}_j(\vec{x}_i) \quad (2.14)$$

$$\hat{h}(\vec{x}_i) = -\frac{\hbar^2}{2m_i} \nabla_i^2 - \sum_{I=1}^M \frac{Z_I e^2}{4\pi\epsilon_0 r_{iI}} \quad (2.15)$$

$$\hat{J}_j(\vec{x}_i)\chi_i(\vec{x}_i) = \left[\int dx_j \chi_j^*(\vec{x}_j) \frac{1}{4\pi\epsilon_0 r_{ij}} \chi_j(\vec{x}_j) \right] \chi_i(\vec{x}_i) \quad (2.16)$$

$$\hat{K}_j(\vec{x}_i)\chi_i(\vec{x}_i) = \left[\int dx_j \chi_j^*(\vec{x}_j) \frac{1}{4\pi\epsilon_0 r_{ij}} \chi_i(\vec{x}_j) \right] \chi_j(\vec{x}_i) \quad (2.17)$$

where ϵ_i is the energy corresponding to the spin orbital $\chi_i(\vec{x}_i)$ and $\hat{F}(\vec{x}_i)$ is the Fock operator, $\hat{h}(\vec{x}_i)$ is a single electron Hamiltonian, $v^{HF}(\vec{x}_i)$ is the average potential experienced by the i th electron due to the presence of the other electrons, $\hat{J}_j(\vec{x}_i)$ is the Coulomb operator representing the coulomb interaction between electrons that occupy orbitals χ_i and χ_j , and $\hat{K}_j(\vec{x}_i)$ is the exchange operator representing exchanges of the electron with coordinates \vec{x}_i in spin orbital χ_j and electron with coordinates \vec{x}_j in spin orbital χ_i .

The HF equation can be solved iteratively using the self consistent field (SCF) method. The solution of the HF eigenvalue problem produces a set of orthonormal HF spinorbitals, $\chi_i(\vec{x}_i)$. The approximate electronic energy of the electronic ground state is calculated as

$$E_{el}(HF) = \sum_{i=1}^N \epsilon_i - \frac{1}{2} \sum_{i=1}^N \sum_{j=1}^N (J_{ij} - K_{ij}) \quad (2.18)$$

where, J_{ij} and K_{ij} are the matrix elements of the coulomb and exchange operators, equations (2.16) and (2.17), respectively.

The resulting value will be an upper bound to the exact energy within the limitation imposed by the single determinantal wave-function and the particular basis set employed. Hence the best single determinantal wave-function is formed by minimizing the expectation value of the energy with respect to the coefficients $C_{\mu i}$. In practice, one solves the HF equation numerically by introducing a set of known spatial basis functions, equation (2.10), then the HF equation can be converted to a set of algebraic equations, the Roothaan-Hall equations (2.19),⁽⁹⁹⁾ which are solved by standard matrix techniques

$$\mathbf{FC} = \mathbf{SC}\boldsymbol{\epsilon} \quad (2.19)$$

where, \mathbf{F} is the Fock matrix with elements $F_{\mu\nu} = \int \Phi_{\mu}^*(r) \mathbf{F} \Phi_{\nu}(r) dr$, \mathbf{S} is the overlap matrix with elements $S_{\mu\nu} = \int \Phi_{\mu}^*(r) \Phi_{\nu}(r) dr$, \mathbf{C} is the eigen vectors matrix and $\boldsymbol{\epsilon}$ is the diagonal matrix of the orbital energies, ϵ_i .

2.1.3. Electron Correlation Methods

The lack of the electron correlation which arises from using only single SD is the main deficiency in HF theory. The exact wave-function cannot be expressed as a single

determinant. The neglect of electron correlation leads to a number of quantitative deficiencies in the description of the electronic structure and energies. The difference between the exact and the HF energy is defined as the correlation energy.⁽¹⁰⁰⁾

$$E(\text{exact}) = E_{\text{el}}(\text{HF}) + E(\text{correlation}) \quad (2.20)$$

The electron correlation can be described by mixing of electronic configurations, or equivalently via virtual excitations such as the coupled cluster theory. Two electron correlation methods involving a linear combination of SDs are briefly outlined below.

2.1.3.1. Møller-Plesset Perturbation Method

The Møller and Plesset (MP) perturbation theory is taking into account the electron correlation by splitting the Hamiltonian into two parts.⁽¹⁰¹⁾ It is known how to solve the first part “reference or unperturbed” but not the second one “perturbed”. The MP model is formulated by introducing the following generalized electronic Hamiltonian (H_λ)

$$\hat{H}_\lambda = \hat{H}_0 + \lambda \hat{V} \quad (2.21)$$

$$\lambda \hat{V} = \lambda(\hat{H} - \hat{H}_0) \quad (2.22)$$

where, \hat{H}_0 is the, λV is the perturbed Hamiltonian, \hat{H} is the exact Hamiltonian, and λ is a dimensionless parameter.

The unperturbed or zero-order Hamiltonian, \hat{H}_0 is the sum of the one-electron Fock operators and its corresponding eigen value to a particular determinant Ψ is the sum of the one-electron energies, ε_i , for the spin orbitals which are occupied in Ψ . Both of the exact wave-function Ψ_λ and the electronic energy for a system can be described by the following perturbation expansion:

$$\Psi_\lambda = \Psi^{(0)} + \lambda^1 \Psi^{(1)} + \lambda^2 \Psi^{(2)} + \lambda^3 \Psi^{(3)} + \dots \quad (2.23)$$

$$E_\lambda = E^{(0)} + \lambda^1 E^{(1)} + \lambda^2 E^{(2)} + \lambda^3 E^{(3)} + \dots \quad (2.24)$$

$$E^{(0)} = \langle \Psi^{(0)} | \hat{H}_0 | \Psi^{(0)} \rangle \quad E^{(1)} = \langle \Psi^{(0)} | \hat{V} | \Psi^{(0)} \rangle \quad E^{(2)} = \langle \Psi^{(0)} | \hat{V} | \Psi^{(1)} \rangle \quad (2.25)$$

Where, $\Psi^{(0)} \equiv \Psi_0$ i.e. the HF wave-function, $E^{(0)} = \sum_{i=1}^N \varepsilon_i$, and ε_i is the one electron orbital energy.

The first-order Møller-Plesset energy can be obtained by summing $E^{(0)}$ and $E^{(1)}$ which is equal to the HF energy. As a consequence, the correlation energy is recovered only starting from truncation after the second-order “MP2”⁽¹⁰¹⁾. More accurate treatments but also more computational demands can be obtained by truncation after the third-order “MP3” or after the fourth-order “MP4”.

2.1.3.2. Coupled Cluster Method

The coupled cluster (CC) method takes into account electron correlation by construction of multi-electron wave-functions using the exponential cluster operator based on the HF wave-function. It provides the exact solution to the time-independent Schrödinger equation. The idea is to include all corrections of a given type to infinite order. The CC wave-function “ Ψ_{CC} ”, the exponential cluster operator “ e^T ”, and the cluster operator “ T ” itself can be expressed as the following

$$\Psi_{CC} = e^T \Psi_0 \quad (2.26)$$

$$e^T = 1 + T + T^2 + T^3 + T^4 + \dots = \sum_{k=0}^{\infty} \frac{1}{k!} T^k \quad (2.27)$$

$$T = T_1 + T_2 + T_3 + T_4 + \dots + T_N \quad (2.28)$$

Acting on the HF reference wave-function, the T_i operator generates all i -th excited SD. Now the exponential cluster operator “ e^T ” can be rewritten as

$$e^T = 1 + T_1 + \left(T_2 + \frac{1}{2} T_1^2 \right) + \left(T_3 + T_1 T_2 + \frac{1}{6} T_1^3 \right) + \dots \quad (2.29)$$

The first and the second terms generate the reference HF wave-function and all singly excited determinants. The first parenthesis generates all doubly excited states including the true doubly excited states by T_2 and product of singly excited states by the product $T_1 T_1$. The second parenthesis generates all triply excited states including the true triply excited states by T_3 , product of singly and doubly excited states by the product $T_1 T_2$, and product of singly excited states by the product $T_1 T_1 T_1$. Generally including only T_1 will not improve over HF. So the lowest level in CC treatment is starting from including the doubly excited state i.e. $T = T_2$ which is referred to coupled cluster doubles (CCD). The most applicable one has arisen from including both single and double excitations i.e. $T = T_1 + T_2$ referring to

coupled cluster singles and doubles (CCSD).⁽⁵⁷⁾Including single, double, and triple excitations which is referred to CCSDT is applicable only for small systems.

2.1.4. Density Functional Theory

Density functional theory (DFT) is an approach including approximately the electron correlation by focusing on the electronic density " $\rho(r)$ " rather than the wave function. The term functional makes a correspondence between a number "E" and the function $\rho(r)$, i.e. $E(\rho)$. For a given system with N electrons and M nuclei, $\hat{H}_{el} = \hat{T} + \hat{V}_{ee} + \hat{V}$ where, $\hat{V} = v(r)$ is the external potential due to M nuclei, \hat{T} and \hat{V}_{ee} are defined explicitly by (2.5). Modern DFT is based on the following two theorems according to Hohenberg and Kohn:⁽¹⁰²⁾1- The ground state density " $\rho(r)$ " determines the ground state wave function " Ψ " and the external potential " $v(r)$ " which indicates that any observable of the static many-particle system is a functional of its $\rho(r)$. The functional $F = \langle \Psi | \hat{T} + \hat{V}_{ee} | \Psi \rangle$ is universal and has no dependence on $\rho(r)$, so F is given for all electronic systems with \hat{V}_{ee} interaction.2- The total energy functional " $E_v(\rho^t)$ " (superscript t means trial density) corresponding to the external potential $v(r)$, is equal to the exact ground state energy " $E_v(\rho)$ " if the ground state density ρ^0 is taken. This is equivalent to the variational principle i.e. $E_v(\rho^t) > E_v(\rho)$ for $\rho^t \neq \rho^0$ where $E_v(\rho^t) = \langle \Psi | \hat{T} + \hat{V}_{ee} + \hat{V} | \Psi \rangle$.

Applying the variational principle, the electronic energy can be expressed as follows

$$E_v(\rho) = \text{Min}_\rho(E_v(\rho^t)) = \text{Min}_\rho \left(F + \int v(r)\rho(r)dr \right) \quad (2.30)$$

Equation (2.30) is exact but F is unknown. The true system can be treated as a non-interacting system ($F=T_s$, which is the Kohn–Sham kinetic energy) with an effective external potential and one can write the following:

$$E_v(\rho) = T_s(\rho) + J(\rho) + E_{xc}(\rho) + \int v(r)\rho(r)dr \quad (2.31)$$

$$J(\rho) = \frac{1}{2} \int \frac{\rho(r)\rho(r_1)}{|r - r_1|} dr_1 dr_2 \quad (2.32)$$

with $E_{xc}(\rho)$ contains the exchange-correlation energy plus a correlation kinetic term. If one suppose that $E_{xc}(\rho)$ is known, the total energy, $E_v(\rho)$, can be minimized with respect to the density ρ , yielding the Kohn-Sham equations that can be solved self-consistently.

$$\varepsilon_i = \left[-\frac{\hbar^2}{2m_i} \nabla^2 + \int \frac{\rho(r_1)}{|r - r_1|} dr_1 + v(r) + v_{XC}(r) \right] \quad (2.33)$$

where,

$$v_{XC}(r) = \frac{\delta E_{XC}(\rho)}{\delta \rho} \quad (2.34)$$

These equations are exact but the exact XC functional of ρ is unknown. The most pragmatic way is to build approximate XC functional of ρ and solve these equations iteratively.

For construction of DFT functionals, different approximations⁽¹⁰²⁻¹⁰⁷⁾ are usually made:

- 1- Both Local density approximation and local spin density approximation depend on the value of the electron density at a certain point only. Moreover, the latter approximation takes into account the spin density.
- 2- Gradient corrected functionals are functionals of both the electron density and its gradient.
- 3- Hybrid exchange functionals combine the correct HF exchange expression with the gradient corrected functional.

Common functionals are a combination of different exchange and correlation functionals. An example is the B3LYP functional (composed of Beck's 1988 exchange functional and Lee-Yang-Parr correlation functional).^(107,108) This functional is combined by three parameters, which are derived by fitting the results of DFT calculations for test systems to experimental data. The B3LYP functional has the mathematical form:⁽¹⁰⁸⁾

$$E_{XC} = a_0 E_X^{HF} + (1 - a_0) E_X^{LDA} + a_x \delta E_X^B + (1 - a_c) E_C^{VWN} + a_c \delta E_C^{LYP} \quad (2.35)$$

The exchange-correlation terms are parameterized by a_0 , a_x and a_c with fixed values of 0.20, 0.72 and 0.81 respectively. These values are derived from fitting thermodynamic and spectroscopic properties of various systems.

Empirical Damped Dispersion Correction

Empirical damped dispersion correction is particularly important when the long-range correlation effects become dominant. This dispersion correction energy can be added to the DFT energy as follows:

$$E_{DFT-D} = E_{DFT} + E_{disp} \quad (2.36)$$

For DFT-D2⁽⁵⁸⁾ the dispersion interaction " E_{disp} " is calculated as follow:

$$E_{disp} = -S_6 \sum_{i,j < i}^N f_{damp}(R_{ij}) \frac{C_6^{ij}}{R_{ij}^6} \quad (2.37)$$

where, N is total number of atoms, R_{ij} is the interatomic distance of atoms i and j , S_6 is a global scaling parameter depending on the choice of the functional used and the C_6^{ij} value are calculated from atomic dispersion coefficients C_6^i and C_6^j in the following way:

$$C_6^{ij} = \sqrt{C_6^i C_6^j} \quad (2.38)$$

The function f_{damp} damps the dispersion correction for shorter inter-atomic distances and is given by:

$$f_{damp}(R_{ij}) = \frac{1}{1 + \exp(-\alpha (R_{ij}/(R_{vdW}^i + R_{vdW}^j) - 1))} \quad (2.39)$$

where, R_{vdW}^i and R_{vdW}^j are the van-der-Waals radius for atom i and j , respectively, and α is a parameter that is usually set to 23 or 20.^(59,109)

For DFT-D3,⁽⁵⁸⁾ E_{disp} is the sum of the two- and three-body contributions to the dispersion energy.

$$E_{disp} = E^{(2)} + E^{(3)} \quad (2.40)$$

$$E^{(2)} = \frac{1}{2} \sum_{i \neq j} \sum_{n=6,8} S_n \frac{C_n^{ij}}{R_{ij}^n} f_{damp,n}(R_{ij}) \quad (2.41)$$

$$E^{(3)} = \frac{C_9^{ijk} (3 \cos \theta_a \cos \theta_b \cos \theta_c)}{(R_{ij} R_{jk} R_{ki})^3} f_{damp}(R_{ij}) \quad (2.42)$$

$$C_9^{ijk} \approx -\sqrt{C_6^{ij} C_6^{jk} C_6^{ki}} \quad (2.43)$$

where, θ_a , θ_b , and θ_c are the internal angles of the triangle formed by R_{ij} , R_{jk} , and R_{ki} .

2.2. Solvation Effect

Solvation of the molecular system can be introduced implicitly or explicitly. Implicit incorporation of the solvent can be studied by the continuum solvation models such as the conductor-like screening model. Explicit studies for the solvent effect can be introduced by immersing the molecular system in a solvent box and treating them by means of a force field.

2.2.1. Conductor-Like Screening Model

The conductor-like screening model (COSMO) is a continuum solvation model (CSM), where the solute molecule forms a cavity within the dielectric continuum of permittivity ϵ that represents the solvent.⁽¹¹⁰⁾ The charge distribution of the solute polarizes the dielectric medium. The response of the medium is described by the generation of screening charges on the cavity surface. COSMO is using simple boundary condition of vanishing electrostatic potential for a conductor with ideal solvent has $\epsilon = \infty$, i.e.

$$\Phi^{\text{tot}} = \Phi^{\text{sol}} + \mathbf{A}\mathbf{q} = 0 \quad (2.44)$$

where, Φ^{tot} , and Φ^{sol} are the total and the solute electrostatic potentials respectively, \mathbf{A} is the Coulomb matrix of the screening charge interactions, and \mathbf{q} is the vector of the screening charges.

The total free energy of the solvated molecule “ E ” is equal to the sum of the energy of the isolated system which calculated with the solvated wave function “ $E(\Psi^{\text{solv}})$ ” and the dielectric energy “ E_{diel} ” which is half of the solute-solvent interaction energy, i.e.

$$E = E(\Psi^{\text{solv}}) + E_{\text{diel}} = E(\Psi^{\text{solv}}) + \frac{1}{2} \frac{\epsilon - 1}{\epsilon + \frac{1}{2}} \mathbf{q}\Phi^{\text{sol}} \quad (2.45)$$

2.2.2. Force Field Molecular Dynamics Simulations

The classical equations of motion for N atoms (nuclei) can be formulated according to Newton’s equations of motion as follows:

$$\frac{dv_i(t)}{dt} = \frac{f_i(t)}{m_i} \quad \& f_i(t) = -\frac{\partial}{\partial r_i} V(r_1, r_2, r_3, \dots, r_N) \quad (2.46)$$

where, m_i , r_i , and v_i are mass, coordinates, and velocity of atom i , respectively, f_i is the force on atom i , V is the potential energy or the interaction function, and t is the time. The Hamiltonian of a molecular system “ $H(\mathbf{p}, \mathbf{r}; m, s)$ ” has the form

$$H(\mathbf{p}, \mathbf{r}; m, s) = T(\mathbf{p}; m) + V(\mathbf{r}; s) \quad (2.47)$$

where, $T(\mathbf{p}; m)$ and $V(\mathbf{r}; s)$ are kinetic energy of the system and the atomic interaction function, respectively, \mathbf{p} and m are the momentum and mass of particles, and s is force field parameters.

$$T(\mathbf{p}; m) = \sum_{i=1}^N \frac{\mathbf{p}_i^2}{2m_i} = \sum_{i=1}^N \frac{1}{2} m_i v_i^2 \quad (2.48)$$

In the current study, the interaction function of the GROMOS force field is used which is expressed as follows:⁽¹¹¹⁾

$$\begin{aligned}
 V(\mathbf{r}; \mathbf{s}) = & \sum_{n=1}^{N_b} \frac{1}{4} K_{b_n} (b_n^2 - b_{0_n}^2)^2 + \sum_{n=1}^{N_\theta} \frac{1}{2} K_{\theta_n} (\cos\theta_n - \cos\theta_{0_n})^2 + \sum_{n=1}^{N_\xi} \frac{1}{2} K_{\xi_n} (\xi_n - \xi_{0_n})^2 \\
 & + \sum_{n=1}^{N_\phi} K_{\phi_n} (1 + \cos(\delta_n) \cos(m_n \phi_n)) + \sum_{\text{pairs } i,j} \left[\frac{C_{12}(i,j)}{r_{ij}^{12}} - \frac{C_6(i,j)}{r_{ij}^6} \right] \\
 & + \sum_{\text{pairs } i,j} \frac{q_i q_j}{4\pi\epsilon_0\epsilon_1} \left[\frac{1}{r_{ij}} - \frac{C_{rf} r_{ij}^2}{2R_{rf}^3} - \frac{1 - \frac{1}{2}C_{rf}}{R_{rf}} \right] \quad (2.49)
 \end{aligned}$$

The first four terms represent the bond-stretching, bond angle, improper dihedral angle, and proper dihedral angle interactions, respectively while the last two terms represent the Lennard-Jones and electrostatic interaction, respectively. The sums run over all bonds N_b , bond angles N_θ , improper and proper dihedral angles N_ξ and N , and non-bonded atom pairs. K_{b_n} , K_{θ_n} , K_{ξ_n} , and K_n are the force constants for a covalent bond, bond angle, improper and proper dihedral angles, respectively. The actual and equilibrium values for bond distances, bond angles, and improper dihedral angles are b_n and b_{0_n} , θ_n and θ_{0_n} , and ξ_n and ξ_{0_n} , respectively. Values of δ_n and m_n are restricted to 0 or π , and 1, 2, 3, 4, 5, or 6 respectively.⁽¹¹¹⁾ The parameters C_6 and C_{12} depend on the type of atoms i and j , r_{ij} is the distance between the atoms i and j , q_i and q_j are the partial charges of atoms i , and j , ϵ_0 and ϵ_1 are the dielectric permittivity of the vacuum and the relative permittivity of the medium, C_{rf} is the medium reaction-field constant, and R_{rf} is a cutoff distance.

2.3. Quantitative Structure–Activity Relationship

Quantitative structure–activity relationship (QSAR) is a regression method used in different branches of science such as chemistry, biology, etc. QSAR aims to find a relationship between some molecular descriptors of interested compounds and their biological activity or chemical property.⁽⁹⁴⁾ These descriptors consist of physicochemical properties or theoretical molecular parameters. In general, QSAR can be expressed mathematically by a linear equation as follow:

$$\text{Activity} = C_0 + C_1P_1 + C_2P_2 + C_3P_3 + C_4P_4 + \dots \quad (2.50)$$

Wehre P_1, P_2, \dots are the molecular descriptors; and C_0, C_1, \dots are coefficients which can be determined using multiple-linear regression.

Multiple-linear regression attempts to model the relationship between two or more variables (in our case are “descriptors”) and response variable (in our case is “activity”). Some important parameters for description of the regression model are written down.

$$SSE = \sum_i^n (y_i - \hat{y}_i)^2 \quad \& \quad MSE = \frac{SSE}{n - p - 1} \quad (2.51)$$

$$SSR = \sum_i^n (\hat{y}_i - \bar{y})^2 \quad \& \quad MSR = \frac{SSR}{p} \quad (2.52)$$

$$SST = \sum_i^n (y_i - \bar{y})^2 \quad \& \quad MST = \frac{SST}{n - 1} \quad (2.53)$$

$$R^2 = \frac{SSR}{SST} \quad \& \quad \text{adjusted } R^2 = 1 - \frac{MSE}{MST} \quad (2.54)$$

$$F_{\text{statistic}} = \frac{MSR}{MSE} \quad (2.55)$$

Where y_i : the dependent observable variables, \bar{y} : mean of the dependent observable variables, \hat{y}_i : the estimated value of the dependent observable variables obtained from the fitting, n : number of dependent observable variables, p : number of the independent variables, SSE : sum of squares due to the error, SSR : sum of squares due to the regression, SST : sum of total squares, MSE : mean of squares due to the error, MSR : mean of squares due to the regression, MST : mean of total squares, R^2 and adjusted R^2 are proportional to the total variation in y , and $F_{\text{statistic}}$: measures significance of the model describing the data.

3. MATERIALS AND METHODS

This chapter is organized to include details about soil site and sampling (3.1), systematic modification of the soil organic matter (3.2), analytical methods (3.3), hexachlorobenzene (3.4), adsorption kinetics of HCB on original soil sample (3.5), adsorption isotherms of HCB on soil samples (3.6), and finally SOM modelling and quantum chemical calculations (3.7). In section 3.2, hot water extraction (3.2.1) and off-line pyrolysis of soil sample (3.2.2) are introduced. C, N, S elemental analysis (3.3.1), Py-FIMS (3.3.2), and C and N K-edge XANES (3.3.3) are represented in section 3.3.

3.1. Soil Site and Sampling

The soil was sampled from an unfertilized rye plot of the long-term Eternal Rye Cultivation experiment at Halle (Saale), Germany in 2002. This experiment had been established in 1878 by J. Kühn.⁽¹¹²⁾ It is the world's second oldest long-term fertilization trial and its objective is to investigate the effects of long-term organic and mineral fertilizations on crop yields and soil fertility as a number of studies reported.⁽¹¹³⁻¹¹⁵⁾ The long-term impacts of fertilization and rotation (rye, maize, and potato) on yields and SOM contents after 120 years have been published previously.⁽¹¹⁶⁾ Differences in SOM composition have been examined by means of modern methods of pyrolysis.⁽¹¹⁷⁾

Representative samples of the Ap horizon (0–20 cm depth) were taken using a soil corer. These samples were air dried and sieved (<2 mm). On average they contain about 10% clay, 18% silt and 72% sand (texture sandy loam). The clay fraction contains dioctaedric three-layer-silicates such as illite (39%), illitic mixed layer minerals (17%) and smectite (10%), quartz (14%), feldspars (5%), kaolinite (4%) and chlorite (2%). The fine silt fraction contains less dioctaedric three-layer-silicates (43%) and kaolinite (1%) but more quartz (40%), feldspars (11%) and chlorite (5%).⁽¹¹⁸⁾ Major inorganic elements are Al (8.05 g kg⁻¹), Ca (2.44 g kg⁻¹), Fe (12.00 g kg⁻¹), K (0.90 g kg⁻¹), Mg (1.39 g kg⁻¹), Mn (0.32 g kg⁻¹), Na (0.24 g kg⁻¹), and P (0.31 g kg⁻¹). Also concentrations of the active pedogenic oxides for Al, Fe, Mn, and P in the soil sample are 0.73, 1.60, 0.24, and 0.20 g kg⁻¹ soil, respectively. The pH value is 5.3 and the cation exchange capacity is 10 cmol₍₊₎kg⁻¹.

3.2. Systematic Modification of the Soil Organic Matter

SOM modification is aiming to produce soil samples with same mineralogy and different SOM composition. Such differences in the chemical composition of SOM will have a

significant effect on binding of HCB to SOM. Thus, this will be helpful for explanation and understanding adsorption of HCB on the soil based on the different functional groups as well as the building blocks of SOM.

In the original soil sample, the SOM composition was changed systematically in two ways. First, by removal and addition of hot-water extract (HWE), that contains mostly polar functional groups, from/to the original soil to decrease/increase the polar character of the SOM in the sample. The carbohydrates, N-containing compounds including peptides and thus polar functional groups can be extracted from the soil by hot-water.^(32,119,120) The second way was to pyrolyze the original soil to decrease the polar character of SOM. This type of modification generally increases the proportions of unsaturated C, substituted aromatic C, and N in nitriles and/or N in aromatic compounds.⁽¹²¹⁾ These two contrasting treatments, HWE removal and addition, and thermal heating may result in SOM modification that is comparable to natural processes such as additions of rhizodeposits or dissolved organic matter from plants and manure⁽¹²²⁾ and prescribed burning of vegetation residues or wildfires⁽¹²³⁾ in the environment.

3.2.1. Hot Water Extraction

A sample of 15 g dry original soil was boiled in 45 ml of de-ionized water for 60 min followed by centrifugation for 20 min at 3500 ×g. The supernatant was filtrated (Whatman no. 1442 110) to separate the dissolved HWE from specific light particulate organic matter. This was added to the precipitated solid material, and the residue of the extraction was used in further experiments and was termed as 'soil residue'. The original soil was modified by adding HWE in the following proportions: an extract of 45 g soil was added to 15 g original soil to get soil:HWE in a ratio 1:3 (soil+3 HWE). Similarly, an extract of 90 g soil was added to 15 g of original soil to get soil: HWE in a ratio 1:6 (soil+6 HWE). After addition of the HWE to the original soil sample, the mixtures were freeze-dried in beakers closed by a permeable tissue. Then they were finely ground to obtain as homogenous samples as possible for further analyses.



Figure 7. Scheme is showing how remove/addition HWE from/to original soil was performed.

3.2.2. Off-Line Pyrolysis

About 4 g of the original soil sample was heated in a specifically designed oven (Wösthoff, Bochum, Germany) at 600 °C under nitrogen flow for 60 min, and then allowed to cool down to room temperature in the presence of nitrogen flow to prevent SOM oxidation.

3.3. Analytical Methods

3.3.1. C, N, S Elemental Analysis

Total nitrogen (N_t), total carbon (C_t), and total sulfur (S_t) contents for all soil samples as well as the HWE were determined by dry combustion using a Vario EL C/N/S-analyzer (Elementar, Hanau, Germany). Three replicates were measured and the mean standard errors were 0.38 g kg⁻¹ for C_t , 0.01 g kg⁻¹ for N_t and 0.06 g kg⁻¹ for S_t .

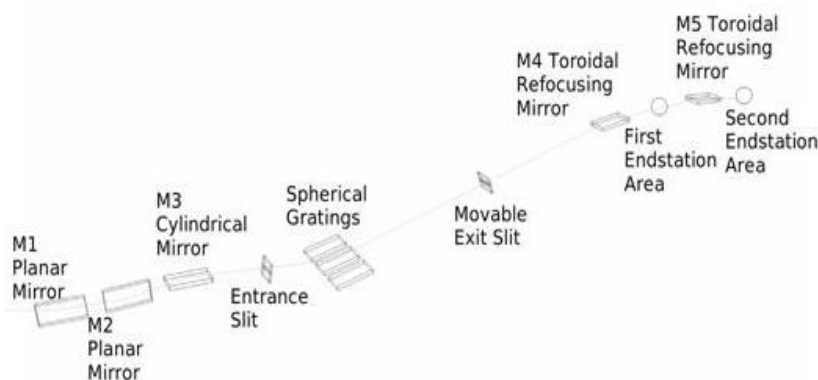
3.3.2. Pyrolysis-Field Ionization Mass Spectrometry (Py-FIMS)

For Py-FIMS, about 5 mg of each sample (except for HWE only about 100 µg) was thermally degraded in the ion source of a modified Finnigan MAT 95 high-performance mass spectrometer. The samples were heated under a high vacuum from 110 to 700 °C at heating rate of 20 K min⁻¹ (three replicates). After about 20 min of total registration time, about 60 magnetic scans were recorded for the mass range of 55 to 500 a.u. (single spectra). The single-scan spectra were integrated in time and the different scans were added to obtain one summed spectrum. In general, the summed spectra of three replicates were averaged to give the final survey spectrum. These survey spectra, in particular the assignment of marker signals to chemical compounds, were interpreted as described by Schulten and Leinweber.⁽¹²⁴⁾ These are carbohydrates with pentose and hexose subunits (CHYDR), phenols and lignin monomers (PHLM), lignin dimers (LDIM), lipids, alkanes, alkenes, bound fatty acids, and alkyl monoesters (LIPID), alkyl aromatics (ALKY), non-peptidic (e.g., nitriles, N-heterocyclic compounds) N-containing compounds (referred to as N-containing compounds) (NCOMP), sterols (STEROL), peptides (PEPTI), suberin (SUBER), and free fatty acids (FATTY). Besides the series of marker signals, the volatilization temperature was also considered for identification. For each of the 60 single scans, the ion intensities of these marker signals were calculated. The average ion intensities for each compound class were plotted against the pyrolysis temperature, giving characteristic thermograms. All samples were weighted before and after Py-FIMS to normalize ion intensities per milligram of sample. Detailed descriptions of the Py-FIMS methodology⁽¹²⁵⁾ and statistical evaluations of

sample weight and residue, volatilized matter, and total ion intensities were given by Sorge et al.⁽²⁵⁾

3.3.3. Carbon and Nitrogen K-edge XANES

A piece of silicon wafer with the rough side exposed was attached to a stainless steel holder by double-sided carbon tape. Afterwards, a gold surface was deposited onto the prepared holder. The samples were deposited onto the coated wafer by drop coating. A small amount of finely ground, air-dried samples was mixed with ultrapure water. This suspension was pipetted onto the wafer and the water was allowed to evaporate in a desiccator. Carbon and nitrogen K-edge XANES spectra were collected at the high resolution spherical grating monochromator (SGM) beam line of the Canadian light source synchrotron, Saskatoon, Canada. The C-XANES spectra were energy calibrated using the $1s \rightarrow \pi^* C=O$ transition of glutaric acid at 288.6 eV.⁽¹²⁶⁾ Carbon features were assigned based on a review of the literature.^(40,127-129) The N-XANES spectra were energy calibrated using the $1s \rightarrow \pi^*$ vibrational manifold of N_2 gas at 400.8 eV evolved from $(NH_4)_2SO_4$.⁽¹³⁰⁾ Nitrogen spectral features were assigned based on a wide range of reference compounds published by Leinweber et al.⁽⁴¹⁾ Spectra were recorded in total fluorescence yield mode using a two-stage multichannel plated detector. All N-XANES spectra were normalized to the intensity of the incident beam, which measured simultaneously as the current emitted from a freshly sputtered gold mesh. To correct C-XANES spectra for inevitable steady signals of C contaminants a background signal was scaled linearly and then subtracted from the spectra to yield a flat pre-edge region. Afterwards, the spectra were normalized to the intensity of the incident beam. For all samples up to five scans were recorded and the beam was



moved to a "fresh" sample spot after each scan. Spectra of individual scans were averaged and then background corrected by subtracting a linear regression fit through the pre-

edgeregionfromthewhole spectrum,andthen normalizedtothemeanofthelast20data points.

Figure 8. The optical layout of the Canadian spherical grating monochromator beam line.⁽¹³²⁾

3.4. Hexachlorobenzene

The used POP in this study is named as hexachlorobenzene (HCB), or perchlorobenzene. It was introduced for the first time in 1945 as a fungicide for seed treatment, especially for control of bunt of wheat. HCB is also a by-product of the manufacturing of industrial chemicals including carbon tetrachloride, perchlorethylene, trichloroethylene and pentachlorobenzene. HCB is an animal carcinogen and is considered to be a probable human carcinogen. It has been banned globally under the Stockholm convention on persistent organic pollutants.⁽¹³¹⁾

HCB is a white crystalline solid with molecular formula C_6Cl_6 , and negligible solubility in water (around 0.005 ppm at 25 °C) and variable solubility in different organic solvents. It is soluble in hot benzene, chloroform, ether, and *n*-hexane. Its vapour pressure is 1.09×10^{-5} mmHg at 20 °C. Its flash point is 242 °C and it sublimes at 322 °C.

A stock solution of 100 mg/l HCB (CAS number 118-74-1, Sigma-Aldrich) was prepared in *n*-hexane.



Figure 9. The chemical as well as the three-dimensional structure of HCB.

3.5. Adsorption Kinetics of HCB

One gram of air-dried original soil sample was mixed with 30 ml of 10.0 mg/l HCB (prepared in 0.01 M $CaCl_2$ solution) in 50 ml Teflon centrifugal tubes. To this suspension

100 μl NaN_3 (100 mg/l) was added to suppress the microbial activity. The suspension was shaken at 22 revolutions per minute using a special overhead rotator (GFL overhead rotator 3040). At different times (1, 4, 8, 24, 48, 72, 120, and 168 h), the suspension was centrifuged for 20 min at 3500 g. Samples of HCB (50 μl of *n*-hexane layer) were withdrawn. Concentrations of these HCB withdrawn samples were determined by using a G1530A (Agilent Technologies, Santa Clara, USA) gas chromatograph (GC) with two parallel capillary columns with different polarities, each equipped with an electron capture detector (ECD), i.e. GC-ECD. The separation was performed by a 60 m Varian FactorFour capillary column VF-5ms (5% phenylmethyl- and 95% dimethylpolysiloxane) with an inner diameter of 0.25 mm and a film thickness of 0.25 μm and by a J & W capillary column DB-1701P (14% cyanopropylphenyl- and 86% dimethylpolysiloxane) with 60 m length, 0.25 μm film thickness and an inner diameter of 0.25 mm.

3.6. Adsorption Isotherms of HCB

One gram of each air-dried soil sample (original soil, soil+3 HWE, soil+6 HWE, and pyrolyzed soil samples) was mixed in Teflon tubes with 30 ml of HCB (prepared in 0.01 M CaCl_2 solution) at different initial concentrations (0.25, 0.50, 0.75, 1.00, 2.00, 3.00, 4.00, 5.00 mg/l). To each suspension, a 100 μl NaN_3 (100 mg/l) was added. The suspensions were shaken at 22 r/min for 24 hours and centrifuged for 20 min at 3500 g. For HCB analysis, 50 μl of *n*-hexane layer was sampled from each tube. For each soil sample, two blank measurements (one of them is without soil sample and the other is without HCB) were also processed at the same time. These adsorption experiments for the different HCB concentrations as well as the blank measurements were performed in duplicates. In a split less mode, 1 μl of HCB sample was injected to GC-ECD. HCB concentrations were determined by comparison of the peak height of the analyte with that of HCB standards.

The adsorption isotherms were fitted using the Freundlich equation,

$$X = K_F C_{eq}^n \quad (3.1)$$

where, X is amount of adsorbed HCB on the soil sample (given either in $\mu\text{g/g}$ soil or in $\mu\text{g/g}$ total carbon, C_{tot}), K_F is Freundlich unit capacity factor, n is Freundlich exponent, and C_{eq} is the HCB equilibrium concentration in mg/l. Notice that this model assumes that the adsorption enthalpy depends on the amount of adsorbed HCB. In the limit of small X where

the adsorption enthalpy should not depend on X one could describe the isotherm by a Langmuir equation as well, i.e.

$$X = X_{max} \frac{K_L C_{eq}}{1 + K_L C_{eq}} \quad (3.2)$$

where X_{max} is the maximum amount of adsorbed HCB on the soil samples which is required to have a complete saturation of all binding sites and K_L is the equilibrium Langmuir constant.

3.7. Soil Organic Matter Modelling and Quantum Chemical Calculations

To reduce the problems arising from polymer-like modelling of SOM or modelling of SOM by few numbers of functional groups, we developed a new approach for SOM modelling. We modelled the SOM by separate representative systems covering almost all functional groups as well as analytically determined compound classes of SOM which appears most promising. Development of a SOM model for studying HCB-SOM-interaction has been based on detailed elemental analyses by Py-FIMS and XANES at the C- and N-edges.^(31,82) Hence, in the test set of representative SOM compound classes and functional groups (Figure 10) PHLM is modeled by phenol, catechol, and 3,4,5-trimethoxy cinnamic acid (lignin monomer). ALKY is modelled by benzene, methylbenzene, and ethylbenzene. Moreover bicyclic aromatic compounds, like naphthalene and ethylnaphthalene, are added to study effect of increasing number of aromatic rings. CHYDR is represented by the most abundant monomer glucose in the open and cyclic forms. PEPTI is modelled by the main abundant monomer glycine and hexa-glycine. NCOMP is represented by ethylnitrile, and five- and six-membered heterocyclic compounds pyrrole and pyridine. The acetic acid is modelled as carboxylic acid representing free fatty acids. LIPID, alkane, alkene compounds are represented by short chain alkane (*n*-butane) and conjugated alkene (1,3-butadiene), and long chain alkane (*n*-decane) and conjugated alkene (1,3,5,7,9-decapentaene). Effects of sterols enter into the model via the hydroxyl group in methanol, and short/long alkanes and alkenes. Moreover, based on the functional groups analysis by XANES we were added to our model set carbonyl in acetamide, acetaldehyde, dimethylketone, and methylacetate, amine like methylamine, protonated methylamine, and aniline, and quinone. In addition, coronene and silicon hydroxide trimer were added to study the effect of pyrolysis products on binding of HCB to the soil.

Initial geometries of complexes of these test set compounds with HCB are constructed by selecting the expected preferential binding situations for each complex. Full geometry optimization⁽¹³³⁾ has been performed for all individual species and their complexes by using HF, DFT (both BLYP and B3LYP) with and without dispersion correction with 6-31G, 6-31++G, and 6-311++G(d,p) basis sets. For complexes with HCB, in case geometry optimization gave more than one configuration, these are explicitly treated and the most stable one selected. An exception is the HCB-glycine complex, which has two equivalent configurations.

The binding energies of HCB to the test set compounds in these complexes were calculated as the difference between the total energies of the complexes and the individual molecules.

$$E_{B_i} = E_{HCB-i \text{ complex}} - (E_{HCB} + E_i) \quad (3.3)$$

where, E_{B_i} is the binding energy of HCB to the compound i , $E_{HCB-i \text{ complex}}$ is the energy of the complex of HCB with the compound i , E_{HCB} is energy of HCB, and E_i is energy of the test set compound i .

After obtaining the favorable optimized structures, single point calculations have been performed for all individual species and complexes to check effect of dispersion correction, basis sets, DFT-functionals, and different theoretical methods on binding of HCB within these complexes. Effect of including dispersion correction has been studied using HF, B3LYP without and with dispersion corrections at different basis sets. Hence, we have used two types of empirical dispersion correction (D2 and D3) that introduced by Grimme and coworkers. Effect of different basis sets such as 6-31G, 6-31++G, 6-311++G(d,p), 6-311++G(2d,2p), and aug-cc-pvdz as well as effect of different DFT-functionals such as the Becke, Lee-Yang-Parr hybrid functional (BLYP), Becke, three-parameter, Lee-Yang-Parr hybrid functional (B3LYP), B3LYP5, and Handy and coworkers' long range corrected version of B3LYP (CAM-B3LYP) been explored. All the above quantum mechanical calculations have been performed using both Terachem program packages.⁽¹³⁴⁾

Moreover, benchmark calculations using standard methods such as MP2 and CCSD have been performed at aug-cc-pvdz basis set to check ability of DFT in description this interaction type. Both MP2 and DFT including dispersion corrections (DFT-D) calculations

have been corrected from the basis set superposition error (BSSE)⁽¹⁵⁹⁾ by counterpoise correction.⁽¹⁶⁰⁾ Effects of the BSSE have been neglected in case of DFT-D due to the binding energies in case of the uncorrected DFT-D from BSSE are closer to those obtained by corrected MP2 than those in case of the corrected DFT-D from BSSE. Solvation by water has been included within the conductor-like screening model (COSMO).⁽¹¹⁰⁾ Based on the optimized geometries in the gas phase, full geometry optimization has been performed using B3LYP-D3 under effect of solvation via COSMO model. Then the binding free energies of all complexes of the test set compounds were calculated. These quantum mechanical calculations have been performed using Turbomole program packages.⁽¹³⁵⁾

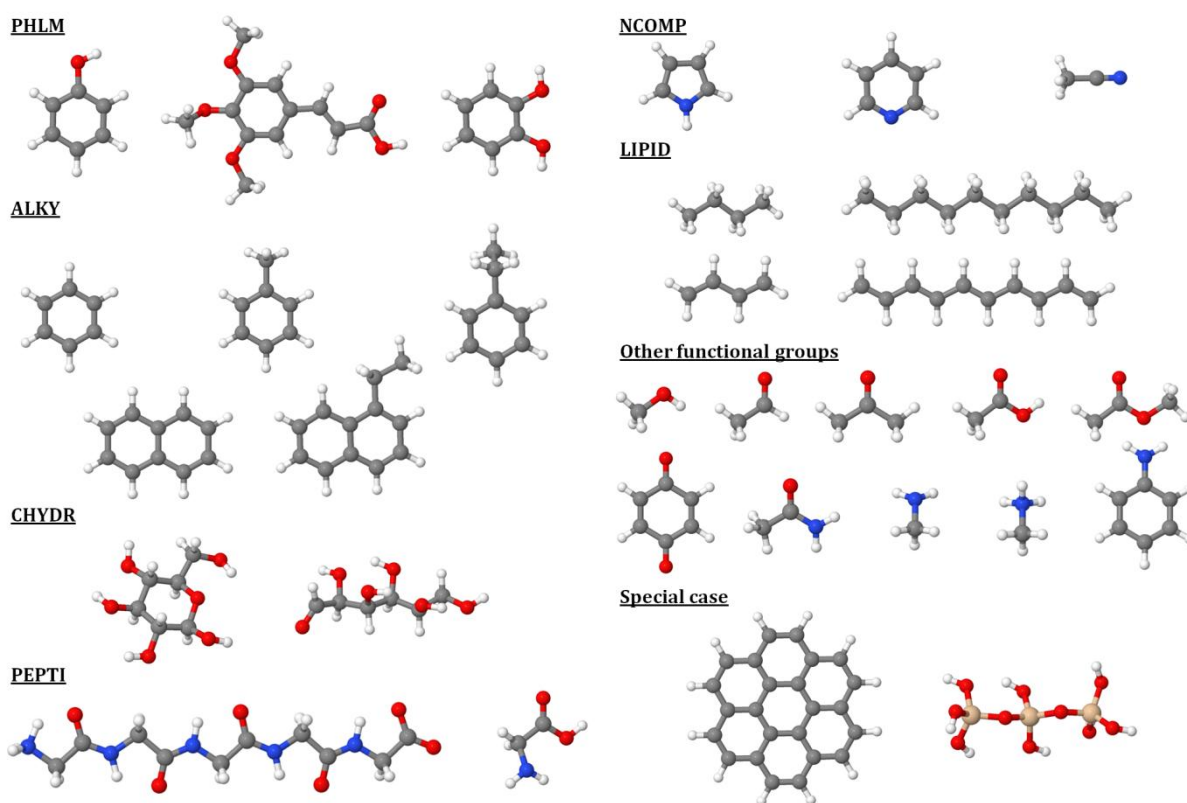


Figure 10. The developed test set for studying the interaction of HCB with different SOM functional groups including PHLM, ALKY, CHYDR, PEPTI, NCOMP, LIPID, O- and N-functional groups, and special cases such coronene, and silicon hydroxide.

3.8. Molecular Dynamics Simulations

To check ability of the force-field approach to describe HCB interactions with the modeled SOM systems, single point calculations have been performed based on the optimized geometries obtained at B3LYP-D3/6-311++G(d,p). Additionally, molecular dynamics (MD) simulations have been done for some of HCB-SOM complexes. Each HCB-SOM complex is inserted into cubic box containing 900 equilibrated water molecules. Then

equilibration of the HCB-SOM complex inside this water box has been taken place. These water molecules are introduced by the simple point charge (SPC) model, in which the water molecule has three centers of concentrated charge. After the equilibration, the MD simulations have been taken place using a canonical ensemble (NVT ensemble) where the temperature and the box volume along the trajectory are fixed at 300 K and 27000 Å³, respectively. The MD simulations are run for 100 ps with a 0.2 fs time step. The binding energies between HCB and SOM systems have been calculated using the Van der Waals interaction as well as electrostatic interaction between HCB and each SOM system. The Van der Waals interaction is given by Lennard-Jones interaction which is introduced as the fifth term in equation (2.49). The electrostatic interaction is represented by three contributions including, coulomb interaction, Poisson-Boltzmann reaction field interaction, and distance-independent reaction field interaction. Total binding energy between HCB and each SOM representative system is calculated as sum of all these interactions. These single point calculations as well as MD simulations have been performed using the GROMOS96 package⁽¹³⁶⁾ and the GROMOS force-field parameters 53A6.⁽¹¹¹⁾

3.9. Quantitative Structure-Activity Relationship

Moreover, QSAR analysis has been done to correlate the binding energy (E_B) of HCB to SOM representative systems with the appropriate physical parameters governing this interaction. In this correlation, the binding energies are those including the solvation energy using COSMO model as well as obtained from MD simulations. Isotropic polarizability (P_1), quadrupole moment (P_2), sum of C atoms charges (P_3), sum of N atoms charges (P_4), molecular-mass (P_5), and molar volume (P_6) of the representative systems are introduced as descriptors. These physical properties are correlated to the binding energies via the following equation.

$$E_B = C_0 + C_1P_1 + C_2P_2 + C_3P_3 + C_4P_4 + C_5P_5 + C_6P_6 \quad (3.4)$$

The coefficients C_0 , C_1 , C_2 , C_3 , C_4 , C_5 , and C_6 are determined by multiple-linear regression.

4. EXPERIMENTAL RESULTS AND DISCUSSION

4.1. General Characterization of Samples

The C_t , N_t and S_t concentrations in Table 1 show that the content of organic compounds increases in the order: pyrolyzed soil < soil residue < original soil < soil+3 HWE < soil+6 HWE < HWE. The C_t/N_t ratios are around 13.4 for all soil samples. For HWE, the C_t/N_t ratio is 10.0 which can be explained by large proportions of N-containing compounds most likely amino acids and peptides in the HWE.⁽¹¹⁹⁾ The losses in C_t and N_t concentrations in cases of the pyrolyzed soil sample and the soil residue sample, and the gains in C_t and N_t concentrations, in cases of the soil+3 HWE and soil+6 HWE samples with respect to the original soil sample are calculated from the data in Table 1. The loss in the pyrolyzed soil sample is 24.1% for C_t and 25.0% for N_t . This means that the off-line pyrolysis at 600 °C produced a soil sample that had lost 25% of the organic matter compared to the original soil sample. For the soil residue sample, the losses in C_t and N_t are not significant compared to C_t and N_t of the original soil sample. The addition of 3 HWE to the original soil increases C_t by 3.2%, and N_t by 5.0% of the corresponding values in the original soil. The addition of 6 HWE to the original soil increases C_t by 13.7% of the original soil C_t , and N_t by 12.5% of the original soil N_t . Comparing the gains in C_t and N_t concentrations in the case of addition of 3 HWE and 6 HWE with the original soil sample, the heterogeneity of the chemical composition in the soil becomes very clear. Comparing the loss in the case of the pyrolyzed soil sample with the loss in the case of the soil residue sample or/and the gain in the case of the addition of HWE indicates that the modification by pyrolysis is stronger than that achieved by the remove/addition of HWE. The S_t concentration remains almost constant for all samples except HWE.

Table 1. Concentrations of total carbon (C_t), nitrogen (N_t), sulfur (S_t) and the C_t/N_t ratio for the samples pyrolyzed soil, soil residue, original soil, soil+3 HWE, soil+6 HWE, and HWE.

sample	C_t	N_t	S_t	C_t/N_t
	$g\ kg^{-1}$			
pyrolyzed soil	8.13	0.60	0.30	13.55
soil residue	10.52	0.78	0.29	13.49
original soil	10.71	0.80	0.30	13.39
soil+3 HWE	11.05	0.84	0.35	13.15
soil+6 HWE	12.18	0.90	0.40	13.53
HWE	158.92	15.90	7.34	10.00

In order to test whether removal/addition of HWE from/to soil resulted in a dominant change of the SOM composition only, without influencing the mineralogy, the major

elements were determined. Concentrations of these major elements were measured for both the original soil and HWE using the inductively coupled plasma atomic emission spectroscopy (ICP-AES). Table 2 shows that about 9.02% Al, 13.35% Fe, 75.20% Mn, and 64.74% P of the total concentrations of these elements were extracted by oxalate and, thus, bound in low crystalline, “active” pedogenic oxides. Furthermore, the HWE contains 0.005 g kg⁻¹ Al, 0.018 g kg⁻¹ Ca, 0.003 g kg⁻¹ Fe, 0.007 g kg⁻¹ K, 0.004 g kg⁻¹ Mg, 0.0002 g kg⁻¹ Mn, 0.014 g kg⁻¹ Na, and 0.002 g kg⁻¹ P (these concentrations are in g kg⁻¹ soil). These concentrations are equivalent to 0.06% Al, 0.74% Ca, 0.02% Fe, 0.83% K, 0.25% Mg, 0.06% Mn, 5.62% Na, 0.64% P of the total elements concentrations, and 0.69% Al, 0.19% Fe, 0.08% Mn, and 1.00% P of the “active” pedogenic oxides. This indicates that the mineral matrix of soil was not significantly affected by the HWE extraction. Thus, we have obtained soil samples with similar mineralogy but significant differences in the SOM content and polarity.

Table 2. Concentrations of total Al, Ca, Fe, K, Mg, Mn, Na, and P in both original soil and HWE samples in addition to concentrations of the pedogenic oxides in the original soil sample.

	Al	Ca	Fe	K	Mg	Mn	Na	P
	g kg ⁻¹ soil							
original soil	8.05	2.44	12.00	0.90	1.39	0.32	0.24	0.31
HWE	0.005	0.018	0.003	0.007	0.004	0.0002	0.014	0.002
pedogenic oxides	0.73	-----	1.60	----	-----	0.24	-----	0.20

4.2. Pyrolysis-Field Ionization Mass Spectrometry

Figure 11 shows the Py-FIMS thermograms as well as the spectra of the samples ordered by decreasing organic matter content, which is reflected by a decrease of the total ion intensity (TII) in the thermograms (inserts). The thermogram for the freeze-dried HWE (a) shows two peaks and one shoulder. The first peak has a maximum at about 180 °C, while the second one has a maximum at about 350 °C and a shoulder at 450 °C. Further, this thermogram shows high ion intensities, which reflect a high amount of SOM in the sample as already confirmed by the C_t and N_t concentrations. The thermograms of the soil+6 HWE (b), soil+3 HWE (c) as well as the original soil (d) and the soil residue (e) look quite similar with no volatilization below 250 °C and only one peak with a maximum temperature at about 450 °C. Small differences are observed between these thermograms. The peak heights in the thermograms follow the order: soil+6 HWE > soil+3 HWE > original soil > soil residue samples. Also we can see that there is still a small volatilization above 600 °C in case of the soil+6 HWE and the soil+3 HWE, in contrast to the original soil and soil residue. The

fact that the thermograms of the soil+6 HWE (b) and the soil+3 HWE (c) have no maximum at 200 °C strongly indicates a stabilization of the labile compounds by adsorption and, moreover, the presence of a strong interaction between the SOM and the soil matrix, which is absent in the HWE. The TII thermogram of the pyrolyzed soil (f) shows nearly no volatilization (see the 20 times magnified thermogram in Figure 12). This small total ion intensity agrees with the low C_t and N_t concentrations in Table 1 and can be explained by volatilization of most of the thermally labile SOM during off-line pyrolysis of the sample.

Figure 11 shows similar spectra for the soil+6 HWE (b), soil+3 HWE (c), original soil (d) and soil residue (e) samples. These spectra differ from that of the pyrolyzed soil (f) and HWE sample (a) spectra. Each of them continues over a wide m/z range from about 55 to 400 but only the range of interest will be discussed. The signal pattern in the Py-FI mass spectrum for HWE (a) shows marker signals at m/z 59, 125, and 167, which indicate the presence of N-acetylmuramic acid from microbial cell walls. Also there are marker signals at m/z 84, 96, 110, and 126, which are assigned to carbohydrates, while the marker signals at m/z 156, 170, and 184 are assigned to alkyl naphthalenes. The marker signals at m/z 196 and 208 are assigned to lignin monomers as well as the marker signal at m/z 308, which is assigned to C_{22} -alkene.

The spectra of the soil+6 HWE (b), soil+3 HWE (c), original soil (d) and soil residue (e) show marker signals at m/z 58, 82, 84, 96, and 110, which are due to carbohydrates as well as at m/z 156, 170, and 184 which are assigned to alkyl naphthalenes. There are marker signals at m/z 194, 196, 208, and 210, which are assigned to lignin monomers. Also there are marker signals at m/z 244, 252, 266, and 308, which are assigned to alkenes. The spectrum of the pyrolyzed soil (f) is dominated by a background noise and typical products of char as benzonitrile at m/z 103, C_3 - and C_4 -alkyl benzenes at m/z 120 and 134, respectively, and naphthalene at m/z 128. By comparing the alkene signal markers for HWE (m/z 308) and original soil (m/z 244, 252, 266, and 308), one can conclude that the hot waterpreferentially extracted alkanes/alkenes with longer C-chains.

A more quantitative analysis is provided in Table 3, which shows increasing TII in the order: pyrolyzed soil < soil residue < original soil < soil+3 HWE < soil+6 HWE < HWE in agreement with the order of organic of matter contents (Table 1). For all samples, the average molecular weight by number (M_n) and weight (M_w) and the polydispersity,

synonymous to heterogeneity index (M_w/M_n), are in the range of 181.2 to 199.8, 205.4 to 318.8, and 1.134 to 1.743, respectively. These values indicate a high similarity between the original soil sample and those samples, which are obtained by adding and removing the HWE to and from the original soil sample. Furthermore, the M_w/M_n values, which measure the heterogeneity of sizes of molecules in a mixture, show that the chemical composition is more heterogeneous in the pyrolyzed than the other soil samples. In contrast, there is a significant difference between the original soil and the pyrolyzed one, which have different M_w and, thus, M_w/M_n values. For all samples except the pyrolyzed one, the percentage of organic compound classes according to the relative ion intensity has the order: alkyl aromatic compounds > phenols and lignin monomers > carbohydrates > non-peptidic N-containing compounds (aliphatic nitriles and N-heterocyclic compounds) > lipids, alkanes, alkenes, bound fatty acid and alkyl monoester > lignin dimmers > peptides > sterols > free fatty acids > suberin. On the other hand, it is very difficult to assign correctly the compound classes and their relative ion intensities for the pyrolyzed soil sample because of the extremely low TII.

Table 3 reveals that the hot-water extraction preferentially extracts organic compounds, which are characterized by the presence of polar functional groups. This can be concluded from the increase of the percentage of the carbohydrates, N-containing compounds, peptides and fatty acids and the decrease of the percentage of phenols and lignin monomers, lignin dimers, lipids, alkanes, alkanes and alkyl aromatics in HWE compared with the original soil. For the same reason, the percentage of the carbohydrates, N-containing compounds and peptides in the soil+3 HWE and soil+6 HWE is higher while the percentage of each of the phenols and lignin monomers, lignin dimers, lipids and alkyl aromatics is lower in the soil+3 HWE and soil+6 HWE than that in the original soil sample. In contrast, the percentage of the carbohydrates, N-containing compounds and peptides in the soil residue is lower while the percentage of lignin dimers and lipids in the soil residue is higher than that in the original soil. Upon pyrolysis, the amount of organic compounds decreases as reflected by the TII, which is only about 10% of the TII of the original soil. This low amount of volatile organics makes assignments to compound classes meaningless. The Py-FIMS data in Figure 11(d) and Table 3 show that the amount of volatile organic matter in our original soil sample is less than that published by Schmidt et al.⁽¹¹⁶⁾ Differences in the TII-thermograms and proportions of compound classes are explained by inter-annual

differences in the incorporation of fresh plant materials, richer in carbohydrates and lipids, into the SOM.

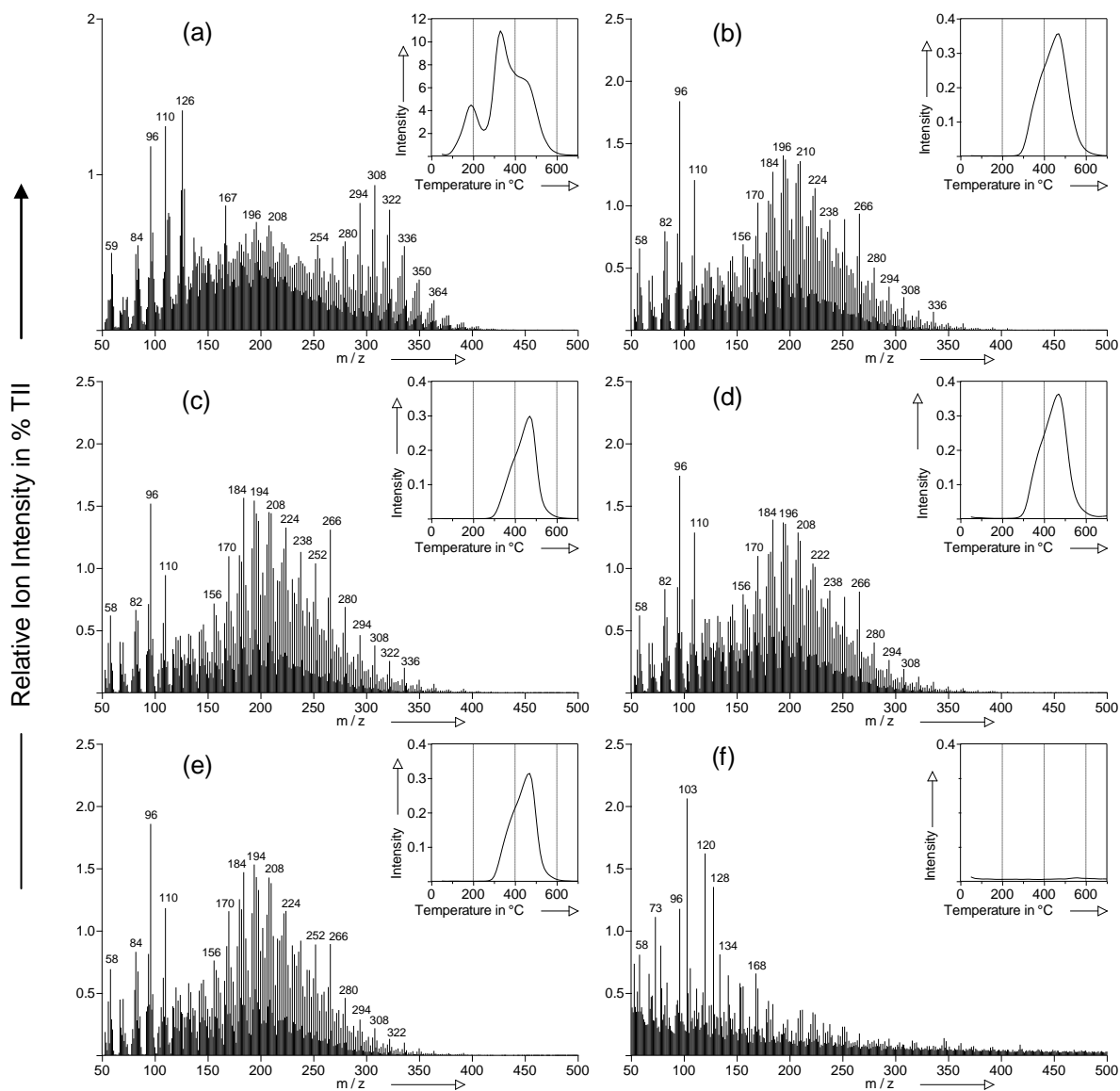


Figure 11. Thermograms of ion intensity in 10^6 counts mg^{-1} (inserts), and summed and averaged pyrolysis-field ionization mass spectra in % of total ion intensity (TII) of HWE (a), soil+6 HWE(b), soil+3 HWE (c), original soil (d), soil residue (e), and pyrolyzed soil (f).

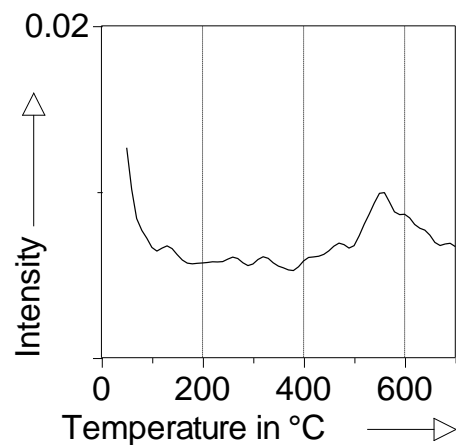


Figure 12. The 20 times magnified thermogram of the pyrolyzed soil sample.

Table 3. Volatile matter (VM), average molecular weight by number (M_n) and weight (M_w), polydispersity (M_w/M_n), total ion intensity (TII) and relative proportions of ion intensity of different compound classes: carbohydrates = CHYDR, phenols + lignin m monomers = PHLM, lignin dimers = LDIM, lipids = LIPID, alkyl aromatics = ALKY, heterocyclic nitrogen containing compounds = NCOMP, sterols = STEROL, peptides = PEPTI, suberin = SUBER, free fatty acids = FATTY for pyrolyzed soil, soil residue, original soil, soil + 3 HWE, soil + 6 HWE and HWE.

sample	VM	TII	M_n	M_w	M_w/M_n	ion intensity of compound classes(% TII)									
	%	$10^6 \text{ countmg}^{-1}$	g mol^{-1}	-----	CHYDR	PHLM	LDIM	LIPID	ALKY	NCOMP	STEROL	PEPTI	SUBER	FATTY	
pyrolyzed soil	0.6	0.455	182.9	318.8	1.743	correct assignment is impossible because of the extremely low TII									
soil residue	7.3	3.908	188.2	214.1	1.138	6.5	15.8	4.0	6.6	17.4	6.1	0.2	2.5	0.0	0.1
original soil	4.8	4.388	181.2	205.4	1.134	7.8	16.9	3.4	5.9	17.5	6.9	0.1	2.9	0.0	0.0
soil+3 HWE	3.3	5.145	181.5	207.5	1.143	8.1	16.5	3.1	5.6	16.5	7.2	0.1	3.0	0.0	0.1
soil+6 HWE	4.1	5.555	181.5	209.6	1.155	8.0	15.5	3.3	5.8	15.5	7.6	0.1	3.2	0.0	0.1
HWE	42.8	229.718	199.8	233.1	1.167	8.9	11.4	2.0	5.3	11.6	9.0	0.4	3.4	0.0	0.8

4.3. Carbon K-edge XANES Spectroscopy

The C-XANES spectra in Figure 13 show 12 features, (a) to (l), which are characteristic for most of the samples. Features (a) and (b) at 284.7 and 285.0 eV are assigned to C=C in alkylated aromatic compounds and alkenes^(137,138) and appeared in all the samples. Feature (c) at 285.7 eV is assigned to C=N in pyridines⁽¹³⁸⁾ and/or C≡C,⁽⁴²⁾ which clearly appeared in the pyrolyzed soil sample. Feature (d) at 286.0 eV is assigned to aromatic C bound to aldehyde.⁽¹²⁷⁾ For all samples the features (e) and (f) appeared at 286.4 and 286.6 eV, which are assigned to aromatic C bound to urea,⁽¹²⁷⁾ and/or carbamates, C=N in pyrroles,⁽¹³⁹⁾ NCHNH in imidazoles and purines,^(140,141) aliphatic nitriles,⁽¹³⁸⁾ aldehydes and/or ketones⁽¹²⁹⁾. For all samples the feature (g) at 288.5 eV is assigned to aliphatic carboxylic acids^(129,142,143) and/or carbohydrate hydroxyl C⁽⁴²⁾. Feature (h) at 289.4 eV, appearing in all samples except the pyrolyzed one, is assigned to C=O in urea,⁽¹²⁹⁾ aliphatic C in C-OH,⁽¹³⁸⁾ and/or aromatic C bound to CONH and HNCONH in thymine, guanosine and uracil⁽¹⁴¹⁾. Feature (i) is assigned to C in carbonate and/or carbamate,⁽¹²⁹⁾ and it is more intensive in the pyrolyzed compared to the other samples. Feature (j), appearing in all samples at 291.0 eV, is assigned to C=O in amide functional group.⁽¹⁴²⁾ Features (k) at 297.4 eV and (l) at 299.9 eV are assigned to potassium compounds and found in all samples.⁽¹⁴⁴⁾

Figure 13 shows that the most abundant features are those corresponding to unsaturated and aromatic compounds (features (a) and (b)), aliphatic nitriles, ketones, aldehyde and/or N-heterocyclic compounds (features (e) and (f)), carboxylic acids and/or carbohydrates (feature (g)), and potassium compounds (features (k) and (l)). In all spectra except the HWE spectrum, the potassium features are the most intensive peaks. The intensity ratio of the potassium/organic compounds features decreases in the order: pyrolyzed sample > soil residue sample > original sample > soil+3 HWE > soil+6 HWE. This indicates that the organic matter content increases in this order, in agreement with the data obtained from the elemental analysis and Py-FIMS. According to similarities in the shape of the spectra the samples can be divided into three groups. The first group includes the soil+3 HWE, soil+6 HWE, and HWE samples; the second one comprises the original soil and the soil residue samples and the third group contains the pyrolyzed soil sample. In the first group, the order for the abundance of features is carboxylic acids and/or carbohydrates > N-heterocyclic compounds > aromatic compounds. The intensity ratio (carboxylic acids and/or carbohydrates)/(heterocyclic compounds) is larger for the soil+6 HWE than that for soil+3

HWE. This indicates that the addition of HWE increases the amount of the polar functional groups as intended. In the second group, the order of the abundant features is carboxylic acids and/or carbohydrates ~ N-heterocyclic compounds > aromatic compounds while for the pyrolyzed soil, the order is N-heterocyclic compounds > aromatic compounds > carboxylic acids and/or carbohydrates.

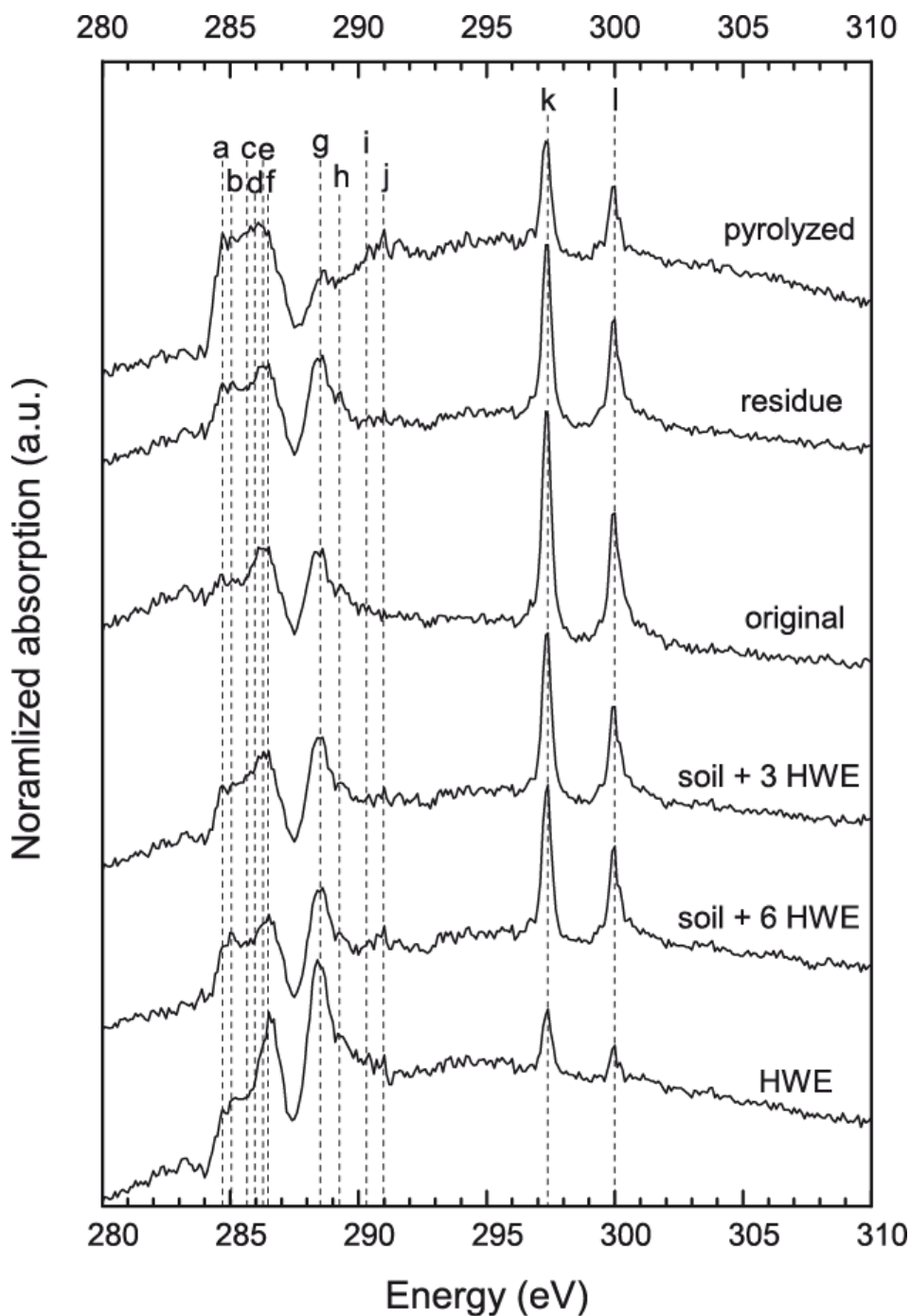


Figure 13. Normalized stacked Carbon K-edge XANES spectra of pyrolyzed soil, soil residue, original soil, soil+3 HWE, soil+6 HWE, and HWE

In summary, these data indicate that the modification by thermal heating enriches the soil mainly in the heterocyclic and aromatic compounds and decreases the polar compounds while the addition of HWE enriches the soil with polar compounds (especially carboxylic acids and/or carbohydrates) and N-containing compounds and decreases the aromatic compounds.

A comparison of the present data set (Figure 13) with C-XANES data for two Canadian soils (Elstow and Melfort) published by Gillespie et al.⁽⁴²⁾ indicates similarities in aromatic C at 285.2 eV, C≡C at 285.7 eV, N-substituted aromatic C at 286.8 eV, carbohydrate hydroxyl C at 288.7 eV, and carbonate C at 290.5 eV and dissimilarity in quinone C at 283.7 eV, phenolic C at 287.1 eV, aliphatic C at 287.5 eV.

4.4. Nitrogen K-edge XANES Spectroscopy

The N K-edge spectra in Figure 14 exhibit the features (a) to (d) which vary in their intensities. The energies of the peak features are at 398.8 eV (a), 399.7 eV (b), 401.0 eV (c) and 405.9 eV (d). For the pyrolyzed soil, feature (d) is shifted from 405.9 eV to 406.0 eV. These features can be assigned according to published spectra of a wide range of N-reference compounds⁽⁴¹⁾. Feature (a) is assigned to the six-membered heterocyclic N-containing compounds (pyridines and pyrazines). Feature (b) is assigned to nitriles and five membered heterocyclic N-containing compounds (pyrazoles). Feature (c) is assigned to the N-amide functional group and feature (e) is a result of all $1s \rightarrow \sigma^*$ excitation combined with nitrate resonances.

The above assignments and relations of peak areas indicate that amides included in proteins are the most abundant organic N-compounds. The order of the N-compounds in all samples is amides > nitriles, five-membered heterocyclic N-containing compounds > six-membered heterocyclic N-containing compounds. Also Figure 14 shows that the ratio of the integrated peak features c:b:a increases in the order: pyrolyzed soil < soil residue < original soil < soil+3 HWE < soil+6 HWE < HWE. This indicates that the abundance of heterocyclic compound increases in the order: HWE < soil+6 HWE < soil+3 HWE < original soil < soil residue < pyrolyzed soil. The N-XANES of HWE in Figure 14 shows much less nitrate than in lyophilized soil leachates from arable and fallow soils⁽¹⁴⁵⁾ in which nitrate forms the most abundant N-functional group. This can be explained by the predominance of the organic over inorganic N in HWE, which is a major difference to the above discussed soil leachates.

The N-XANES data of the original soil in Figure 14 are similar to N-XANES spectra of a range of Canadian soils (Lethbridge, Macklin, St. Denis;⁽⁴³⁾ Elstow and Melfort⁽⁴²⁾). Furthermore, the pyrolyzed soil has an N-XANES spectrum similar to a spectrum that was obtained by heating a soil sample to 600 °C under a normal atmosphere ⁽¹⁴⁶⁾.

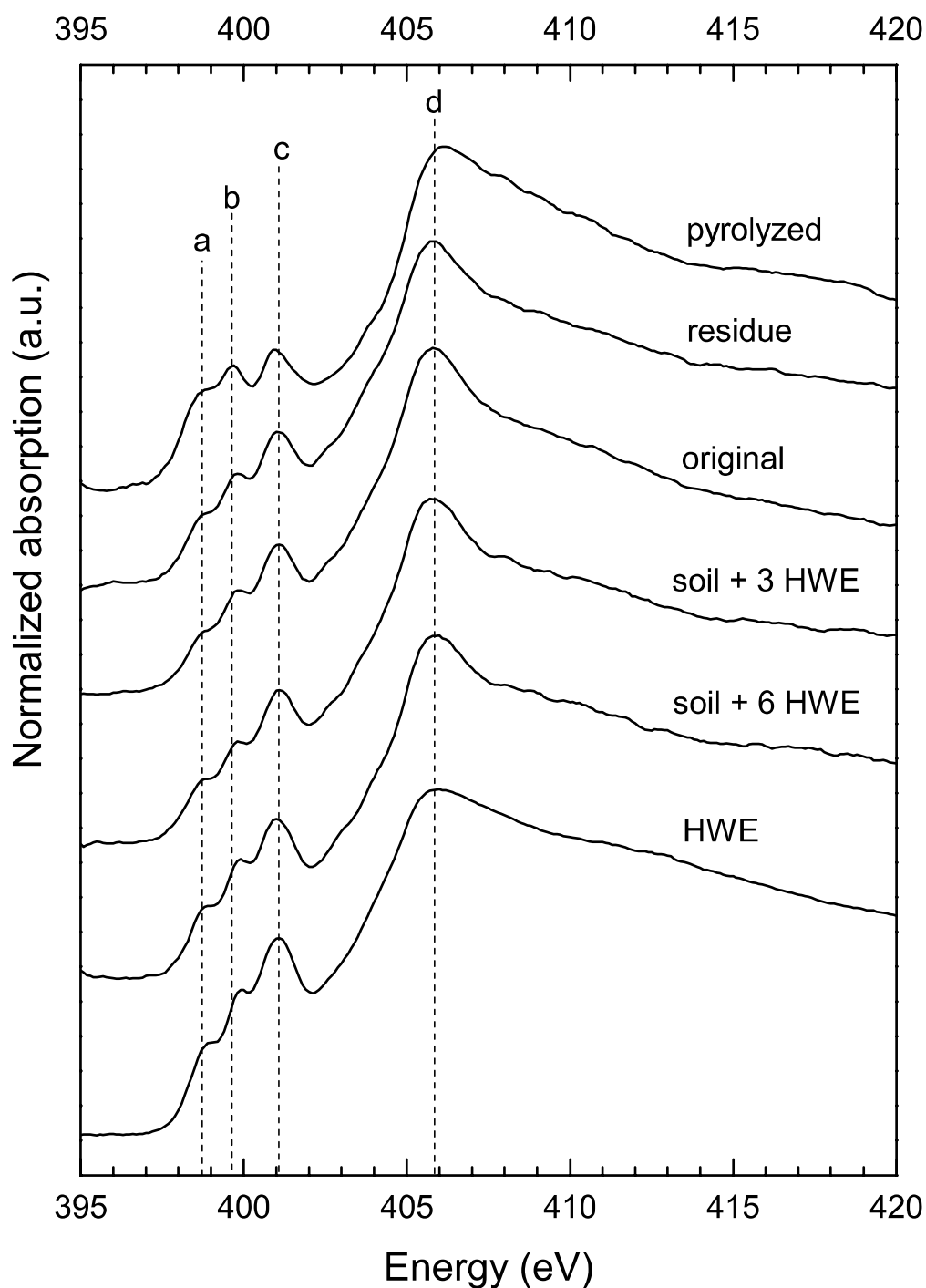


Figure 14. Normalized stacked Nitrogen K-edge XANES spectra of pyrolyzed soil, soil residue, original soil, soil+3 HWE, soil+6 HWE, and HWE.

4.5. HCB Adsorption Kinetics

Kinetics of HCB adsorption on the original soil sample has been performed in duplicates. The standard errors from duplicate data are ranged from 0.017 to 0.163 mg/l HCB giving rise to average is equal to 0.080 mg/l HCB. The free HCB concentrations in mg/l versus time in hours are introduced in Figure 15. An initial rapid adsorption stage of HCB on the soil sample is observed in the first 24 hours due to increasing of the free HCB concentration in this period. This fast stage is a surface phenomenon. As a result to the hydrophobic behaviour of HCB, the vacant sites in the soil are filled up rapidly in the initial stage following linear variation. Normally it is known that this fast step is followed by slow step taking a long time till reaching equilibrium. For example, it was observed by Deane et al.,⁽¹⁵⁵⁾ that HCB didn't reach sorption equilibrium on consolidated sediments and saturated soil even on long range time such as 512 days. Over our short time, decreasing the free HCB concentration is observed after 24 hours. To be sure about this behaviour, adsorption kinetics of HCB on different soil sample (mais soil) has been performed under the same condition. The same behaviour has been reproduced. This behaviour had been obtained for adsorption of endosulfan on different soil samples in Palestine and India.^(156,157) We expected that the reason for increasing of HCB concentration may be desorption of HCB from the soil. This can be explained by temporary saturation of soil surfaces by HCB, then competition between the soil and *n*-hexane with respect to HCB. Therefore, *n*-hexane withdraws part of the adsorbed HCB to the solution phase. The second reason may be raised from evaporation of the *n*-hexane during withdrawing the HCB samples for analysis. This leads to increasing of the HCB concentration. Finally, this motivates to conduct the adsorption experiments of HCB on the different soil samples for 24 hours.

4.6. HCB Adsorption Isotherms

Adsorption of HCB on the original soil, soil+3 HWE, soil+6 HWE, and pyrolyzed soil samples are shown in Figure 16. Amount of the adsorbed HCB on the different soil samples has been normalized to the total mass of the soil (Figure 16 A). Various studies have been reported the strong relationship between total organic carbon in the soil and the mobility of the pesticides.⁽¹⁵⁶⁾ For this reason, Amount of the adsorbed HCB on the different soil samples has been normalized to the total carbon mass in the soil sample (Figure 16 B). The adsorption of HCB on the original soil sample increased upon addition of HWE resulting in the order: original soil sample < soil+3 HWE sample < soil+6 HWE sample. This is valid for the adsorbed HCB concentrations normalized to the total soil mass (Figure 16 A) and the total carbon concentration (Figure 16 B). Adsorption of HCB on the pyrolyzed soil sample

exceeded that of soil+6 HWE at low initial concentrations when normalized to the total soil mass. By increasing of HCB concentration, the adsorption of HCB on the pyrolyzed soil sample became smaller (Figure 16 A). The same is valid over a larger range of HCB concentrations when normalized to the total C concentrations (Figure 16 B).

The adsorption data were fitted to Freundlich (Figure 17) as well as to Langmuir equation (Figure 18). The fitted parameters of adsorption isotherms yielded comparable squared correlation coefficients (r^2) close to one for both equations (Table 4). The agreement with the Langmuir model is not surprising since the hydrophobic HCB is unlikely to form a multilayer. Considering the Freundlich model, the nature of the obtained isotherms characterized by their shape testifies to the prevailing sorption mechanism of a given substance in the system. Nonlinearity of Freundlich exponents (n : 0.56 to 0.80) in case of all soil sample indicates that sorption mechanism is predominant by adsorption⁽¹⁵⁸⁾ process over absorption process. One should note that the exponent n indicates the diversity of the free energies associated with adsorption of HCB on a heterogeneous surface. The $n < 1$ for all soil samples evidences that upon increasing the HCB concentration binding is reduced, i.e. the binding free energies decrease. The only significant difference is observed for the pyrolyzed sample ($n = 0.56$). HCB adsorption on the pyrolyzed sample is described fairly well by the Langmuir equation. The order of adsorption isotherms: original soil < soil+3 HWE < soil+6 HWE (Figures 16, 17, and 18) is reflected by the increase of K_F and X_{max} in Table 4. The Freundlich isotherm parameters for the soil+3 HWE and soil+6 HWE are similar to those obtained for samples from a red and a paddy Chinese soil, respectively⁽¹⁴⁷⁾. Although these authors did not report C concentration, one could explain this by similarity in the organic matter contents because the mineralogy must be completely different from the present soil.

To correlate finding of the adsorption with the SOM composition, the absolute ion intensity (A_{II}) of each compound class, with effective value, for the different soil samples are compiled from Table 3 and collected in Table 5. For each compound class, the A_{II} increased in the order: original soil (A_{II1}) < soil+3 HWE (A_{II2}) < soil+6 HWE (A_{II3}), indicating a contribution of all SOM constituents to HCB adsorption. In order to investigate the effect of chemical composition of SOM on HCB adsorption, we introduce X_1 "amount of adsorbed HCB on original soil", X_2 "amount of adsorbed HCB on soil+3 HWE", and X_3 "amount of adsorbed HCB on soil+6 HWE". For a given equilibrium concentration, the difference in

the adsorbed concentrations between the original soil and soil+3 HWE (X_2-X_1) is always greater than that between the soil+3 HWE and soil+6 HWE (X_3-X_2) (Figures 16, 17, and 18). For comparison of (X_2-X_1) and (X_3-X_2) with the molecular SOM composition we denote the differences in All for each compound class $\Delta All_1 = All_2 - All_1$, and $\Delta All_2 = All_3 - All_2$. For LIPID and LDIM $\Delta All_1 < \Delta All_2$ but for PHLM, ALKY, CHYDR, NCOMP, and PEPTI $\Delta All_1 > \Delta All_2$. This suggests the conclusion that the later compound classes are more likely to explain the above differences in HCB adsorption among samples enriched in hot water extracted organic matter. Especially PHLM, and ALKY, having the largest $\Delta All_1 : \Delta All_2$ values, might contribute to the binding of HCB to SOM more significantly than the other compound classes. This will be supported by the binding energy calculations presented in chapter 5. Moreover, this correlation can be established by using the differences in the Freundlich unit capacities (K_F 's) providing the same results obtained by using the differences in amount of adsorbed HCB on the different soil samples (X 's).

The low total ion intensity in Py-FIMS of the pyrolyzed soil did not allow determining the All of each compound class. However, it is well known that pyrolysis in general decreases the amount of SOM and increases the proportion of unsaturated, substituted aromatic, heterocyclic, and aliphatic nitrile compounds, besides producing charcoal.^(82,121,146) Hence it is reasonable to assume that such changes are responsible for the behaviour shown in Figure 16.

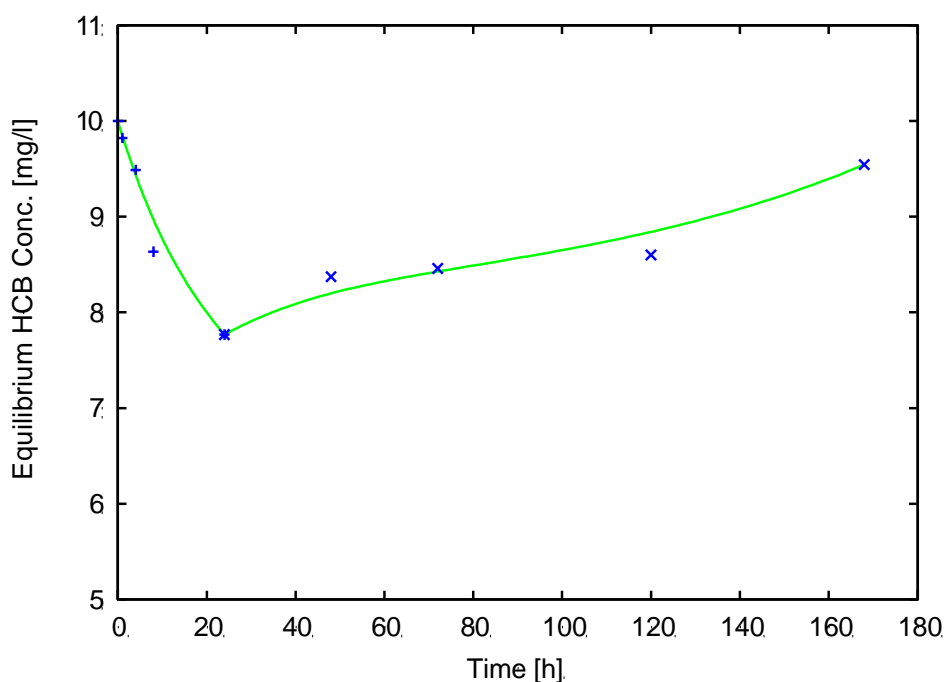


Figure 15. Sorption kinetics of HCB on the original rye soil sample.

Table 4. Fitted parameters with respect to Freundlich and Langmuir equations which are normalized to the total soil mass as well as the total carbon mass for the original soil, soil+3 HWE, soil+6 HWE, and the pyrolyzed soil samples.

soil sample	Freundlich				Langmuir			
	K_F	n	r^2	K_L	X_{\max}	r^2		
	total soil	C_t			total soil	C_t		
original soil	4.02	374.96	0.75	0.99	0.48	13.35	1245.78	0.99
Soil+3 HWE	7.04	637.32	0.80	1.00	0.39	27.03	2445.47	0.99
Soil+6 HWE	10.24	840.99	0.76	0.99	0.48	33.67	2764.42	0.99
pyrolyzed soil	8.66	1065.22	0.56	0.96	0.66	24.81	3051.57	0.98

Table 5. The absolute ion intensity in 10^4 counts mg^{-1} of original soil (AII_1), soil+3 HWE (AII_2), soil+3 HWE (AII_3); the absolute ion intensity difference between original soil and soil+3 HWE (ΔAII_1), and between soil+3 HWE and soil+6 HWE (ΔAII_2).

	PHLM	ALKY	CHYDR	NCOMP	PEPTI	LIPID	LDIM
AII_1	74.2	76.8	34.2	30.3	12.7	25.9	14.9
AII_2	84.9	84.9	41.7	37.0	15.4	28.8	15.9
AII_3	86.1	86.1	44.4	42.2	18.3	32.2	18.3
ΔAII_1	10.7	8.1	7.5	6.7	2.7	2.9	1.0
ΔAII_2	1.2	1.2	2.7	5.2	2.9	3.4	2.4

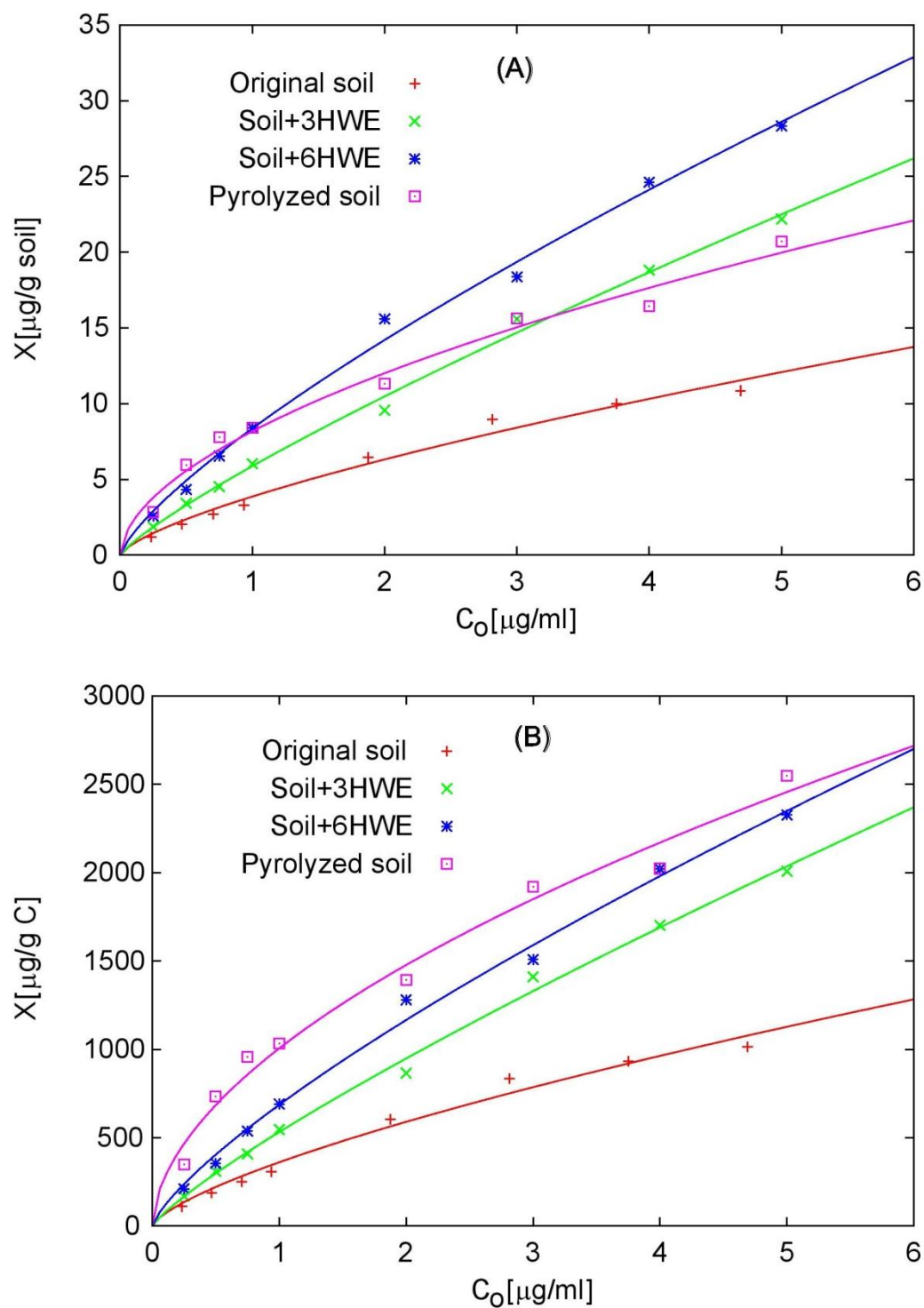


Figure 16. The adsorption isotherms of HCB on the soil samples in which amount of adsorbed HCB normalized to the total soil mass, in $\mu\text{g HCB/g soil}$, (A) and the total carbon content, in $\mu\text{g HCB/g } C_{\text{tot}}$, (B) were plotted versus the corresponding initial HCB concentrations (C_0). The lines were, obtained from an exponential correlation, plotted as guide for eye.

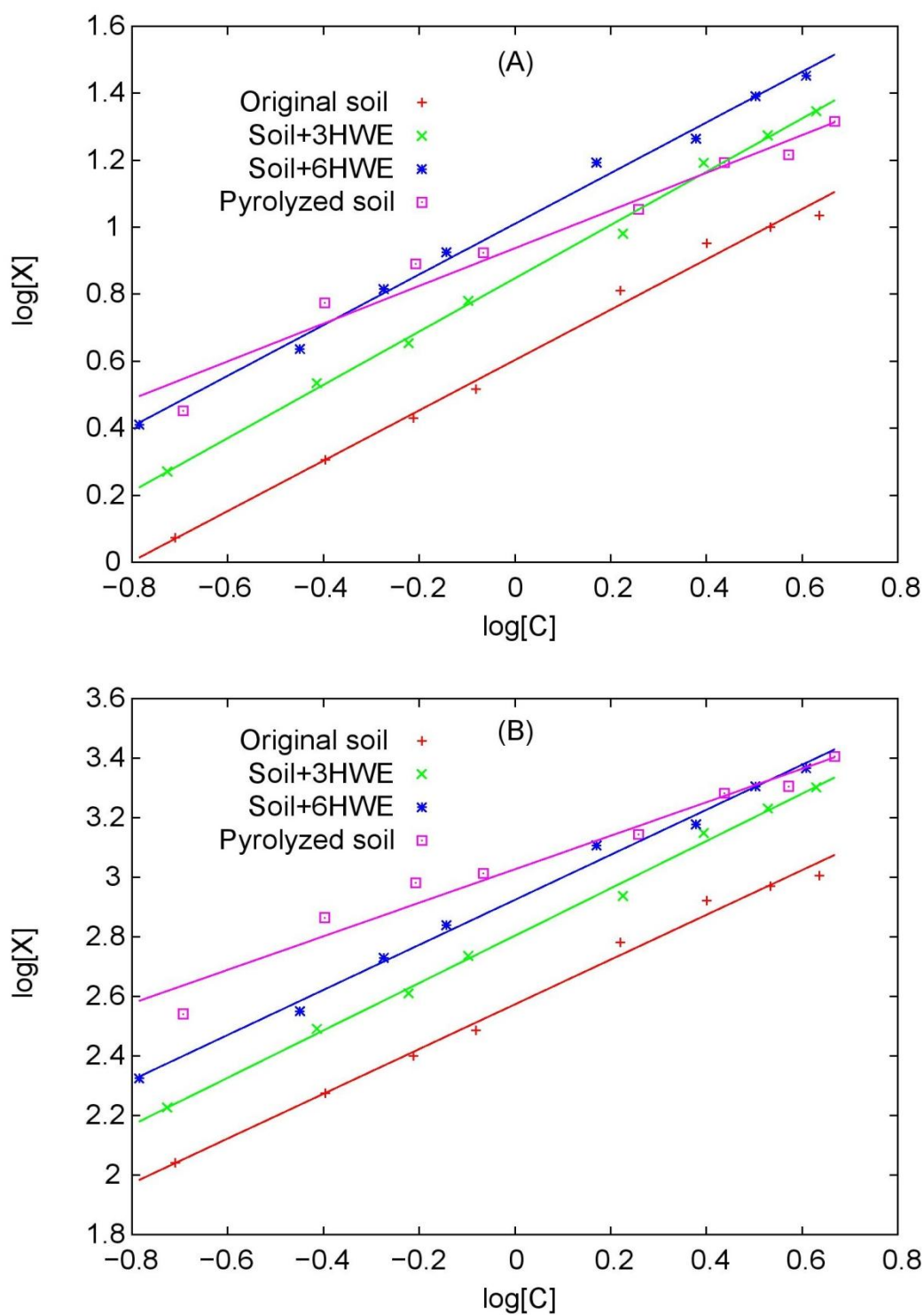


Figure 17. The Freundlich fitted adsorption isotherms of HCB on the soil samples normalized to the total soil mass, in $\mu\text{g HCB/g soil}$, (A) and the total carbon content, in $\mu\text{g HCB/g } C_{\text{tot}}$, (B).

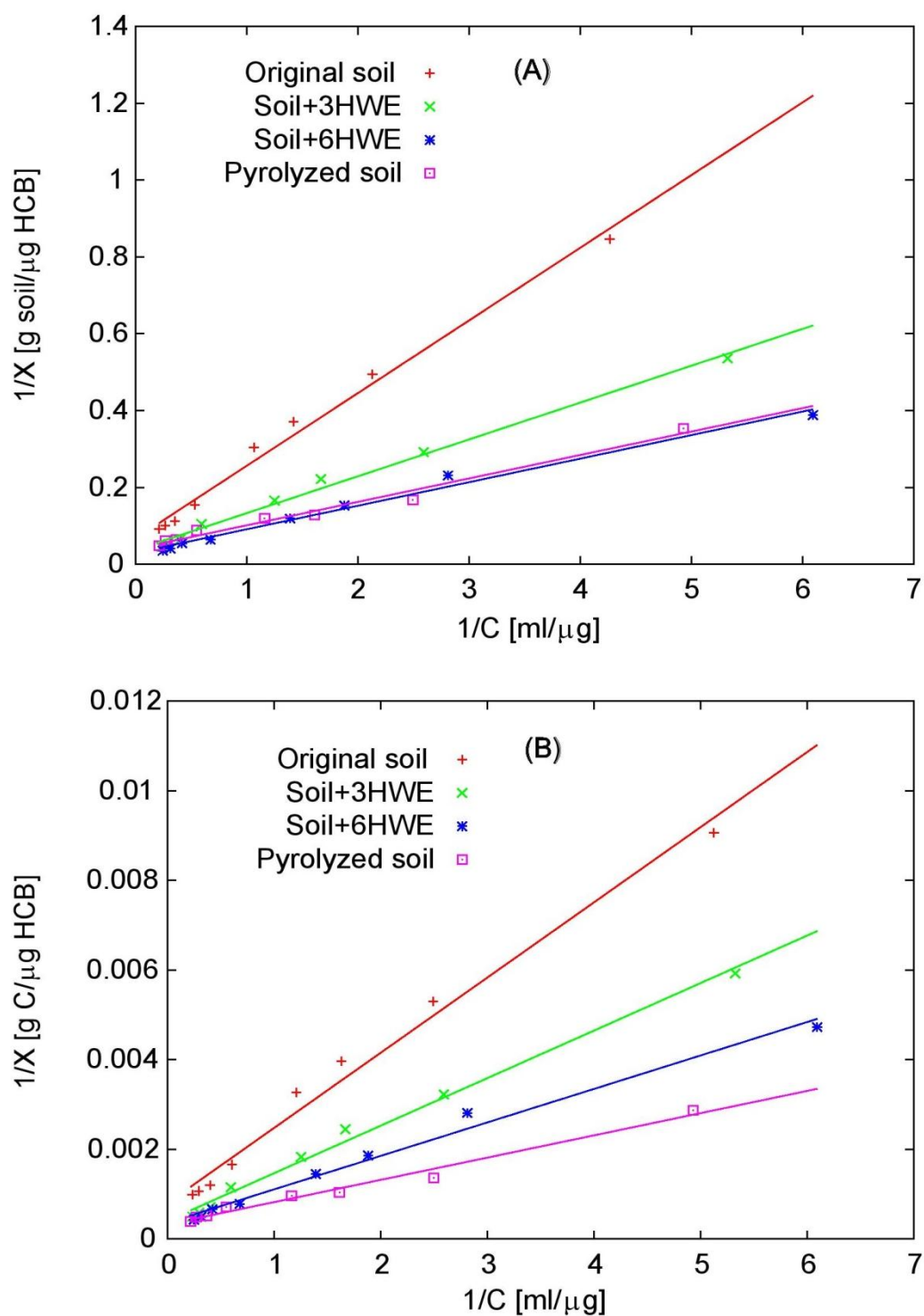


Figure 18. The Langmuir fitted adsorption isotherms of HCB on the soil samples normalized to the total soil mass, in μ g HCB/g soil, (A) and the total carbon content, in μ g HCB/g C_{tot} , (B).

4.7. Summarizing Discussion

To the best of our knowledge, this is the first study describing the controlled experimental modification of SOM in a well-defined soil sample and investigating of this modification by a multi-methodological approach. The combination of elemental analyses, Py-FIMS, and C- and N-XANES provides complementary information about the SOM chemical composition and its alteration by HWE addition and pyrolysis. The C_t - and N_t -concentrations, the TII in Py-FIMS, and the potassium features in the C-XANES data agreed in showing the same order of the organic matter contents in the different samples. This order is pyrolyzed soil sample < soil residue sample < original soil sample < soil+3 HWE sample < soil+6 HWE sample < HWE sample. Furthermore, the C_t - and N_t -concentrations, the molecular weight characteristics M_n , M_m , and M_m/M_n , the TII thermograms and spectral patterns in Py-FIMS as well as the C- and N-XANES spectra reveal a high degree of similarity in the chemical composition among the original soil, soil residue, and two soil samples modified by HWE addition. For all samples except the pyrolyzed one, the percentage of organic compound classes according to the relative ion intensity has the order: ALKY > PHLM > CHYDR > non-peptidic N-containing compounds (aliphatic nitriles and N-heterocyclic compounds) NCOMP > LIPID > LDIM > PEPTI > STEROL > FATTY > SUBER. For instance, C-XANES and N-XANES showed the presence of C=O (in aldehyde, ketone, carboxylic acid, urea, carbamate, and/or amide), aliphatic C in C-OH, carbohydrate hydroxyl, aliphatic nitriles, alkenes, $C\equiv C$, aromatics, aromatic C bound to CONH and HNCONH (in thymine, guanosine and uracil), N-heterocyclic compounds (pyrroles, pyrazoles, imidazoles, pyridines, pyrazines, purines), carbonate, and potassium compounds in these samples. On the other hand, these complementary methods also agreed in showing that the off-line pyrolysis strongly alters the chemical composition of the soil sample. This confirms recent results that showed strong alterations in the chemical structure of SOM upon heating from 400 °C on using the same analytical techniques ⁽¹⁴⁶⁾. Comparing the two approaches for modification of the soil samples, unequivocally it is revealed that the addition or removal of HWE modify the sample much less than thermal heating. However, perhaps pyrolysis at a lower temperature would have resulted in samples with less drastic changes in SOM and more similarity of the original and HWE-modified samples.

The modification by thermal heating enriched the soil mainly in heterocyclic and aromatic compounds and decreased the polar compounds. The addition of HWE to the soil sample

increased the relative proportions of CHYDR, NCOMP, and PEPTI, and decreased the relative proportion of PHLM, LDIM, and LIPID. The addition of different proportions of HWE to the original soil increased the C_t - and N_t -concentrations by 3.2 and 5.0% (3 HWE) and 13.7 and 12.5% (6 HWE). This indicates that either the HWE was not constant in its chemical composition and/or not completely uniformly distributed in the soil samples. Our HWE generally agreed with those published by Leinweber et al.⁽¹¹⁹⁾ in the Py-FI thermogram although the first peak in Figure 11(a) occurred at a higher temperature (180 °C) than in the cited study (120 °C). This slight dissimilarity is explained by the lower organic matter content in the present study (159 g kg⁻¹ C and 15.9 g kg⁻¹ N, Table 1) as compared with the cited reference (235–248 g kg⁻¹ C and 25.8–25.9 g kg⁻¹ N). Furthermore, the organic matter in our HWE seems to be less labile than in the study by Leinweber et al.⁽¹¹⁹⁾ which is confirmed by small proportions of N-containing compounds and carbohydrates. This difference can be explained by a possible precipitation of alkyl aromatic compounds and phenols/lignin monomers in previous studies where HWE was obtained by a decantation of the cooled extract. In the present study we avoided this by filtrating the centrifuged HWE immediately after boiling. Furthermore, our HWE was substantially different from that extracted from forest floors⁽¹²⁰⁾ as it had less C and N, and smaller proportions of phenols and lignin monomers, lipids, sterols, suberin and fatty acids. Despite these differences, the addition of HWE in general appears suitable to enrich a soil sample in the polar functional groups, but the degree of this enrichment depends on the origin of the HWE. These changes in the SOM structures may have agronomic implications because soil amendments with, e.g. compost, were also reflected by the chemical composition of dissolved organic matter and extracted humic substances.^(148,149) Therefore, HWE addition to soil may be a model for the addition of organic amendments which release soluble organics into soil. Elemental analysis and Py-FIMS show that the pyrolyzed soil sample contains only a small amount of volatile SOM because most organic matter was volatilized during off-line pyrolysis (Table 1). The losses in C_t and N_t were 24.1% and 25.0%, respectively, for the pyrolyzed soil compared to the original soil. The off-line pyrolysis of the soil decreased the proportions of volatile organic matter so strongly (the TII for the pyrolyzed soil is 10.4% of the TII for the original soil) that an assignment of the remaining m/z signals to compound classes appeared to be not straightforward. The C- and N-XANES (Figures 13 and 14) agreed in showing that the most abundant organic functional groups in the pyrolyzed sample were aromatics, aliphatic nitriles, aldehydes, nitrogen in five-membered heterocyclic rings, and aliphatic carboxylic

acids. This composition is typical for soil samples that are thermally heated experimentally in the laboratory or by wildfires.^(123,146,150,151) For soil+3 HWE, soil+6 HWE, and HWE samples, the order of the abundant features is carboxylic acids and/or carbohydrates > N-heterocyclic compounds > aromatic compounds. For original soil, and the soil residue samples, the order of the abundant features is carboxylic acids and/or carbohydrates ~ N-heterocyclic compounds > aromatic compounds while for the pyrolyzed soil, the order is N-heterocyclic compounds > aromatic compounds > carboxylic acids and/or carbohydrates.

Generally, adsorption of HCB on the soil samples increased upon addition of HWE resulting in the order: original soil < soil+3 HWE < soil+6 HWE. Adsorption of HCB on the pyrolyzed soil sample exceeded that on soil+6 HWE at low initial concentrations when normalized to the total soil mass. The same is valid over a larger range of HCB concentrations when normalized to the total C concentrations. The adsorption isotherms were fitted to both Langmuir and Freundlich equations. It was found that the difference in the adsorbed concentrations between the original soil and soil+3 HWE (X_2-X_1) is always greater than that between the soil+3 HWE and soil+6 HWE (X_3-X_2). These adsorption results were correlated to the difference in the absolute ion intensities (ΔAII_1 and ΔAII_2). As a result for this correlation, it was suggested that both PHLM and ALKY have the largest impact on adsorption of HCB on soil samples enriched in hot water extracted organic matter. Moreover, it was suggested that the unsaturated, substituted aromatic, and heterocyclic compounds besides charcoal are the most effective compound types controlling adsorption of HCB on the pyrolyzed soil sample.

5. THEORETICAL RESULTS AND DISCUSSION

5.1. Test Set Systems Classification

HCB-SOM complexes are developed by combination of each representative test set system, in Figure 10, with HCB. Geometries of these complexes are optimized in the gas phase and will be discussed in the next section. The gas phase equilibrium geometries of the test set complexes at B3LYP-D3/6-311++G(d,p) level of theory are shown in Figure 19. The numbering of these complexes in Figure 19 and all the following figures is according to increasing the binding energy of HCB with the representative system at B3LYP-D3/6-311++G(d,p) in the gas phase (except the inorganic silicon hydroxide which has the number **32**). For the PHLM compound class, phenol, catechol, and 3,4,5-trimethoxy cinnamic acid have the numbers **22, 26**, and **30**, respectively. Benzene, methylbenzene, ethylbenzene, naphthalene, and ethylnaphthalene in ALKY compound class have the numbers **17, 18, 24, 28**, and **29**, respectively. Regarding CHYDR compound class, the open and cyclic forms of glucose have the numbers **2** and **15** respectively, while for PEPTI, HCB-glycine complex has two energetically equivalent configurations with the numbers **9** and **10**, and hexa-glycine has the number **27**. Ethylnitrile, pyridine, and pyrrole in NCOMP have the numbers **3, 13**, and **16**, respectively. In LIPID, *n*-butane, 1,3-butadiene, 1,3,5,7,9-decapentaene, and *n*-decane have the numbers **12, 14, 20**, and **23**, respectively. Acetamide, methanol, acetaldehyde, acetic acid, dimethylketone, methylamine, methylacetate, quinone, protonated methylamine, and aniline have the numbers **1, 4, 5, 6, 7, 8, 11, 19, 21**, and **25**. Finally, coronene, and silicon hydroxide trimer have the numbers **31**, and **32**, respectively.

Figure 19 shows that HCB interacts through its positively charged hydrophobic ring center with the negatively charged center of most modelled systems. There are three exceptions (acetamide (**1**), glucose in the open form (**2**), and charged methylamine (**8**)) that bind HCB in a different way. In complexes of these systems, two chlorine atoms in HCB interact with one or two H atom(s). Furthermore, Figure 19 clearly shows that there is no covalent bond formed between HCB and the SOM model set, i.e. binding is due to dispersion interaction except for the charged system (**21**) which has electrostatic interaction. Figure 19 shows that the polar aliphatic compounds and pyridine bind to HCB in such that the most negatively charged atom is directed to the positively HCB ring center. On the other hand, the non-polar aliphatic compounds, and aromatic compounds bind to HCB in such

that both planes containing these representative systems and HCB are parallel to each other.

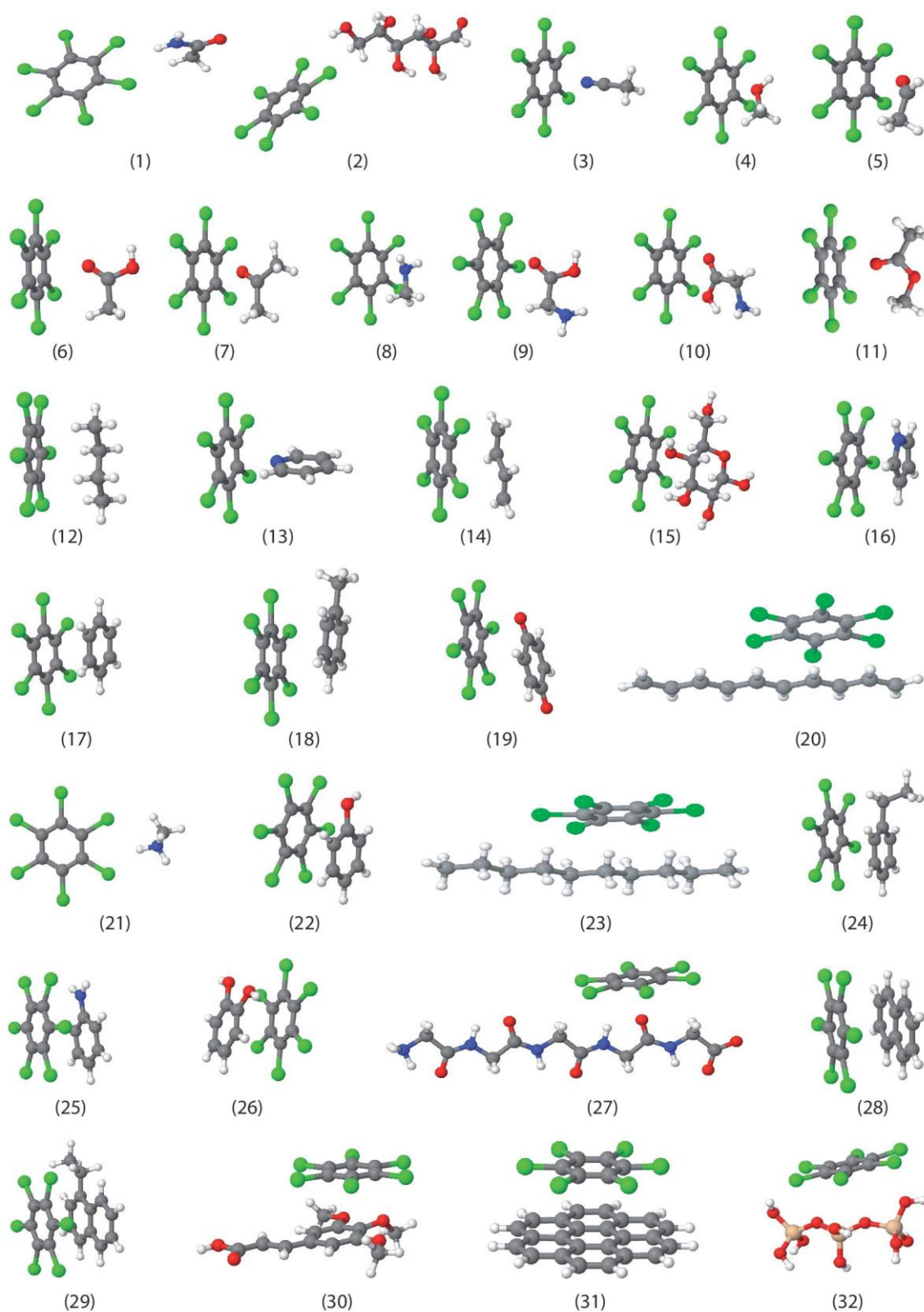


Figure 19. The gas phase equilibrium geometries of the test set complexes with HCB optimized at B3LYP-D3/6-311++G(d,p).

5.2. Geometry Optimization

Figure 20 shows the binding energy of HCB with each SOM representative system. The three-dimensional structures of HCB, the individual representative systems, and their complexes with HCB are optimized using B3LYP with Grimme correction for dispersion interaction D3 (DFT-D3) employing three different basis sets, i.e. 6-31G, 6-31++G, and 6-311++G(d,p). The binding energies between HCB and the SOM representative systems as well as the dipole moments of the complexes show that the three basis sets describe this interaction in similar way. The calculated binding energies at 6-31++G basis set are closer to that at 6-311++G(d,p) basis set than that at 6-31G basis set. Noticeable deviations in the binding energies of HCB with glucose in both forms (**2**) and (**15**), and ketone (**7**) are shown at 6-31G basis set with respect to the other basis sets. Moreover, the root mean square deviation (RMSD) in the binding energies calculated at 6-311++G(d,p) and 6-31G basis sets with respect to that at 6-31++G basis set, are 0.863 and 1.279 kcal/mol, respectively. Clearly, most of the HCB-SOM complexes have typically similar dipole moments at the three used basis sets especially 6-31++G and 6-311++G(d,p). For the complexes of HCB with glucose in the open form (**2**), methylnitrile (**3**), and ketone (**7**) deviation in the dipole moment values are observed at 6-31G basis set with respect to the other basis sets. Considering structures of HCB-SOM complexes at 6-31++G basis set as a references, Figure 20 shows the structure RMSD of each HCB-SOM complex for 6-31G and 6-311++G(d,p) basis sets. It is obvious that RMSD of 6-31G basis set with respect to 6-31++G basis set are larger than that for 6-311++G(d,p) basis set which implies that HCB-SOM complexes at 6-31++G and 6-311++G(d,p) basis sets are typically close to each other. This can be shown in case of the complexes of glucose in both forms (**2**), and (**15**), ketone (**7**), butane (**12**), and quinone (**19**) which have large structure deviations at 6-31G basis set with respect to 6-311++G one. Combining the three panels of Figure 20 one can conclude that 6-31++G basis set at B3LYP-D3 is sufficient for geometry optimization of these HCB-SOM complexes to obtain the minima of the representative systems as well as their complexes.

Nevertheless since the optimized geometries at B3LYP-D3/6-311++G(d,p) are obtained, they will be taken for further calculations in the following sections. These geometries are used as starting point for geometry optimization at the same level of theory by including the water as a solvent via COSMO model. Also single point calculations including different quantum mechanical levels of theory have been performed based on these geometries.

Moreover, some of them are used as starting configurations for running molecular dynamics simulations.

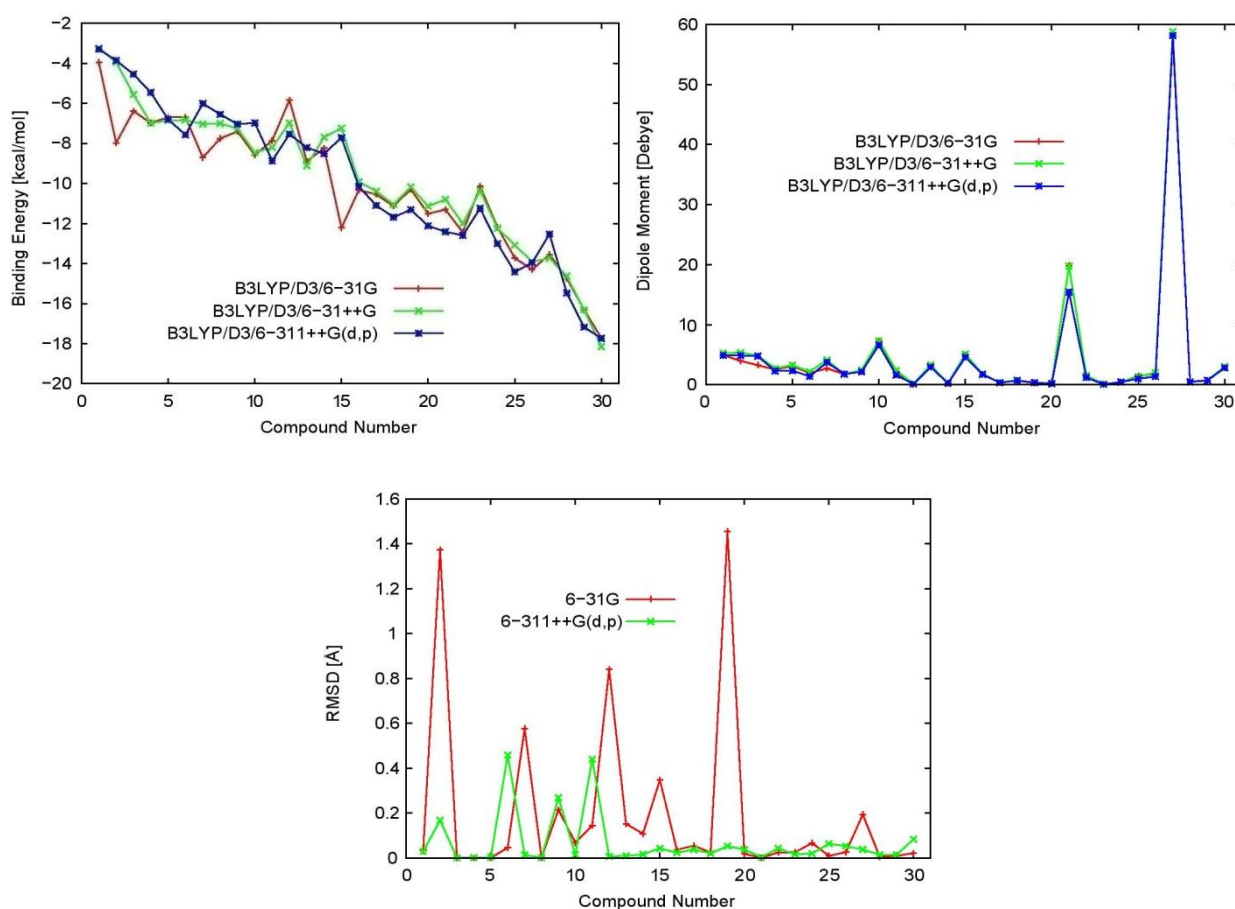


Figure 20. The binding energies of HCB with the SOM representative systems (upper-left panel), dipole moments of HCB-SOM complexes (upper-right panel) at 6-31G, 6-31++G, and 6-311++G(d,p) basis sets, and structure RMSD of each HCB-SOM complex (lower panel) at 6-31G and 6-311++G(d,p) basis sets with respect to structures at 6-31++G basis set.

5.3. Effect of Dispersion Correction

Geometry optimization of the HCB-SOM complexes using HF and DFT without dispersion correction produced configurations with significant differences compared with those obtained by DFT including dispersion corrections like D2 and D3. To study effect of dispersion on binding energy, single point calculations are performed on the optimized structures of HCB-SOM complexes as well as their individual systems. These calculations have been done using HF, B3LYP without dispersion correction, B3LYP-D2, and B3LYP-D3 at different basis sets. In the next section effect of the basis set will show that 6-311++G(2d,2p) is sufficient basis set for study this type of interaction. So Figure 21 shows effect of including dispersion correction in the level of theory on the calculated binding energies in these complexes at 6-311++G(2d,2p) basis set. It is clear that both HF and B3LYP

without dispersion correction have the same trend in description of the interaction of the HCB-SOM complexes. These complexes seem to be more stable in case of B3LYP compared with HF level of theory. In general, the binding energies for most of these complexes are positive values which indicate instability of these complexes at these levels of theory. There is one exception, charged amine (**21**), which has a positive binding energy value with HCB. This complex is stable due to the positive charge on the nitrogen atom of the amine system. By including the dispersion correction D2 or D3, substantial changes in the binding energy values of HCB-SOM complexes are observed compared to that calculated using HF and B3LYP without dispersion correction. All these complexes have negative binding energies which mean stability of these complexes by including the dispersion correction. This indicates the importance of involving empirical dispersion corrections in the different types of the quantum mechanical levels of theory for studying of this non-covalent interaction.

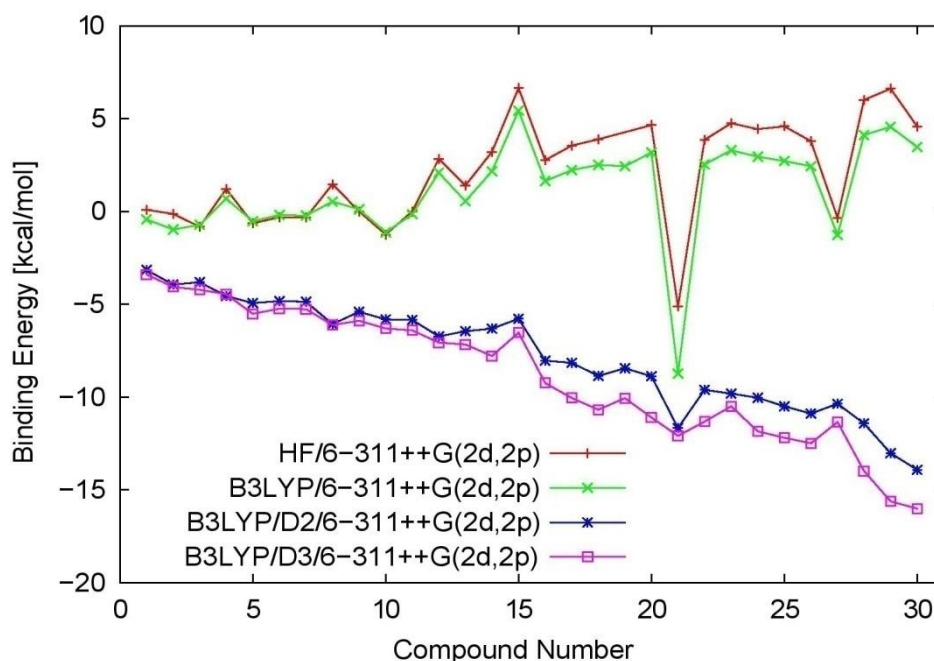


Figure 21. The binding energies of HCB with the SOM representative systems at 6-311++G(2d,2p) using HF, B3LYP, B3LYP-D2, and B3LYP-D3.

Comparing the different types of dispersion correction D2 and D3, one can observe that HCB is more stabilized with the developed test set in case of including D3 than D2. This can be explained by the additional terms including $1/r^8$ term as well as the three-body contributions to the dispersion energy in case of D3. This leads to increasing the total energy of the complex in case of D3 as compared with D2. Thus greater binding energies are obtained in case of D3 compared with D2.

Figure 21 shows that a great contribution in description of these binding energies comes from the dispersion interactions while small effects come from the electrostatic interactions. This indicates that the dispersion interaction is the most important interaction type in the HCB-SOM complexes. This opens the floodgates for using a cheap method, including some empirical corrections for dispersion interactions, such as force field approach for studying this interaction. Thus one can run a molecular dynamics simulation for a long time in addition to study the effect of the solvent.

5.4. Effect of Basis Sets

Effect of different basis sets such as 6-31G, 6-31++G, 6-311++G(d,p), 6-311++G(2d,2p), and aug-cc-pvdz at B3LYP-D3 on the binding energies and dipole moments of HCB-SOM complexes is introduced in Figures 22 and 23. The reference geometries are the optimized HCB, SOM representative systems, and HCB-SOM complexes at B3LYP-D3/6-311++G(d,p). It is clear from Figure 22 that all these basis sets describe the interaction of the HCB-SOM complexes by the same trend while only there are small fluctuations between them. Figure 23 shows the deviations in the binding energy of these complexes as well as the deviations in the dipole moment.

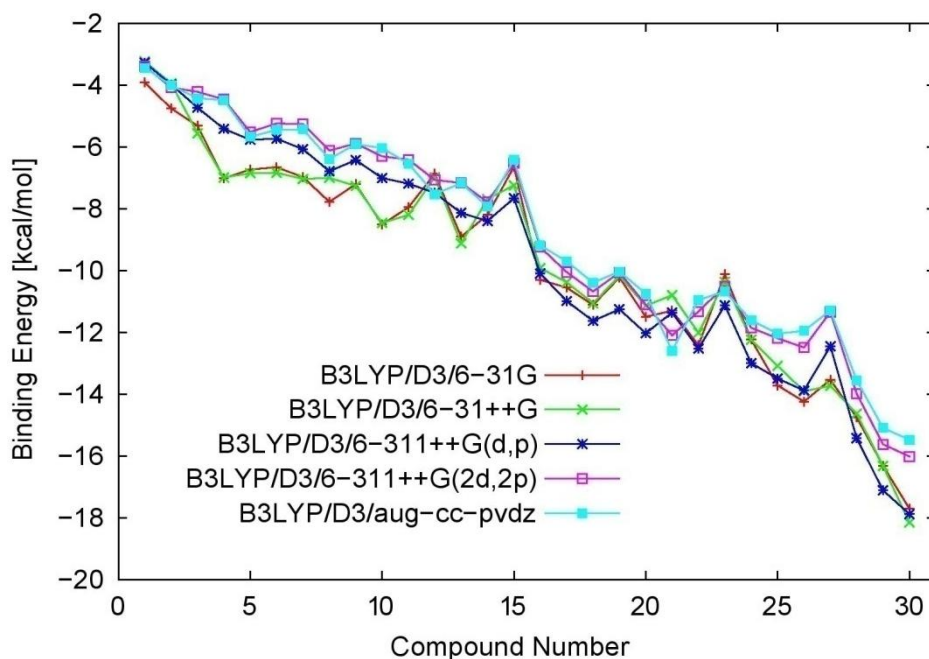


Figure 22. The binding energies of HCB with the SOM representative systems using B3LYP-D3 at 6-31G, 6-31++G, 6-311++G(d,p), 6-311++G(2d,2p), and aug-cc-pvdz basis sets.

Taking aug-cc-pvdz basis set as a reference, the maximum deviations in the binding energy for 6-31G, 6-31++G, 6-311++G(d,p), and 6-311++G(2d,2p) basis sets are around 2.6, 2.8, 2.4, and 0.6 kcal/mol, respectively. Similarly, the maximum deviations in the dipole moment for

6-31G, 6-31++G, 6-311++G(d,p), and 6-311++G(2d,2p) basis sets are around 1.2, 1.5, 0.8, and 0.2 Debye, respectively. The RMSD in the binding energies of all complexes with respect to aug-cc-pvdz basis set are 1.377, 1.370, 1.151, and 0.285 kcal/mol for 6-31G, 6-31++G, 6-311++G(d,p), and 6-311++G(2d,2p) basis sets, respectively. The RMSD in the dipole moments with respect to aug-cc-pvdz basis set are 0.375, 0.444, 0.181, and 0.063 Debye for 6-31G, 6-31++G, 6-311++G(d,p), and 6-311++G(2d,2p) basis sets, respectively. So one can mention that by increasing size of the basis set, the binding energies are being almost constant starting from 6-311++G(2d,2p) basis set. This results indicates that 6-311++G(2d,2p) basis set is sufficient basis set and recommended for studying interaction of HCB to SOM constituents.

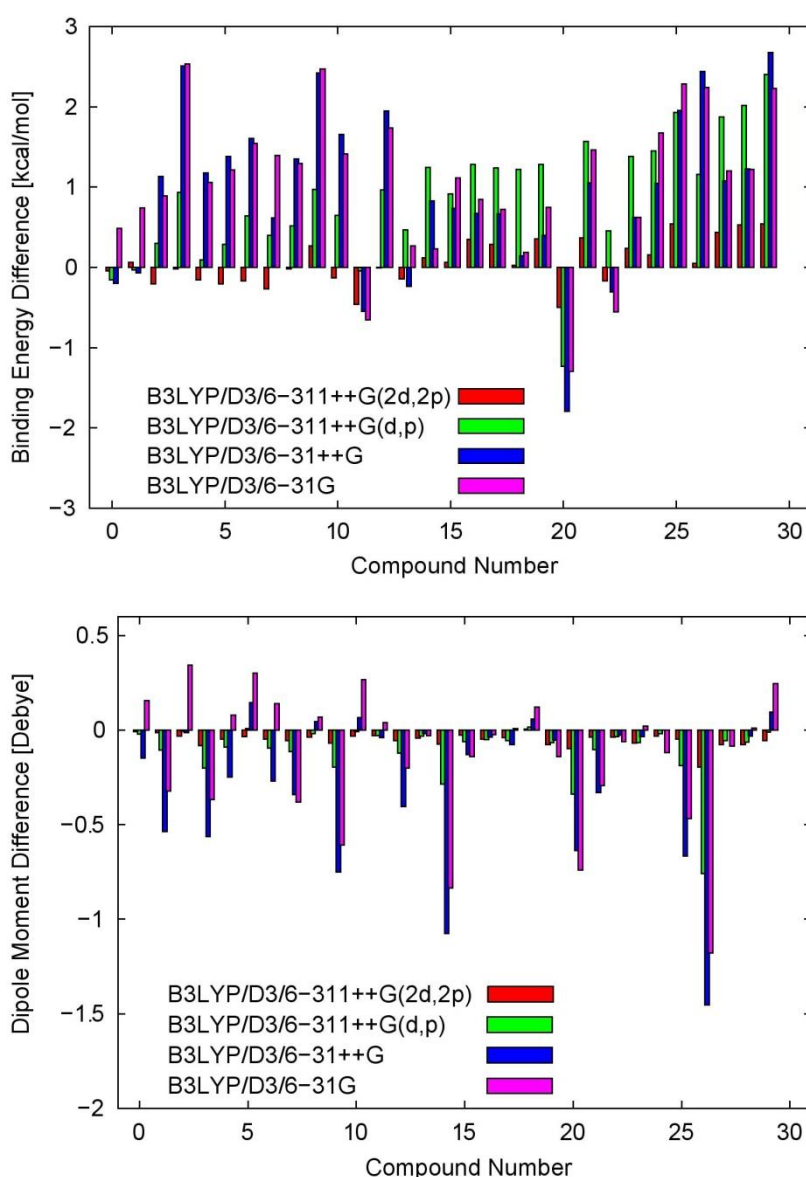


Figure 23. The binding energy differences of HCB with the SOM representative systems, dipole moment differences of the HCB-SOM complexes using B3LYP-D3 at 6-31G, 6-31++G, 6-311++G(d,p), 6-311++G(2d,2p) basis sets with respect to aug-cc-pvdz basis set.

5.5. Effect of DFT-Functionals

Effect of different DFT-functionals on the binding of HCB to the SOM test set systems is represented in Figures 24 and 25. Here single point calculations are performed using various DFT-functionals including BLYP, B3LYP, B3LYP5, and CAMB3LYP at 6-311++G(2d,2p) basis set. In these calculations D3 dispersion is included. Figure 24 shows that profile of the binding energies of HCB to the SOM representative systems over the HCB-SOM complexes have almost similar behaviour for all the used DFT-functionals. In Figure 24, small deviations can be shown between the different DFT-Functionals.

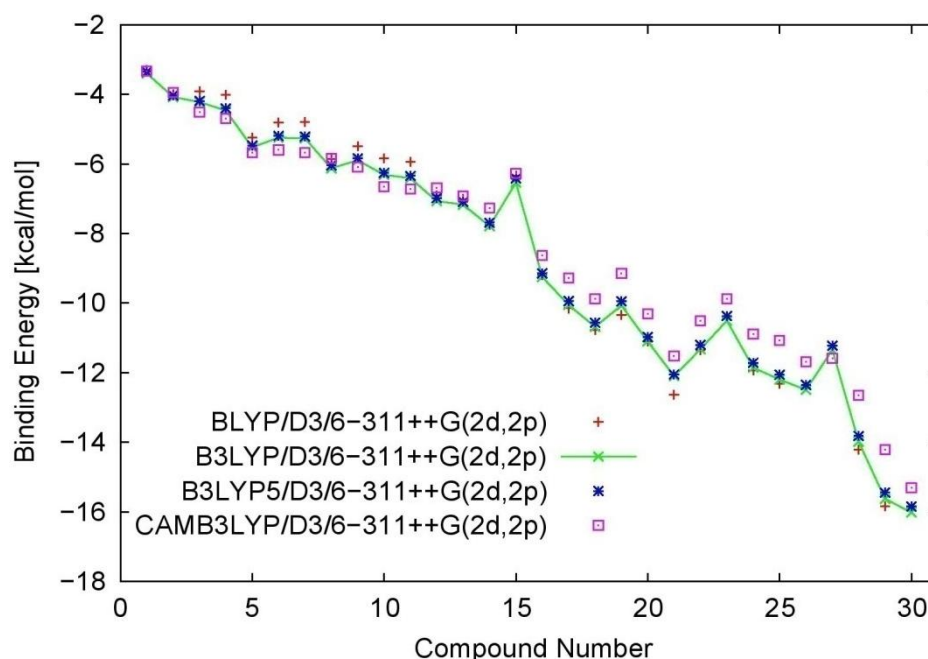


Figure 24. The binding energies of HCB with the SOM representative systems using BLYP-D3, B3LYP-D3, B3LYP5-D3, and CAMB3LYP-D3 at 6-311++G(2d,2p) basis set.

For more details, the deviations in the binding energy and the dipole moment values are calculated with respect to B3LYP and introduced in Figure 25. The maximum deviations in the binding energy are around 0.5, 0.1, and 1.5 for BLYP, B3LYP5, and CAMB3LYP, respectively. For the dipole moments of HCB-SOM complexes, it was found that almost there is no deviation in case of B3LYP5 with respect to B3LYP. The maximum deviations in dipole moments for BLYP and CAMB3LYP are 0.28 and 0.18, respectively. The RMSD in the binding energies are 0.271, 0.104, and 0.670 kcal/mol for BLYP, B3LYP5, and CAMB3LYP, respectively with respect to B3LYP. By similarity, the RMSD in the dipole moments with respect to those of B3LYP are 0.100, 0.001, and 0.073 Debye for BLYP, B3LYP5, and CAMB3LYP, respectively. This indicates that each of these DFT-functionals can describe this weak interaction in acceptable way. Moreover, the averages of the required SCF iteration

time for single point calculations of HCB-SOM complexes for B3LYP, B3LYP5, and CAMB3LYP, are around 0.183, 1.023, and 1.071 times of that for B3LYP. Once these DFT-functionals have the ability to describe the HCB-SOM interaction with similar behaviour, it is recommended to use BLYP in case of time demanding calculations like molecular dynamics simulations based on DFT.

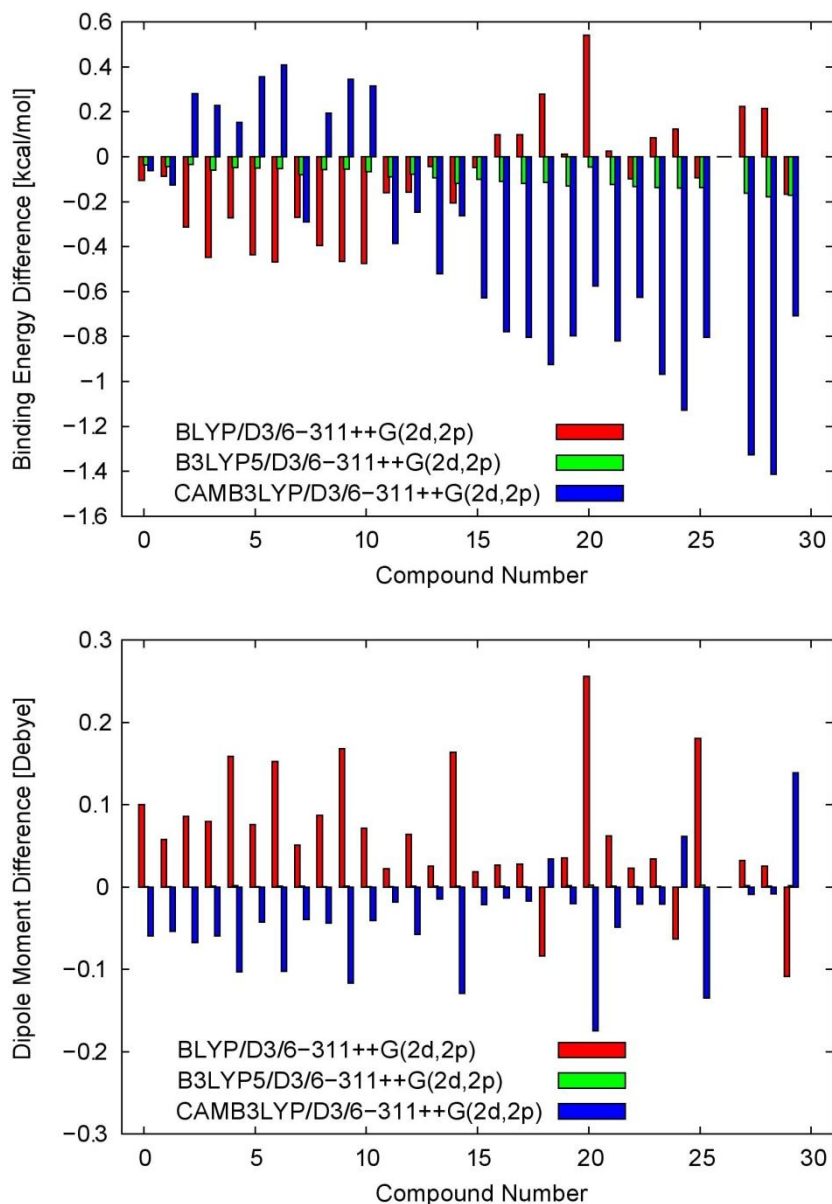


Figure 25. The binding energy differences of HCB with the SOM representative systems, dipole moment differences of the HCB-SOM complexes at 6-311++G(2d,2p) basis set using BLYP-D3, B3LYP5-D3, and CAMB3LYP-D3 with respect to B3LYP-D3.

In the same context, effect of the wave-function convergence on the single point calculations of HCB-SOM complexes is checked at B3LYP-D3. The different used wave-function convergence thresholds (10^{-5} , 10^{-6} , and 10^{-7}) show exactly the same binding

energies and dipole moments. So accuracy of the results is not affected in case of using any one of them.

5.6. Benchmark Calculations

Single point calculations are performed on the optimized HCB, SOM systems and HCB-SOM complexes by the accurate standard methods such as MP2 and CCSD. This has been done to test the obtained results from DFT calculations including dispersion corrections. Figure 26 shows the binding energies of HCB to SOM representative systems using B3LYP-D3, MP2, and CCSD at aug-cc-pvdz basis set. These calculations are performed using Turbomole package even in case of B3LYP-D3. For MP2 calculations, their binding energies are corrected from the basis set super position error (BSSE)⁽¹⁵⁹⁾ via counterpoise correction.⁽¹⁶⁰⁾ Also it is important to mention that we are not able to obtain the complete set of the binding energies in case of CCSD due to its computational demands.

Figure 26 shows the three used methods have the same trend in drawing the picture of interaction of HCB to SOM representative systems. This can be shown from almost increasing of the binding energies of the complexes by increasing the compound number from aliphatic to aromatic compounds. Only small fluctuations can be observed in each case. One can recognize small deviations in the binding energies between B3LYP-D3 (not corrected from BSSE) and the corrected BSSE MP2 for the first 15 complexes. On the other hand, these deviations increase in the last 15 complexes but still are acceptable compared with those obtained using HF or even DFT without dispersion correction. This gives attention that the DFT including dispersion correction (DFT-D) is a sufficient approach for description of this non-covalent interaction. Moreover, close of the binding energy values in case of the corrected BSSE MP2 with DFT-D indicates that the latter approach does not need for BSSE correction. This can be clearly confirmed in Figure 27 which shows the binding energy differences obtained from the raw data at MP2/aug-cc-pvdz and B3LYP-D3/aug-cc-pvdz with respect to the corrected BSSE MP2/aug-cc-pvdz. Figure 27 clearly shows that the deviations of the binding energies at MP2 (not corrected) are larger than that at B3LYP-D3, or in more general DFT-D, with respect to the corrected BSSE MP2. The RMSD in the binding energies are 1.481 and 7.301 kcal/mol for B3LYP-D3/aug-cc-pvdz and MP2/aug-cc-pvdz, respectively with respect to the corrected BSSE MP2/aug-cc-pvdz. This small deviation in case of B3LYP-D3 motivates us to recommend DFT-D3 for further calculations focusing on non-covalent interaction.

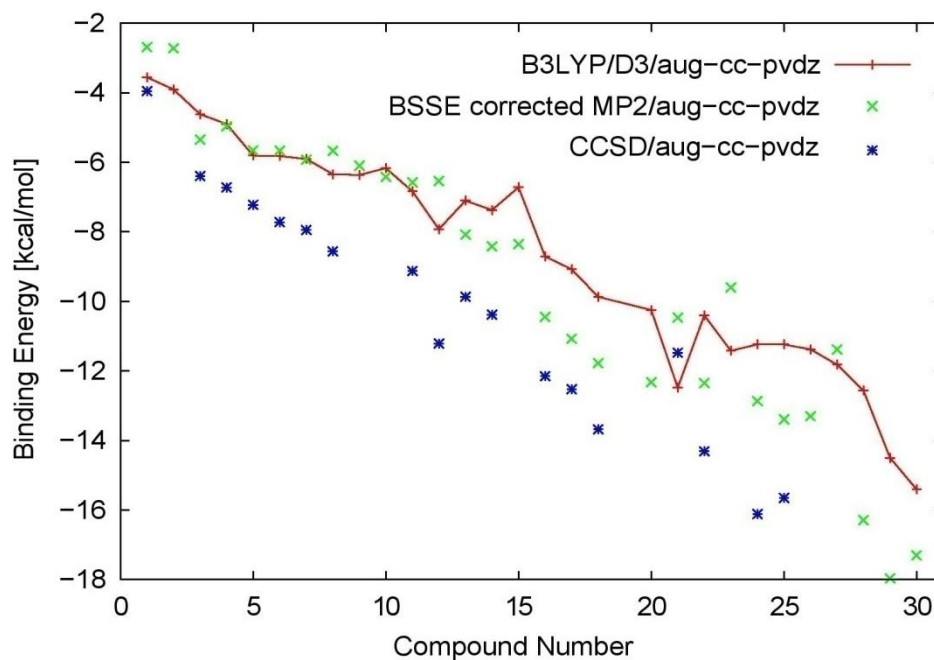


Figure 26. The binding energies of HCB with the SOM representative systems using B3LYP-D3, the corrected BSSE MP2, and CCSD at aug-cc-pvdz basis set.

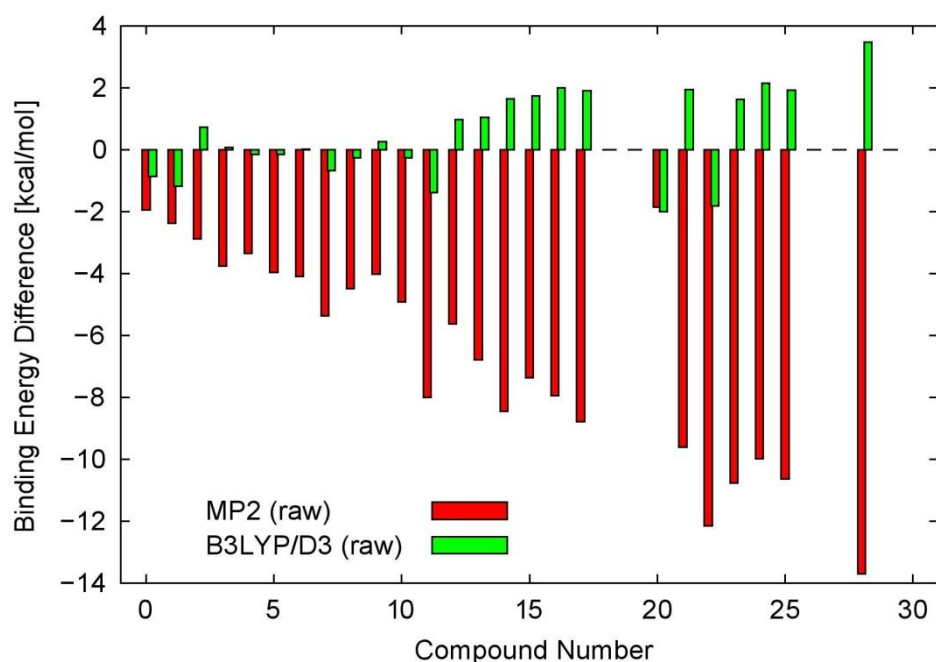


Figure 27. The binding energy differences of HCB with the SOM representative systems at MP2/aug-cc-pvdz (raw data) and B3LYP-D3/aug-cc-pvdz (raw data) with respect to the corrected BSSE MP2/aug-cc-pvdz.

5.7. Gas Phase HCB-SOM Interaction and Effect of Solvent

In this section, the binding energies in the gas phase of HCB with the developed test set systems of the soil especially SOM are correlated to their chemical composition. One should not forget that the soil solution is an important factor controlling this interaction. This soil solution, which is mainly composed of water, is simulated by a continuum

solvation approach. Here we are using the COSMO model which is implemented in Turbomole package. Since the 6-311++G(2d,2p) basis set is not included in Turbomole, the following calculations are performed at 6-311++G(d,p) basis set using B3LYP-D3. In case of using COSMO model, geometry optimization for HCB, the test set compounds, and HCB-test set compounds are performed. Then the binding free energies of HCB to the different representative systems in all complexes are calculated.

In Figure 28, the binding energies in the gas phase for the test set complexes indicate that aromatic compounds (**13**, **16-19**, **22**, **24-26**, and **28-31**) bind to HCB stronger than aliphatic compounds (**1-12**, **14**). This can be explained by the type and strength of the interaction center. For polar aliphatic compounds, the centers of interaction are the partially negatively charged atoms, while for non-polar aliphatic compounds (like alkanes and alkenes) most of the atoms contribute to the interaction. For aromatic compounds, the centers of interaction are the partially negatively charged aromatic rings. Thus, it can be concluded that the binding energy increases with the subjected surface area for the interaction. This also implies that binding energies for HCB with long chain alkanes and alkenes are comparable to that of aromatic compounds. A more detailed inspection of Figure 28 reveals that for aliphatic compounds HCB binds in the order: saturated long chain hydrocarbon (**23**) ~ unsaturated long chain hydrocarbon (**20**) > unsaturated short chain hydrocarbon (**14**) ~ saturated short chain hydrocarbon (**12**) > amine functional group (**8**) > carbonyl functional group (**5-7**) > alcohol functional group (**4**) > nitrile functional group (**3**). In case of aromatics, it was found that HCB binds in the order: aniline (**25**) > ethylbenzene (**24**) > phenol (**22**) > methylbenzene (**18**) > benzene (**17**). Furthermore, HCB binds to carbohydrates, modelled by glucose (**15**), and peptides, modelled by hexaglycine (**27**), within the aromatic's binding range. Due to the above mentioned functional groups effect, binding is stronger to peptides than to carbohydrates. In addition, HCB binds to alkylated aromatic compounds (**17**, **18**, **24**) stronger than heterocyclic ones (**13,16**). Within the aromatic compounds, HCB binds the polycyclic aromatic rings (like the substituted (**29**) and non-substituted (**28**) naphthalene) stronger than monocyclic aromatic rings (like the substituted (**18**, **24**) and non-substituted (**17**) benzene). Note that despite that HCB binds to naphthalenes stronger than to benzenes, the interaction with HCB exceeds that of naphthalenes if benzene is substituted by a strong electron donating functional group (like the lignin monomer (**30**)).

The COSMO calculations show that solvation does not affect significantly the spatial configuration of HCB-test set complexes. The root-mean square deviation between the conformers in the gas phase and the corresponding ones in solution for most of these complexes is less than 0.05 Å which can be shown in Figure 29. Only in the case of HCB-acetic acid and HCB-methylacetate complexes, the systems were rotated by 90° to make the planes containing the system and HCB parallel to each other. The calculated binding free energies show that solvation decreases the binding energy for all HCB-test set complexes from gas phase to solution. This is due to stabilization of the inorganic species as well as the SOM components by water. Nevertheless, the overall picture remains almost unchanged, i.e. HCB binds to both aromatic and nonpolar aliphatic compounds more than to polar aliphatic compounds. Specifically, HCB binds in the order: substituted polycyclic aromatic compounds like naphthalenes (binding free energy: -14.2 kcal/mol) > lignin monomers (binding free energy: -13.7 kcal/mol) > long chain alkanes (binding free energy: -11.4 kcal/mol) > substituted benzenes with alkyl and amino groups ~ long chain alkenes (binding free energy: -9.6 kcal/mol) > phenols (binding free energy: -9.3 kcal/mol) > short chain alkanes (binding free energy: -7.4 kcal/mol) > five membered heterocyclic ring compounds (binding free energy: -7.1 kcal/mol) > short chain alkenes ~ esters (binding free energy: -6.6 kcal/mol) > carbohydrates (binding free energy: -6.2 kcal/mol) > peptides (binding free energy: -5.2 kcal/mol) > six membered heterocyclic ring compounds (binding free energy: -4.5 kcal/mol) > polar aliphatic compounds (binding free energy: -2.9 kcal/mol). As a general trend it has been found that in case the polarity of SOM components increases the binding free energy decreases. An exceptional behaviour is observed for the case of charged amine (**21**), hexaglycine (**27**), and silicon hydroxide trimer (**32**) where a strong decrease in their binding free energies is observed compared with their binding energies in gas phase (marked (I), (II), and (III) respectively in Figure 28). Here the solvation of the positive charge and the highly polar functional groups compensates the other types of the interaction (electrostatic and dispersion).

Figure 28 can be summarized into four points:

- 1- HCB binds to aromatic and non-polar aliphatic compounds stronger than to polar aliphatic and inorganic compounds.
- 2- HCB binds polycyclic aromatic compounds stronger than monocyclic aromatic compounds.

3- As the subjected surface area for the interaction increases, binding of HCB increases as well.

4- Solvation reduces the binding energies in all cases especially for polar aliphatic compounds, peptides, and carbohydrates.

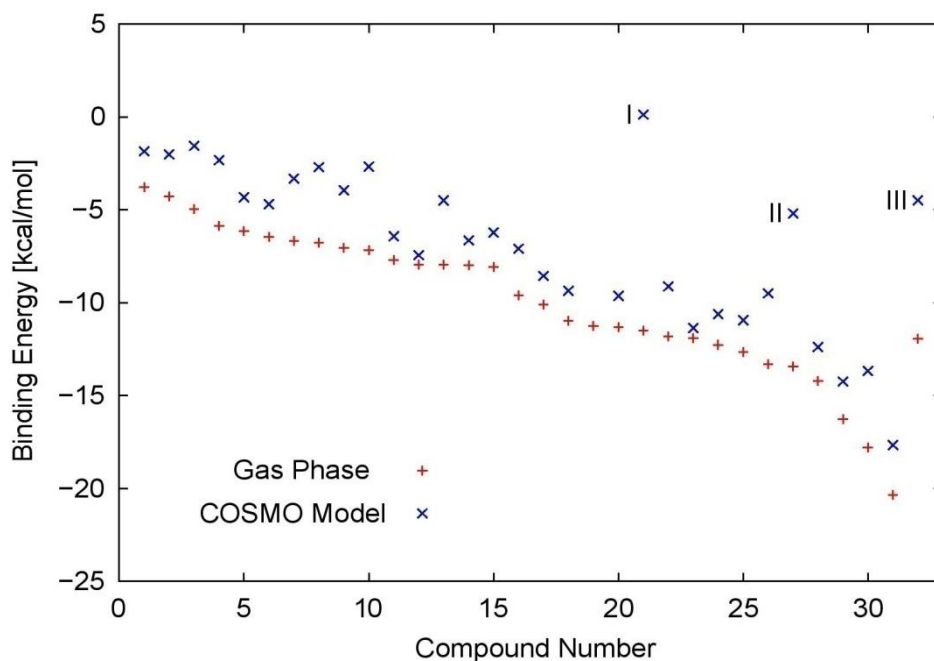


Figure 28. The binding energies for HCB with the test set given in Fig. 19 calculated at the B3LYP-D3/6-311++G(d,p) level of theory in gas phase and using the COSMO model. (I), (II), and (III) mark complexes which are most strongly affected by solvation (21, 27, and 32).

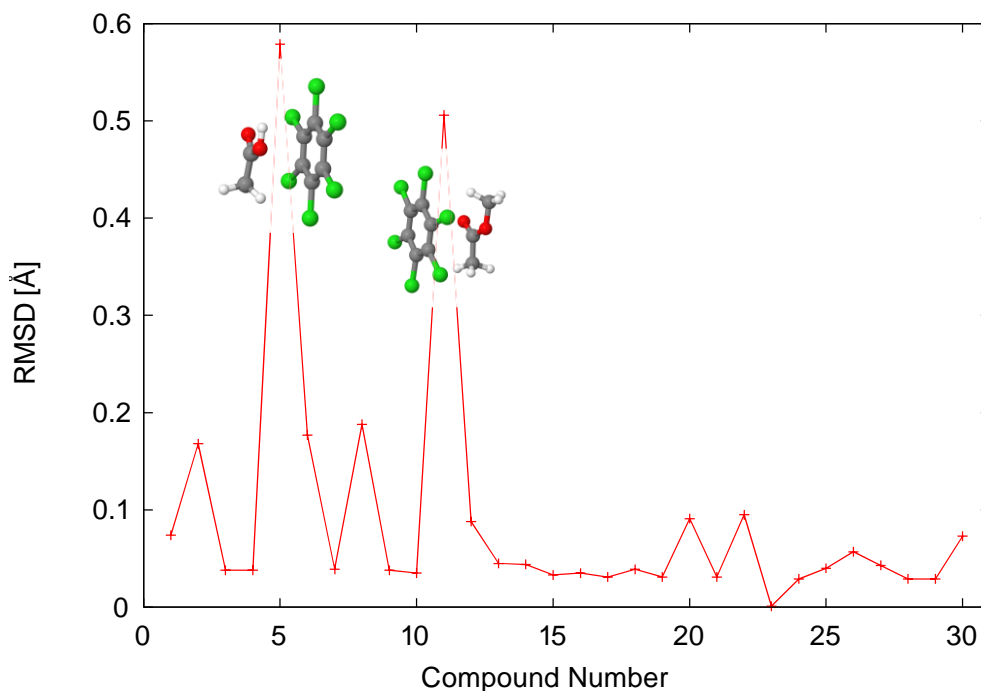


Figure 29. The root-mean square deviation, in Å, between the optimized conformers in the gas phase and solution at B3LYP/D3/6-311++G(d,p).

The role of dispersion interaction for the formation and stability of the test set complexes is further highlighted in Figure 30. This figure reveals a linear correlation between total binding free energy and the contribution of dispersion interaction. It is clear that the dispersion interaction is the most contributed interaction type to the total binding free energy as well as the binding energy in gas phase. Figure 31 shows that the binding energies due to the dispersion interaction in case of solution are quite similar to that in gas phase.

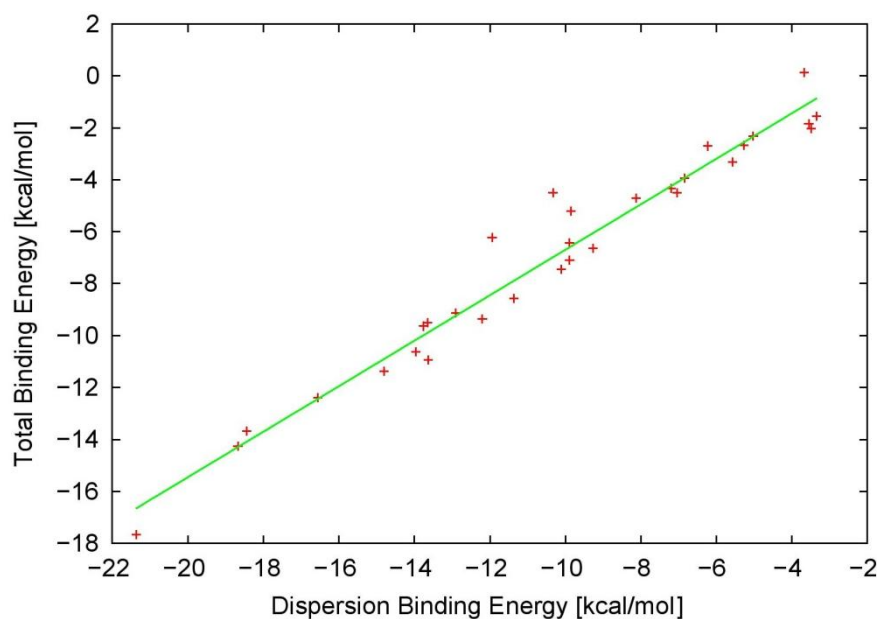


Figure 30. Correlation of the binding free energies for HCB-test set complexes with the dispersion energies at the B3LYP-D3/6-311++G(d,p) level of theory using COSMO model.

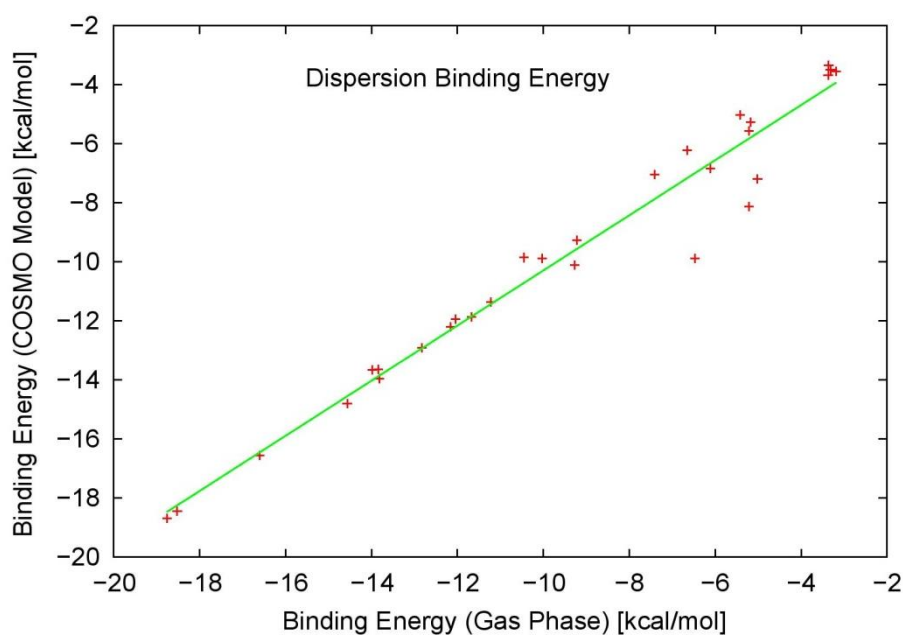


Figure 31. The dispersion binding energy of HCB with the representative systems in gas phase and in solution by using COSMO model.

5.8. Correlation with the Experimental Results

In order to establish a correlation between the computational and experimental results, the binding free energy values of different test set complexes were grouped according to their compound classes. The averaged binding free energies for these compound classes are given in Table 6. Let us denote the total binding free energy (E_B) of HCB to original soil, soil+3 HWE, and soil+6 HWE with $E_{B,org}$, $E_{B,3HWE}$, and $E_{B,6HWE}$, respectively. Next we assume that the E_B for HCB to any soil sample is directly proportional to the AII and the average binding free energy for each compound class in SOM $\langle E_B \rangle_i$, i.e.

$$E_B \propto \sum_i \langle E_B \rangle_i * AII_i \quad (5.1)$$

where the sum runs over all compound classes. Since Figures 16, 17, and 18, and Table 5 suggested that important differences might be seen in the relative changes, using (5.1) we consider

$$E_{B,3HWE} - E_{B,org} \propto \sum_i \langle E_B \rangle_i * (AII_{i,3HWE} - AII_{i,org}) = \sum_i \langle E_B \rangle_i * \Delta AII_{1,i} \quad (5.2)$$

$$E_{B,6HWE} - E_{B,3HWE} \propto \sum_i \langle E_B \rangle_i * (AII_{i,6HWE} - AII_{i,3HWE}) = \sum_i \langle E_B \rangle_i * \Delta AII_{2,i} \quad (5.3)$$

Let us further assume that the ratio of change of the amount of adsorbed HCB is proportional to the change in binding free energy, i.e.

$$\frac{E_{B,3HWE} - E_{B,org}}{E_{B,6HWE} - E_{B,3HWE}} \propto \frac{X_2 - X_1}{X_3 - X_2} \quad (5.4)$$

Inspecting Table 6 one finds that the ratio of binding free energy changes is about 2.8. In fact this is in accord with the observation that $X_2 - X_1 / X_3 - X_2 > 1$. The largest contribution to $E_{B,3HWE} - E_{B,org}$ is due to PHLM and ALKY. This is not out weighted by any of the contribution to $E_{B,6HWE} - E_{B,3HWE}$. Thus we find clear indications that PHLM and ALKY compound classes are dominating the adsorption behaviour of HCB on the considered soil samples.

To explain behaviour of HCB adsorption on the pyrolyzed soil, additionally, coronene (**31**) and silicate (**32**) segment (silicon hydroxide trimer) were added to the model set to mimic the highly aromatic character and the soil mineral respectively. Taking into account the solvent effect, the binding free energies of HCB to coronene and silicate segments are -17.67 and -4.49 kcal/mol, respectively. First, we note that these values are in accord with the widely accepted view that SOM has a higher impact on adsorption of hydrophobic

organic compounds on soil than soil minerals.⁽¹⁵²⁻¹⁵⁴⁾ Second, these data in combination with the fact that the SOM content in the pyrolyzed soil sample is around 75% of that in the original soil sample, explains the behaviour of the adsorption isotherm. The pyrolyzed soil sample is of highly aromatic character and contains unsaturated organic compounds. These compounds bind HCB strongly so that for small HCB concentrations, the pyrolyzed sample will adsorb stronger than the other samples. By increasing HCB concentration, the pyrolyzed soil sample is saturated before the other soil samples. This is due to its low SOM content compared to the other soil samples. This leads to gradual decrease in the adsorption of HCB on the pyrolyzed soil sample compared to the other soil samples. This argument is in good agreement with Freundlich exponent n for adsorption of HCB on the pyrolyzed soil sample which has the lowest value (0.56) compared to the other soil samples. This indicates that the binding free energy decreases for the pyrolyzed samples stronger than for the other soil samples. An intuitive picture, which is in accord with the polymer-like models, would be that with increasing HCB concentration pathways for diffusion through the SOM complex to potential binding sites are blocked.

Table 6. The average binding free energy ($\langle E_B \rangle$) in kcal/mol for the different SOM compound classes and the absolute ion intensity difference in 10^4 counts ΔAII_1 , and ΔAII_2 which are taken from Table 5.

	PHLM	ALKY	CHYDR	NCOMP	PEPTI	LIPID	LDIM
$\langle E_B \rangle$	-10.8	-11.0	-6.2	-5.8	-5.2	-8.8	-----
ΔAII_1	10.7	8.1	7.5	6.7	2.7	2.9	1.0
ΔAII_2	1.2	1.2	2.7	5.2	2.9	3.4	2.4

5.9. Molecular Dynamics Simulations

In general, some valuable points should be highlighted in this section. There is no doubt that the force-field level of theory is completely different than the different types of quantum mechanical levels of theory. So we are focusing on a qualitative comparison not a quantitative one between the outcomes of force-field and quantum mechanical calculations. Effect of solvation is treated explicitly by including 900 water molecules around the HCB-SOM complexes. This is different than the implicit treatment of solvent in case of COSMO which a dielectric continuum outside of a molecular cavity is surrounded these complexes. So one can expect different behaviour for some complexes in case of MD simulations compared with COSMO calculations. In MD simulations, the binding energies of HCB-SOM

complexes under effect of the solvation are calculated at each time step instead of the binding free energies. Both electrostatic and van der Waals interactions between HCB and SOM systems are included in the calculated binding energies.

Based on the force-field approach, single point calculations have been performed for some of HCB-SOM complexes. Geometries of these complexes are obtained from the optimized complexes at B3LYP-D3/6-311++G(d,p) in gas phase. These selected SOM complexes with HCB contain different aliphatic and aromatic SOM representative systems. The binding energies between HCB and SOM systems in these complexes are calculated and introduced in Figure 32. The profile trend of these binding energies looks similar to that in case of the calculated binding free energies at B3LYP-D3/6-311++G(d,p). This indicates to an agreement of the force-field approach with the DFT-D level of theory in description the behaviour of HCB-SOM interaction. Thus, this leads to validity of the force-field to describe this non-covalent interaction. Moreover, this indicates that correlation of the binding energies, obtained using the force field, to the chemical composition of the representative systems is similar that by binding energies obtained using DFT-D3

In general, deviations of the force-field binding energies compared to the DFT-D3 binding free energies increase by increasing the compound number, i.e from left to right. This means that the first SOM systems (polar compounds) have similar binding energies than that for the last SOM systems (non-polar and aromatic compounds). The largest deviation can be introduced in case of charged amine complex (**20**) which has binding energy is completely different than the corresponding one in case of DFT-D in gas phase. This is due to its positive charge in addition to its small size which leads to pronounce the electrostatic interaction compared to the dispersion one. This can be explained by deficiency of the force field approach to describe the electrostatic interactions compared with the quantum mechanical methods. Nevertheless, the force field approach can be used in this study since the dispersion interaction is more valuable than the electrostatic one in HCB-SOM complexes. This can be shown in Figure 33, where the binding energies due to the dispersion interaction using the force-field approach in case of single point calculations as well as MD simulations are introduced. One can observe that there is no significant differences even by including or excluding the electrostatic interaction especially in case of MD simulations in solution. Moreover, to get a quantitative picture for HCB-SOM interaction, one can suggest re-parameterization of the force-field. One can add the terms

containing the $1/r^8$ dependency and the three-body dispersion energy contribution, as in equations (2.41) and (2.42), to the Lennard-Jones potential.

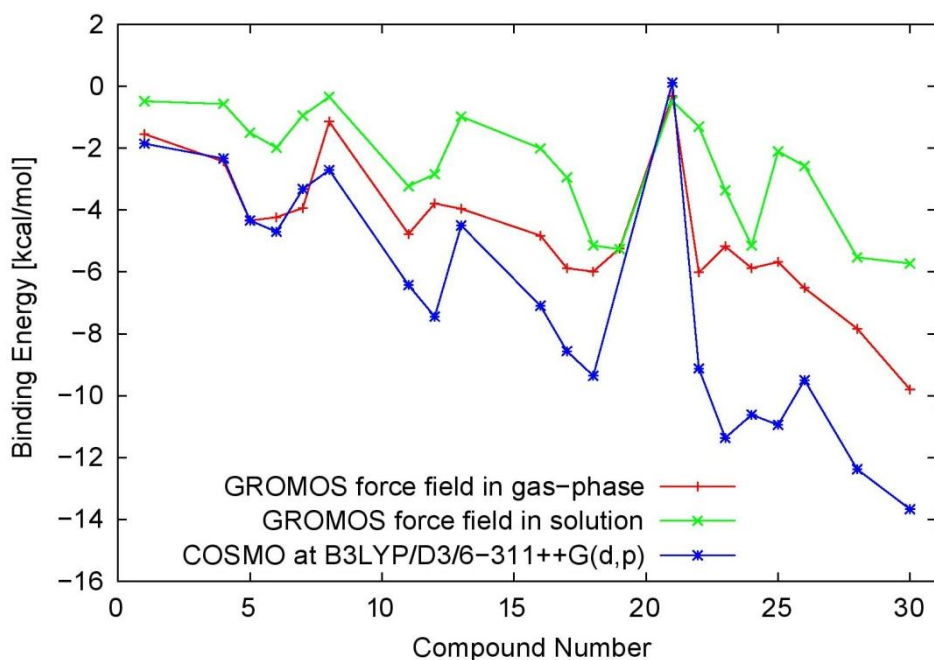


Figure 32. The total binding energies between HCB and the different SOM systems calculated using GROMOS force-field by single point calculations as well as MD simulations, and binding free energies at B3LYP/D3/6-311++G(d,p) using COSMO model.

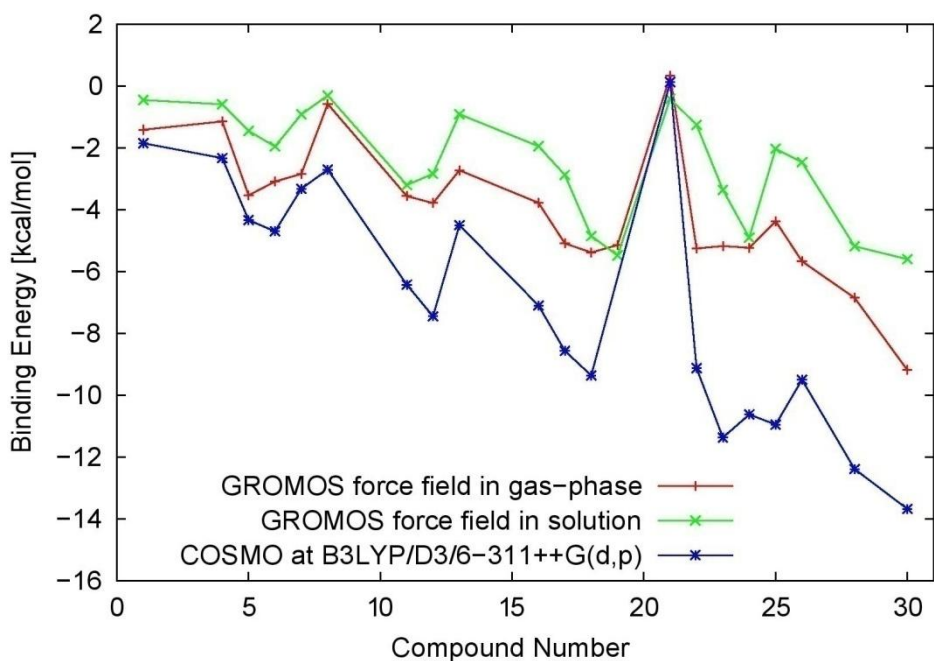


Figure 33. The binding energies due to the dispersion energy of the HCB-SOM complexes calculated using GROMOS force-field by single point calculations as well as MD simulations, and binding free energies at B3LYP/D3/6-311++G(d,p) using COSMO model.

The qualitative agreement of the force-field to DFT-D3 has motivated us to continue and run MD simulations for the same HCB-SOM complexes. The binding energies of these

complexes are calculated every 0.2 fs along 100 ps trajectory. Average of the binding energies along the overall trajectory for each complex is introduced in Figure 32. In addition, the binding energies due to the dispersion interaction are represented in Figure 33. These dispersion binding energies are appeared to be very similar to the total binding energies in Figure 32. This indicates to absence of the electrostatic interaction between HCB and SOM systems in presence of water molecules. A typical trend can be shown by comparing these averages of binding energies to the binding energies obtained from the DFT-D3 calculations. Focusing on both force-field results obtained by gas phase single point calculations and MD simulations in water indicates that the binding energies in these complexes decrease upon solvation. In term of complex SOM, this means that water molecules solvate the different SOM functional groups and blocks the active sites for binding of HCB. This leads to weaken the HCB-SOM interaction and thus decrease the binding energy.

Based on MD trajectories, it has been observed that water molecules solvate both HCB and SOM systems leading to decrease their interaction and thus their binding energies. This can support why the binding free energies obtained from COSMO are smaller than that obtained from gas phase calculations. Generally, this can be explained by number of water molecules in solvation shells which is directly proportional to number of water molecules surrounding each system. It is trivial that increasing number of water molecules and thus decreasing HCB atoms around SOM systems decreases its binding to HCB and vice versa. Along the whole trajectory, number of HCB atoms as well as number of water molecules surrounding each SOM system is averaged. These average numbers with spheres having radii 4, 6, and 8 Å around each SOM systems are given in Figure 34 and Figure 35. The binding energies of these complexes in water can be interpreted in terms number of atoms of HCB as well as water surrounding the SOM system. For first four systems, acetamide (**1**), methanol (**4**), acetaldehyde (**5**), and acetic acid (**6**), the average number inside each sphere (except the sphere of radius 8 Å in case of acetic acid) of HCB neighbour atoms increases and that for water molecules decreases from acetamide to acetic acid. So their binding energies with HCB increase in the same order. Then, the average number of HCB neighbour atoms decreases and that for water molecules increases for dimethylketone (**7**) and methylamine (**8**), so their binding energies decrease than that for first four systems. For methylacetate (**11**) and *n*-butane (**12**), number of water neighbour molecules decreases

and that for HCB increases giving rise to increase in the binding energy. By the same way the decrease and the increase in the binding energy can be explained along the rest of SOM systems. These results can be summarized into increasing the binding energy of HCB to SOM systems by increasing the hydrophobicity of SOM representative systems. Thus, interactions of water molecules to polar SOM systems have been found to be more pronounced than their interactions to HCB. For example, this can be shown in Figure 36 which represents acetic acid system. This Figure shows the HCB-acetic acid, HCB-H₂O molecules, and acetic acid-H₂O molecules binding energies along the overall trajectory. Interactions of water molecules to aromatic SOM systems are less than their interactions to HCB. One example for aromatic systems (methylbenzene) can be shown in Figure 37.

Due to the strong interaction of water to polar SOM systems compared to non-polar SOM, some of polar compounds loss their binding strength to HCB. This leads to weakness or dissociation of their complexes. This behaviour is observed for aliphatic compounds such as acetamide (**1**), methanol (**4**), dimethylketone (**7**), and neutral and charged methylamine (**8,21**) systems. In addition, it has been explored for some complexes containing aromatic compounds having polar character like pyridine (**13**), phenol (**22**), and aniline (**25**). In these weak complexes, the SOM systems and HCB are separated by intermolecular distances in the range of 7.0 to 10.5 Å. For example, dissociation of HCB-acetamide complex takes place at time starting from around 65 ps. Unfortunately, this behaviour cannot be detected using COSMO calculations due to absence of the explicit treatment of solvent molecules. In addition, this behaviour will be completely different in case of using a single macromolecule containing all these functional groups as a SOM model. This is due to the high mass and size which decreases its mobility and diffusion in water and thus prevent dissociation of its complex with the different pollutants. For the rest of SOM systems, stability of their complexes has been detected along the overall trajectory. In these complexes, HCB and SOM systems are separated by intermolecular distances in the range of 3.5 to 6.0 Å.

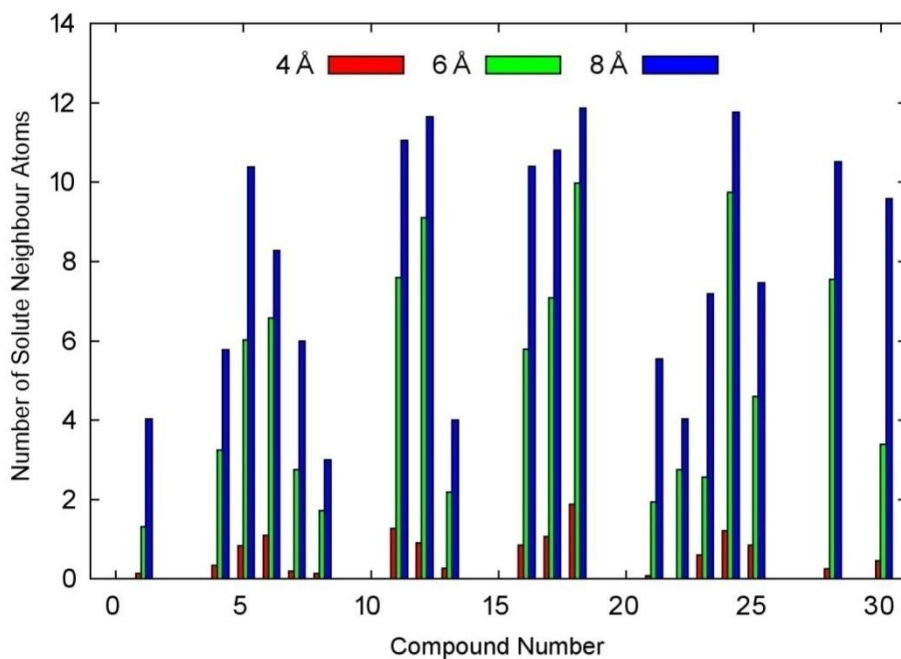


Figure 34. Average number of HCB atoms surrounding the SOM systems in different spheres with radii 4, 6, and 8 Å along 100 ps trajectory.

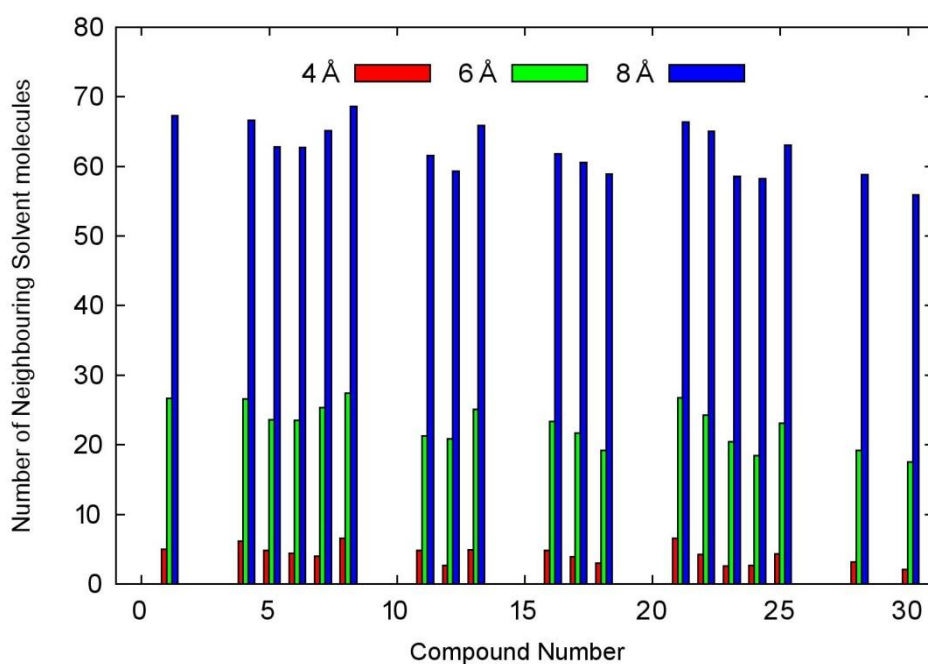


Figure 35. Average number of water atoms surrounding the SOM systems in different spheres with radii 4, 6, and 8 Å along 100 ps trajectory.

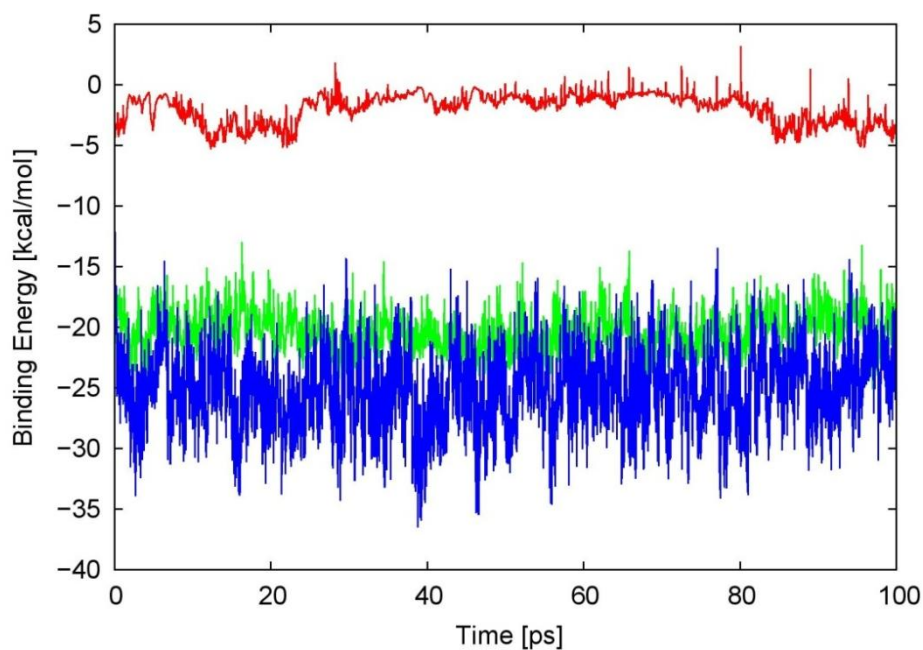


Figure 36. The total binding energies between HCB and acetic acid (red), HCB and water (green), and acetic acid and water (blue) along 100 ps trajectory.

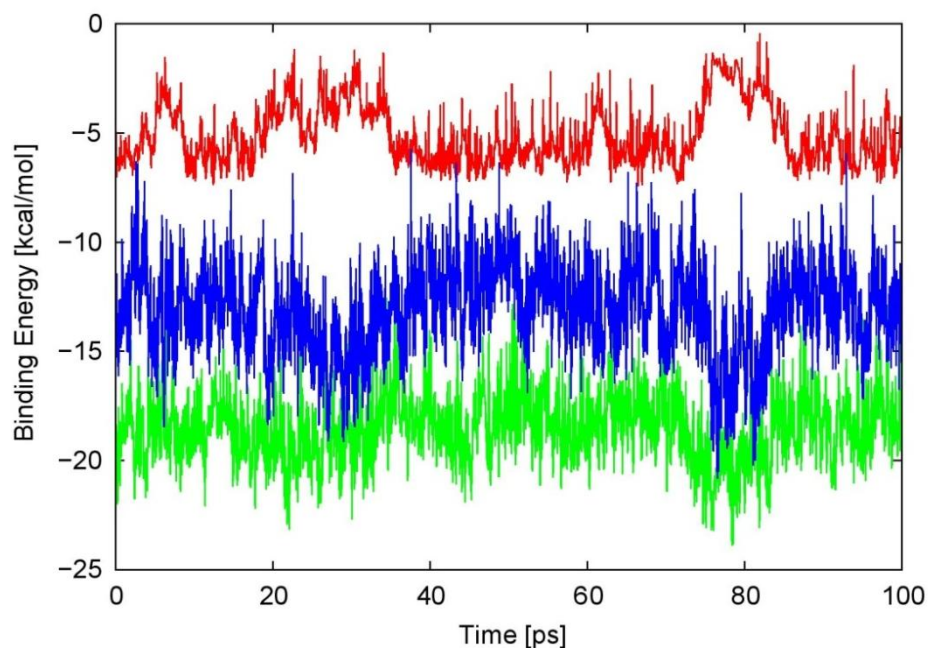


Figure 37. The total binding energies between HCB and methylbenzene (red), HCB and water (green), and methylbenzene and water (blue) along 100 ps trajectory.

5.10. Quantitative Activity-Structure Relationship

The binding free energies of HCB-SOM complexes are correlated to different physical properties of representative SOM systems. This correlation has been done based on the quantitative activity-structure relationship (QSAR). The used binding free energies are those which calculated using COSMO at B3LYP-D3. Several independent descriptors, or in another word physical properties, are checked in this study but those giving rise to the best model are introduced. The most correlated physical properties to the binding free energies are polarizability (P_1), quadrupole (P_2), sum of partial charges on C atoms (P_3), sum of partial charges on N atoms (P_4), molecular-mass (P_5), and molar volume (P_6) of each representative system. The coefficients of equation (3.4), C_0 , C_1 , C_2 , C_3 , C_4 , C_5 , and C_6 , are determined using the multiple-linear regression and given in the following equation.

$$E_B = -2.072 - 0.568P_1 + 0.180P_2 + 1.348P_3 - 0.530P_4 + 0.014P_5 + 0.061P_6 \quad (5.5)$$

The listed binding free energy in the above equation is named as the estimated binding free energy. These estimated binding free energies versus the actual ones are introduced in Figure 38. The fitted parameters of this equation are collected in Table 7. The large value of R^2 , the small difference between R^2 and the adjusted R^2 , and the large value of $F_{\text{statistic}}$ than critical F indicates to a good and an efficient QSAR equation.

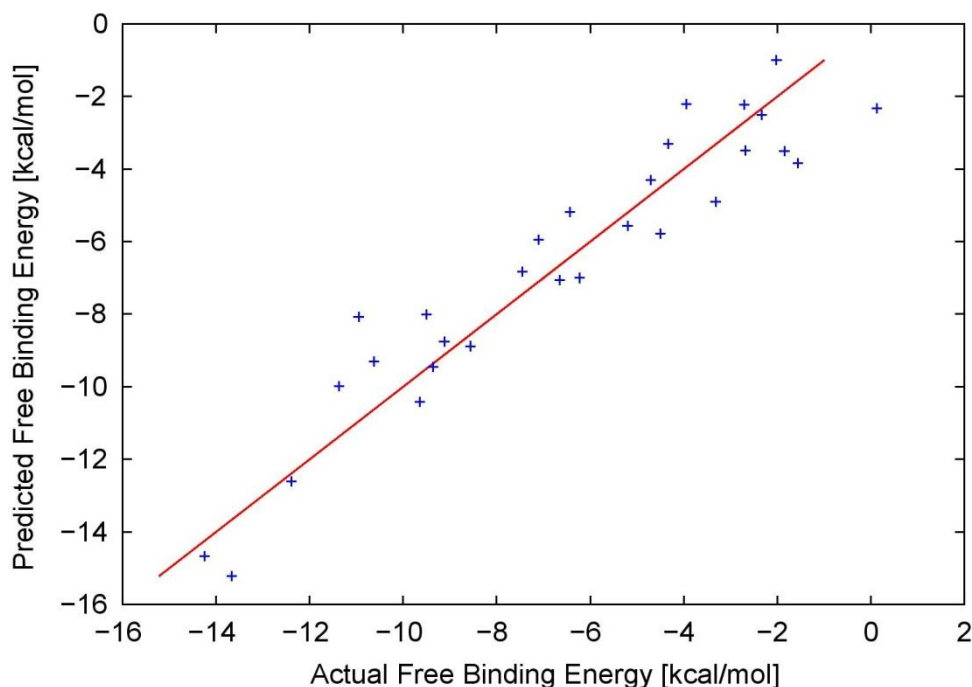


Figure 38. The predicted binding free energies of HCB with the SOM representative systems versus the calculated (actual) binding free energies at B3LYP/D3/6-311++G(d,p) and the red line is a linear correlation plotted as guide for eye.

Since validity of equation (5.5) is proved, correlation as well as contribution of the different descriptors can be introduced. Contribution of each descriptor, in absence of the other descriptors, to the binding free energy is calculated. QSAR analysis indicates that the most correlated descriptors to the binding free energy are the polarizability, sum of the partial charges on C atoms, and the molar volume of the representative SOM systems which contribute to the binding free energy by 79.7%, 29.9%, and 26.4%, respectively. Both polarizability and molar volume of the representative SOM systems are negatively correlated to the binding free energy. On the other hand, sum of the partial charges on C atoms is positively correlated to the binding free energy. This means that increasing the polarizability and/or the molar volume and/or decreasing sum of the partial charges on C atoms of SOM will increase binding of HCB to SOM systems. Moreover, it has been found that the polarizability is highly positively correlated to the molar volume of SOM systems. Sum of the partial charges on C atoms is negatively correlated to N atoms of SOM. The molar volume of SOM has high positive correlation with the molecular mass and the quadrupole SOM systems.

Understanding of nature of HCB-SOM interaction can be highly supported by QSAR. Firstly, since the polarizability of SOM systems is the most predominant property affected this interaction, this means that the dispersion interaction is the predominant type of interaction. This results because the dispersion interaction between to molecular systems is directly proportional to product of their polarizabilities. This confirms what we introduced before about role of dispersion interaction in HCB-SOM complexes. Secondly, importance of the partial charges on C atoms in QSAR indicates the important role of type as well as number of C atoms on binding of HCB to SOM systems. This can support our experimental results i.e. type as well as concentration of C atoms changes the adsorption behaviour. This can be nicely shown in case of the pyrolyzed soil sample compared with the other soil sample. The third point can be conducted from dependence of the binding free energy on molar volume of SOM. This agrees with our theoretical suggestion that in case the subjected surface area of SOM increases, the binding energy increases. Moreover, since the partial charges on C-atoms are negatively correlated with the partial charges on N-atoms, this means that as the partial charges on N-atoms decrease the binding free energy increases. This can be translated into the statement that in case the polarity of SOM system decreases (hydrophobicity increases), its binding to HCB increases. This agrees with what has been obtained before from both quantum mechanical calculations and MD simulations. Due to

agreement and support of QSAR analysis to both experimental and theoretical results, it is highly recommended to use the obtained equation in estimation of binding of HCB to other SOM systems which are not included in our study. Finally, due to significance of the polarizability of SOM systems on HCB-SOM interaction, the respective correlation with the binding free energy is shown in Figure 39.

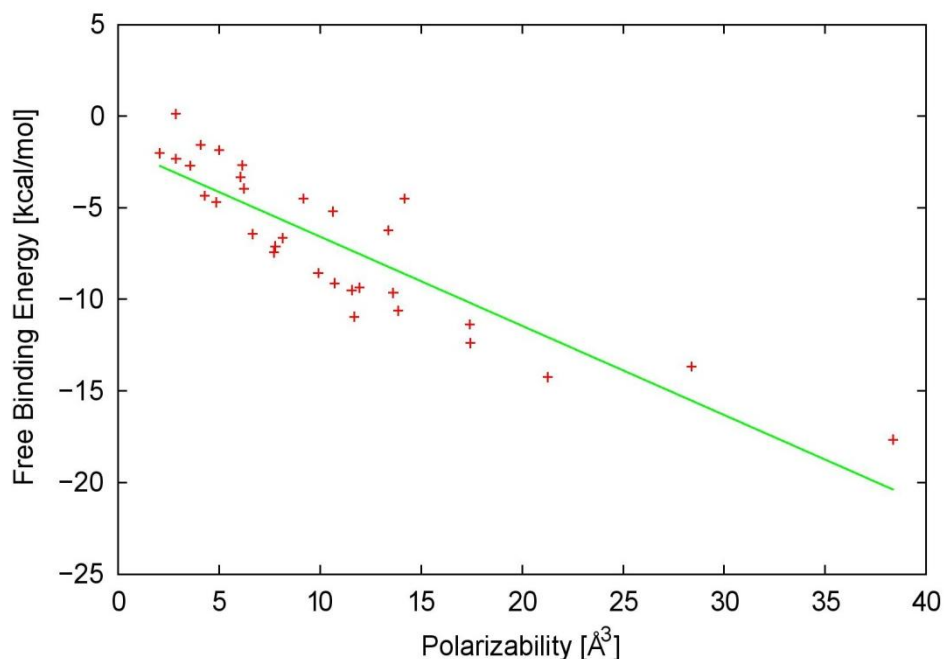


Figure 39. Correlation of the binding free energies for HCB-test set complexes with the polarizability of the test molecule at the B3LYP-D3/6-311++G(d,p) level of theory using COSMO model.

The same descriptors are used to be correlated, using QSAR, with the binding energies obtained from MD simulations. The coefficients of equation (3.4), C_0 , C_1 , C_2 , C_3 , C_4 , C_5 , and C_6 , are given in equation (5.6).

$$E_B = -1.013 - 0.435P_1 + 0.060P_2 + 0.436P_3 - 1.132P_4 + 0.040P_5 + 0.012P_6 \quad (5.6)$$

The fitted parameters of this equation are collected in Table 7. By similarity to the above analysis in case of COSMO binding energy, efficiency of equation (5.6) is indicated. But by comparison of equation (5.6) with equation (5.5), one can find for equation (5.6) that R^2 is smaller, the difference between R^2 and the adjusted R^2 is larger, and $F_{\text{statistic}}$ is smaller than that in case of equation (5.5). This indicates that equation (5.5) is more efficient than equation (5.6). The estimated binding energies from equation (5.6) are plotted, in Figure 40, versus the actual ones.

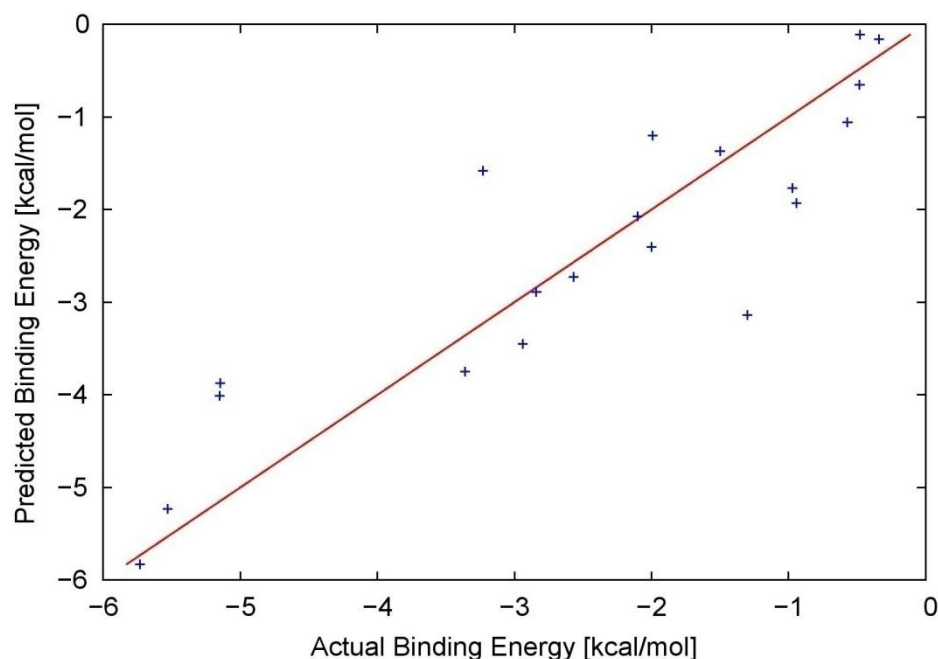


Figure 40. The predicted binding energies of HCB with the SOM representative systems versus the calculated (actual) binding energies from MD simulations and the red line is a linear correlation plotted as guide for eye.

In the following we are focusing on correlations as well as contributions of the different descriptors to the average of binding energy along MD simulations. It has been explored that the binding energy is correlated to the descriptors in the order: polarizability (64.2%) > quadrupole (58.6%) > molecular-mass (55.4%) > molar volume (52.9%) > sum of partial charges on C atoms (39.4%) > sum of partial charges on N atoms (20.5%). The high contributions of the polarizability and the molar volume of SOM system to binding energy fits to the results obtained in case of COSMO DFT-D3 calculations. The low contribution of the C- and N-partial charges with respect to other descriptors indicates to the deficiency of force-field in description of electrostatic interaction compared to the quantum mechanical calculations. The high contribution of the quadrupole moment and its positive correlation to the binding energy indicates to increasing the binding of HCB to SOM by increasing the hydrophobicity of SOM systems. This agrees with what we observed from MD simulations. As the polarity of SOM decreases (or the hydrophobicity increases), number of water molecules surrounding the SOM system decreases and thus the binding energy with HCB increases. Also contribution of molecular-mass of SOM can be highly correlated to stability of HCB-SOM complexes. As the molecular mass of SOM system increases, its motion or mobility in water decreases. This keeps the SOM systems contacted to HCB with small intermolecular distances. In turn this leads to increasing the binding strength of SOM systems to HCB.

Finally, QSAR output can be summarized into: 1- For COSMO calculations and MD simulations, the polarizability and the molar volume of the SOM systems are highly contributing and negatively correlated to the binding energy. 2- Due to ability of the quantum mechanical calculations and deficiency of the force-field approach to describe the electrostatic interaction, the partial charges contribute to the binding energy in the former one more than the latter one. 3- Hydrophobicity of SOM systems, based on values of the quadrupole moments, has shown higher contribution to the binding energy in case of MD simulations than in case of the COSMO calculation.

Table 7. The fitted parameters, correlation of the binding energy with the relevant descriptors, and the most mutual correlated descriptors obtained using QSAR analysis (taking into account that +1.0 and -1.0 indicates to perfect positive and negative correlations, respectively, and 0.0 means that there is no any correlation) in case of COSMO calculations and MD simulations.

fitted parameter	value		correlated descriptor to E_B	correlation value		contribution to E_B (%)		correlated descriptors	correlation value	
	COSMO	MD		COSMO	MD	COSMO	MD		COSMO	MD
SSR	386.31	47.24	P ₁	-0.89	-0.80	79.71	64.20	P ₂ and P ₅	-0.98	-0.99
SSE	45.90	12.43	P ₂	0.43	0.77	18.70	58.58	P ₅ and P ₆	0.98	0.97
SST	432.21	59.66	P ₃	0.55	0.63	29.93	39.36	P ₂ and P ₆	-0.97	-0.98
R ²	89.38%	79.17%	P ₄	-0.31	-0.45	9.47	20.51	P ₁ and P ₆	0.72	0.96
adjusted R ²	86.49%	69.56%	P ₅	-0.46	-0.74	21.44	55.38	P ₁ and P ₅	0.64	0.98
F _{statistic}	30.86	8.24	P ₆	-0.51	-0.72	26.36	52.89	P ₃ and P ₄	-0.61	-0.36
critical F	2.45	2.63						P ₁ and P ₂	-0.60	-0.99

6. SUMMARY AND OUTLOOK

In summary, the interaction of HCB, one of the hazardous POPs, with soil constituents, especially SOM was studied through experimental and computational efforts. Controlled experimental modification of SOM in a well-defined soil sample and investigation of this modification by a multi-methodological approach were established. Well-defined soil samples were prepared by changing the polarity character of SOM in two different ways. Firstly, a HWE fraction was removed from an original soil sample and added into different samples of the same original soil in two different amounts. These amounts are three and six times of the amount of HWE which already included in the original soil sample. Then, we obtained the soil residue (rest of the original soil sample after HWE extraction), soil+3 HWE, and soil+6 HWE samples. Secondly, thermal heating by off-line pyrolysis at 600 °C of the original soil sample was performed. These soil samples were characterized using a combination of Py-FIMS, and C and N K-edge XANES in addition to the elemental analysis. These combined methods showed that the organic matter content in the soil samples followed the order: pyrolyzed soil sample < soil residue sample < original soil sample < soil+3 HWE sample < soil+6 HWE sample < HWE sample. The C=O, aliphatic C in C-OH, carbohydrate hydroxyl, aliphatic nitriles, C=C, C≡C, and aromatic C functional groups, and five and six N-heterocyclic compounds were detected by XANES in these samples. For all samples except the pyrolyzed one, the percentage of organic compound classes had the order: ALKY > PHLM > CHYDR > NCOMP > LIPID > LDIM > PEPTI. Regarding the **SOM** molecular composition, the addition of HWE to the soil sample increased the relative proportions of CHYDR, NCOMP, and PEPTI and decreased ALKY, PHLM, LDIM, and LIPID. Regarding the **total soil** (including all soil constituents), percentage of each compound class, based on the absolute ion intensity, increased in the order: original soil sample < soil+3 HWE sample < soil+6 HWE sample. For each compound class, the differences in the absolute ion intensities between the original soil and soil+3 HWE (ΔAII_1), and between the soil+3 HWE and soil+6 HWE (ΔAII_2) were calculated. It was found that $\Delta AII_1 > \Delta AII_2$ for PHLM, ALKY, CHYDR, NCOMP, and PEPTI while $\Delta AII_1 < \Delta AII_2$ for LIPID and LDIM. Moreover, both PHLM and ALKY have the largest $\Delta AII_1 : \Delta AII_2$ values. On the other hand, pyrolysis enriches the aromatic, unsaturated, N-heterocyclic compounds in addition to charcoal production. These differences in the chemical composition between the different soil samples have a significant effect on the fate of HCB in soil which can be determined through adsorption measurements.

Adsorption of HCB on the pyrolyzed soil, original soil, soil+3 HWE, and soil+6 HWE samples was studied by batch-experiments. The adsorption data were fitted to both Langmuir and Freundlich equations and yielded squared correlation coefficients (r^2) close to one. The adsorption of HCB increased upon addition of HWE in the order: original soil sample < soil+3 HWE sample < soil+6 HWE sample. Adsorption of HCB on the pyrolyzed soil sample exceeded that of soil+6 HWE at low initial concentrations. By increasing HCB concentration, adsorption of HCB on the pyrolyzed soil sample became lower. It was observed that at each initial concentration the difference in the adsorbed concentrations between the original soil and soil+3 HWE (X_2-X_1) is larger than that between the soil+3 HWE and soil+6 HWE (X_3-X_2). These differences were correlated to the ΔAII_1 and ΔAII_2 . This correlation suggested that both PHLM and ALKY are more important for adsorption of HCB on soil samples modified by addition of HWE fractions. The unsaturated, substituted aromatic, and heterocyclic compounds besides charcoal are the most effective compounds type controlling adsorption of HCB on the pyrolyzed soil sample.

For a molecular-level understanding of this interaction, a new approach for SOM modelling has been developed to study interaction of HCB to SOM. SOM has been modelled by separate representative systems covering most of the functional groups and the compound classes in SOM. A test set has been constructed with 32 representative soil constituents especially SOM including PHLM, ALKY, CHYDR, PEPTI, NCOMP, and LIPID. Based on XANES results the most predominant functional groups have been added to the model. In addition, coronene and silicon hydroxide trimer have been added to study effect of soil pyrolysis on adsorption of HCB. Complexes of HCB with the representative systems have been built by selecting the most chemically favorable configuration for each complex. The three-dimensional geometries of HCB, the individual representative systems, and their complexes have been optimized in gas phase as well as using COSMO model.

Geometry optimization in gas phase has shown that convergence of structures takes place at the 6-31++G basis set. Effect of dispersion has been included using HF, B3LYP, B3LYP-D2, and B3LYP-D3. In general, HF and B3LYP have shown positive binding energies which are completely different with respect to B3LYP-D2 and B3LYP-D3. Stability of HCB-SOM complexes at the different levels has the order: B3LYP-D3 > B3LYP-D2 > B3LYP > HF. The dispersion interactions, compared with the electrostatic interactions, have introduced a great contribution to the total binding energies. Effect of different basis sets at B3LYP-D3

has investigated that 6-311++G(2d,2p) is sufficient basis set to describe HCB-SOM interaction. Effect of different DFT-functionals including dispersion correction D3 such as BLYP-D3, B3LYP-D3, B3LYP5-D3, and CAMB3LYP-D3 at 6-311++G(2d,2p) shows similar behaviors for all the used DFT-functionals. Furthermore, validity of DFT-Results as well as neglecting the BSSE correction has been explored using MP2 and CCSD.

HCB interacts mainly through its positively charged hydrophobic ring center with the negatively charged center of most modelled systems. It has been explored that HCB has not the ability of covalent bond formation with the SOM model set. The quantum mechanical calculations, whatever in gas phase or using COSMO solvation model, mainly draw the same picture for HCB-SOM interaction. It has been explored that HCB binds in the order: substituted polycyclic aromatic compounds > lignin monomers > long chain alkanes > substituted benzenes ~ long chain alkenes > phenols > short chain alkanes > five membered heterocyclic ring compounds > short chain alkenes ~ esters > carbohydrates > peptides > six membered heterocyclic ring compounds > polar aliphatic compounds. Generally, this indicates that i- As the subjected surface area for the modelled system increases, binding of HCB increases as well, ii- HCB binds to aromatic and non-polar aliphatic compounds stronger than to polar aliphatic compounds; iii- HCB binds polycyclic aromatic compounds stronger than monocyclic aromatic compounds. Moreover, it has been explored that the solvation reduces the binding of HCB to the modelled systems due to stabilization of both components by water. Furthermore, the dispersion interaction appeared to be the predominant type of interaction.

Correlation of the computational outcome to the experimental one has been established. It has been found that the binding energy differences of HCB between original soil and soil+3 HWE samples ($E_{B,3HWE} - E_{B,org}$) is larger than that between soil+3 HWE and soil+6 HWE samples ($E_{B,6HWE} - E_{B,3HWE}$) which is in accord with the experimental observation that $X_2 - X_1 > X_3 - X_2$. This indicates that PHLM and ALKY compound classes are dominating the adsorption behaviour of HCB on the considered soil samples. For the pyrolyzed soil sample, due to the high organic character, it binds HCB stronger than the other soil samples. By increasing HCB concentration, the pyrolyzed soil sample is saturated before the other soil samples. This is due to its low SOM content compared to the other soil samples. This leads to gradual decrease in the adsorption of HCB on the pyrolyzed soil sample compared to the other soil samples. This can be supported by the low value of Freundlich exponent n .

MD simulations have been performed for some HCB-SOM complexes. Their calculated binding energies of HCB-SOM complexes draw a picture for description of HCB-SOM interaction similar to that obtained using DFT-D3. This indicates to validity of the force-field to describe this type of interaction. It has been observed that water molecules solvate both HCB and SOM systems leading to decrease their binding and thus their interaction energies. Moreover, water molecules interact with polar SOM systems > HCB > non-polar and aromatic SOM systems. This leads to dissociation of some complexes containing SOM systems with polar character such as acetamide, neutral and charged methylamine, dimethylketone, methanol, aniline, phenol, and pyridine systems. For the rest of SOM systems, stability of their complexes has been observed over the all trajectory which kept by intermolecular distances with HCB in range of 2.7 to 6.0 Å. Finally, using QSAR analysis it has been explored that the polarizability, molecular volume and mass, charges and percentage of the C atoms, and quadrupole moments of SOM systems are the most vital parameters controlling this interaction.

Based on the above summarized outcomes of the research, one can introduce the following recommendations:

1. The combination of elemental analysis, Py-FIMS, C-XANES, and N-XANES is well-suited to explore intended modifications of the molecular-level composition of SOM in a soil sample. Therefore, this combination of analytical techniques can be recommended for similar problems that require characterizing the bulk, non-extracted SOM instead of pre-selected compounds or compound classes.
2. Since off-line pyrolysis has been altered the SOM more intensively than stepwise addition of HWE fractions, it would be desirable to have more pyrolyzed samples with a smaller graduation in heat impact to get a refined picture of gradually changing SOM properties and their effect on the pollutant binding.
3. Since the computational results, based on our developed SOM model, substantiate the experimental conclusions, this model can be recommended for further studies focusing on interaction of different xenobiotics to SOM.
4. We recommend use of the most efficient and less computationally demand DFT combined with D3 dispersion correction for studying similar problems.

5. Based on the deep understanding of the HCB-SOM interaction, suitable remediation procedures for HCB can be selected (for example, highly organic character compounds like biochar can be used to immobilize HCB in the contaminant areas).

To focus research on the most urgent gaps in knowledge pollutants-SOM interaction, I propose the following directions for future work to put this research area forward:

1. Selection of different pollutants and study of their interactions with our SOM model.
2. Calculation of the binding free energies in solution of these pollutants with our SOM model.
3. Expansion of this model to huge single molecule of SOM and study its binding free energy with the different pollutants.

REFERENCES

1. Ritter, L.; Solomon, K. R.; Forget, J.; Stemeroff, M.; O'Leary, C. Persistent organic pollutants: An Assessment Report on DDT, Aldrin, Dieldrin, Endrin, Chlordane, Heptachlor, Hexachlorobenzene, Mirex, Toxaphene, Polychlorinated Biphenyls, Dioxins, and Furans. *United Nations Environment Programme Retrieved* **2007**.
2. Jones, K. C.; de Voogt, P. Persistent organic pollutants (POPs): state of the science. *Environ. Pollut.* **1999**, *100*, 209–221.
3. <http://www.eugris.info/FurtherDescription.asp?Ca=2&Cy=0&T=Diffuse%20pollution&e=91>
4. Senesi, N.; Loffredo, E. The fate of anthropogenic organic pollutants in soil: adsorption/desorption of pesticides possessing endocrine disruptor activity by natural organic matter (Humic Substances). *J. Soil Sci. Plant Nutr.* **2008**, *8*, 92–94.
5. <http://en.wikipedia.org/wiki/Biofertilizer>
6. Bollag, J.-M.; Myers, C. J.; D. Minard, R. D. Biological and chemical interactions of pesticides with soil organic matter. *Sci. Total Environ.* **1992**, *123/124*, 205-217.
7. Weber, W. J.; McGinley, P. M.; Katz, L. E. Sorption phenomena in subsurface system: concepts, models and effects on contaminant fate and transport. *Water Res.* **1991**, *25*, 499–528.
8. Chen, Y. X.; Chen, H. L.; Xu, Y. T.; Shen, M. W. Irreversible sorption of pentachlorophenol to sediments: experimental observation. *Environ. Int.* **2004**, *30*, 31–37.
9. Chiou, C. T.; Porter, P. E.; Schmedding, D. W. Partitioning equilibria of nonionic compounds between soil organic matter and water. *Environ. Sci. Technol.* **1983**, *17*, 227–231.
10. Gerzabek, M. H.; Aquino, A. J. A.; Haberhauer, G.; Tunega, D.; Lischka Molecular modelling-opportunities for soil research. *Bodenkultur* **2001**, *52*, 133.
11. Schaumann, G. E.; Thiele-Bruhn, S. Molecular modeling of soil organic matter: Squaring the circle? *Geoderma* **2011**, *166*, 1–14.
12. Birkeland, Peter W. Soils and Geomorphology. 3rd edition. New York: Oxford University Press, **1999**.
13. Chesworth, Edited by Ward (2008), Encyclopedia of soil science, Dordrecht, Netherlands: Springer, xxiv
14. Voroney, R. P., **2006**. "The Soil Habitat". In Soil Microbiology, Ecology and Biochemistry, Eldor A. Paul ed.
15. James A. Danoff-Burg, Columbia University. The Terrestrial Influence: Geology and Soils.
16. McCarthy, David F. (1982). Essentials of Soil Mechanics and Foundations: Basic Geotechnics (2nd ed.). Reston, Virginia: Reston Publishing.
17. Soil Survey Division Staff (1993). "Soil Structure". Handbook 18. Soil survey manual. Soil Conservation Service. U.S. Department of Agriculture. Archived from the original on 16 March 2008. Retrieved 8 July 2008.
18. Donahue, R. L.; Miller, R. W.; Shickluna, J. C. **1977**. Soils: An Introduction to Soils and Plant Growth. Prentice-Hall.
19. Taylor, S. A.; Ashcroft, G. L. **1972**. Physical Edaphology
20. Stevenson, F. J. Humus chemistry. New York: John Wiley and Sons, **1982**.

-
21. Schulten, H.-R. Analytical pyrolysis of humic substances and soils: geochemical, agricultural and ecological consequences. *J. Anal. Appl. Pyrolysis* **1993**, *25*, 97-122.
 22. http://agsci.psu.edu/elearning/course-samples/soils_101/Ln_3/L3_2.htm
 23. <http://en.wikipedia.org/wiki/Soil>
 24. <http://en.wikipedia.org/wiki/Lignin>
 25. Sorge, C.; Müller, R.; Leinweber, P.; Schulten, H.-R. Pyrolysis-mass spectrometry of whole soils, soil particle size fractions, litter materials and humic substances: statistical evaluation of sample weight, residue, volatilized matter and total ion intensity. *Fresenius J. Anal. Chem.* **1993**, *346*, 697-703.
 26. Schnitzer, M.; Schulten, H.-R. Analysis of organic matter in soil, extracts, and whole soils by pyrolysis mass spectrometry. *Adv. Agron.* **1995**, *55*, 167-217.
 27. Schnitzer, M.; McArthur, D. F. E.; Schulten, H.-R.; Kozak, L. M.; Huang, P. M. Long-term cultivation effects on the quantity and quality of organic matter in selected Canadian prairie soils. *Geoderma* **2006**, *130*, 141-156.
 28. Haider, K.; Schulten, H.-R. Pyrolysis field ionization mass spectrometry of lignins, soil humic compounds and whole soil. *J. Anal. Appl. Pyrolysis* **1985**, *8*, 317-31.
 29. Melnitchouck, A.; Leinweber, P.; Eckhardt, K.-U.; Beese, R. Qualitative differences between day- and night-time rhizodeposition in maize (*Zea mays* L.) as investigated by pyrolysis-field ionization mass spectrometry. *Soil Biol. Biochem.* **2005**, *37*, 155-62.
 30. Kuzyakov, Y.; Leinweber, P.; Saponov, D.; Eckhardt, K.-U. Qualitative assessment of rhizodeposits in non-sterile soil by analytical pyrolysis. *J. Plant Nutr. Soil Sci.* **2003**, *166*, 719-723.
 31. Schulten, H.-R.; Leinweber, P. New insights into organic-mineral particles: composition, properties and models of molecular structure. *Biol. Fertil. Soils* **2000**, *30*, 399.
 32. Leinweber, P.; Schulten, H.-R. Advances in analytical pyrolysis of soil organic matter. *J. Anal. Appl. Pyrolysis* **1999**, *49*, 359-83.
 33. Wilcken, H.; Sorge, C.; Schulten, H.-R. Molecular composition and chemometric differentiation and classification of soil organic matter in podzol B-horizons. *Geoderma* **1997**, *76*, 193-219
 34. Lehmann, J.; Solomon, D. Organic carbon chemistry in soils observed by synchrotron-based spectroscopy, synchrotron-based techniques in soils and sediments. *Dev. Soil Sci.* **2010**, *34*, 289-312.
 35. Leinweber, P.; Kruse, J.; Walley, F.; Gillespie, A.; Eckhardt, K.-U.; Blyth, R. I. R, et al. Nitrogen compounds in dissolved and solid environmental samples, synchrotron-based techniques in soils and sediments. *Dev. Soil Sci.* **2010**, *34*, 255-288.
 36. Vairavamurthy, A.; Wang, S. Organic nitrogen in geomacromolecules: insights on speciation and transformation with K-edge XANES spectroscopy. *Environ. Sci. Technol.* **2002**, *36*, 3050-3056.
 37. Christl, I.; Kretzschmar, R. C-1s NEXAFS spectroscopy reveals chemical fractionation of humic acid by cation-induced coagulation. *Environ. Sci. Technol.* **2007**, *41*, 1915-1920.
 38. Kinyangi, J.; Solomon, D.; Liang, B. I.; Lerotic, M.; Wirrick, S.; Lehmann, J. Nanoscale biogeocomplexity of the organomineral assemblage in soil: application of STXM microscopy and C 1s-NEXAFS spectroscopy. *Soil Sci. Soc. Am. J.* **2006**, *70*, 1708-1718.
-

-
39. Solomon, D.; Lehmann, J.; Kinyangi, J.; Liang, B. Q.; Schafer, T. Carbon K-edge NEXAFS and FTIR-ATR spectroscopic investigation of organic carbon speciation in soils. *Soil Sci. Soc. Am. J.* **2005**, *69*, 107–119.
 40. Kruse, J.; Eckhardt, K.-U.; Regier, T.; Leinweber, P. TG-FTIR, LC/MS, XANES and Py-FIMS to disclose the thermal decomposition pathways and aromatic N formation during dipeptide pyrolysis in a soil matrix. *J. Anal. Appl. Pyrolysis* **2011**, *90*, 164–173.
 41. Leinweber, P.; Kruse, J.; Walley, F. L.; Gillespie, A.; Eckhardt, K.-U.; Blyth, R.; Regier, T. Nitrogen K-edge XANES: an overview of reference compounds used to identify ‘unknown’ organic nitrogen in environmental samples. *J. Synchrotron Radiat.* **2007**, *14*, 500–511.
 42. Gillespie, A. W.; Walley, F. L.; Farrell, R. E.; Leinweber, P.; Schlichting, A.; Eckhardt, K.-U.; Regier, T. Z.; Blyth, R. Profiling rhizosphere chemistry: evidence from carbon and nitrogen K-edge XANES and pyrolysis-FIMS. *Soil Sci. Soc. Am. J.* **2009**, *73*, 2002–12.
 43. Leinweber, P.; Walley, F.; Kruse, J.; Jandl, G.; Eckhardt, K.-U.; Blyth, R. I. R.; Regier, T. Cultivation affects soil organic nitrogen: pyrolysis-mass spectrometry and nitrogen K-edge XANES spectroscopy evidence. *Soil Sci. Soc. Am. J.* **2009**, *73*, 82–92.
 44. Khan, S. U. **1978**. The interaction of organic matter with pesticides. In: Schnitzer, M.; Khan, S. U. (Eds), *Soil Organic Matter*. Elsevier Scientific, New York, 138-171.
 45. Pignatello, J. J. Sorption dynamics of organic compounds in soils and sediments. In: B.L. Sawhney and K. Brown (Eds), *Reactions and Movement of Organic Chemicals in Soils*. *Soil Sci. Soc. Am.* **1989**, *22*, 45-80.
 46. Calderbank, A. The occurrence and significance of bound pesticide residues in soil. *Rev. Environ. Contam. Toxicol.* **1989**, *108*, 71-103.
 47. Hsu, T. S.; Bartha, R. Biodegradation of chloroaniline humus complexes in soil and in culture solution. *Soil Sci.* **1974**, *118*, 213-219.
 48. Bollag, J.-M.; Blattmann, P.; Laanio, T. Adsorption and transformation of four substituted anilines in soil. *J. Agric. Food Chem.* **1978**, *26*, 1302-1306.
 49. Helling, C. S.; Krivonak, A. E. Physiochemical characteristics of bound dinitroaniline herbicides in soil. *J. Agric. Food Chem.* **1978**, *26*, 1156-1163.
 50. Saxena, A.; Bartha, R. Microbial mineralization of humic acid 3,4-dichloroaniline with natural organics and microbes. *Soil Biol. Biochem.* **1983**, *15*, 59-62.
 51. Grimme, S.; Ehrlich, S.; Goerigk, L. Effect of the damping function in dispersion corrected density functional theory. *J. Comput. Chem.* **2011**, *32*, 1456–1465.
 52. Brunsveld, L.; Folmer, B. J. B.; Meijer, E. W.; Sijbesma, R. P. Supramolecular Polymers. *Chem. Rev.* **2001**, *101*, 4071-4097.
 53. Grimme, S. Improved second-order Møller–Plesset perturbation theory by separate scaling of parallel- and antiparallel-spin pair correlation energies. *J. Chem. Phys.* **2003**, *118*, 9095.
 54. Takatani, T.; Hohenstein, E. G.; Sherrill, C. D. Improvement of the coupled-cluster singles and doubles method via scaling same- and opposite-spin components of the double excitation correlation energy. *J. Chem. Phys.* **2008**, *128*, 124111-124117.
-

-
55. Tkatchenko, A.; DiStasio, R. A. Jr.; Head-Gordon, M.; Scheffler, M. Dispersion-corrected Møller-Plesset second-order perturbation theory. *J. Chem. Phys.* **2009**, *131*, 094106-094112.
 56. Sherrill, C. D.; Takatani, T.; Hohenstein, E. G. An Assessment of Theoretical Methods for Nonbonded Interactions: Comparison to Complete Basis Set Limit Coupled-Cluster Potential Energy Curves for the Benzene Dimer, the Methane Dimer, Benzene-Methane, and Benzene-H₂S. *J. Phys. Chem. A* **2009**, *113*, 10146-10159.
 57. Raghavachari, K.; Trucks, G. W.; Pople, J. A.; Head-Gordon, M. A fifth-order perturbation comparison of electron correlation theories. *Chem. Phys. Lett.* **1989**, *157*, 479-483.
 58. Grimme, S. Semiempirical GGA-type density functional constructed with a long-range dispersion correction. *J. Comput. Chem.* **2006**, *27*, 1787-1799.
 59. Grimme, S.; Antony, J.; Ehrlich, S.; Krieg, H. A consistent and accurate ab initio parametrization of density functional dispersion correction (DFT-D) for the 94 elements H Pu. *J. Chem. Phys.* **2010**, *132*, 154104-154122.
 60. Piccolo, A. The supramolecular structure of humic substances: A novel understanding of humus chemistry and implications in soil science; **2002**, *75*, 57-134.
 61. Sutton, R.; Sposito, G. Molecular Structure in Soil Humic Substances: The New View. *Environ. Sci. Technol.* **2005**, *39*, 9009.
 62. Schaumann, G. E. Soil organic matter beyond molecular structure Part I: Macromolecular and supramolecular characteristics. *J. Plant Nutr. Soil Sci.* **2006**, *169*, 145.
 63. Kubicki, J. D. Molecular Simulations of Benzene and PAH Interactions with Soot. *Environ. Sci. Technol.* **2006**, *40*, 2298-2303.
 64. Lock, P. A.; Skipper, N. T. Computer simulation of the structure and dynamics of phenol in sodium montmorillonite hydrates. *Eur. J. soil. Sci.* **2007**, *58*, 958.
 65. Jardat, M.; Dufreche, J.-F.; Marry, V.; Rotenberg, B.; Turq, P. Salt exclusion in charged porous media: a coarse-graining strategy in the case of montmorillonite clays. *Phys. Chem. Chem. Phys.* **2009**, *11*, 2023.
 66. Kwon, K. D.; Kubicki, J. D. Molecular Orbital Theory Study on Surface Complex Structures of Phosphates to Iron Hydroxides: Calculation of Vibrational Frequencies and Adsorption Energies. *Langmuir* **2004**, *20*, 9249-9254.
 67. Paul, K. W.; Kubicki, J. D.; Sparks, D. L. Quantum Chemical Calculations of Sulfate Adsorption at the Al- and Fe-(Hydr)oxide-H₂O Interface Estimation of Gibbs Free Energies. *Environ. Sci. Technol.* **2006**, *40*, 7717-7724.
 68. Tribe, L.; Kwon, K. D.; Trout, C. C.; Kubicki, J. D. Molecular Orbital Theory Study on Surface Complex Structures of Glyphosate on Goethite: Calculation of Vibrational Frequencies. *Environ. Sci. Technol.* **2006**, *40*, 3836-3841.
 69. Kubicki, J. D.; Kwon, K. D.; Paul, K. W.; Sparks, D. L. Surface complex structures modeled with quantum chemical calculations: carbonate, phosphate, sulphate, arsenate and arsenite. *Eur. J. soil. Sci.* **2007**, *58*, 932-944.
 70. Zhu, M.; Paul, K. W.; Kubicki, J. D.; Sparks, D. L. Quantum Chemical Study of Arsenic (III, V) Adsorption on Mn-Oxides: Implications for Arsenic (III) Oxidation. *Environ. Sci. Technol.* **2009**, *43*, 6655-6661.
-

-
71. Aquino, A. J.; Tunega, D.; Haberhauer, G.; Gerzabek, M. H.; Lischka, H. Acid-base properties of a goethite surface model: A theoretical view. *Geochim. Cosmochim. Ac.* **2008**, *72*, 3587–3602.
 72. Tunega, D.; Gerzabek, M. H.; Haberhauer, G.; Totsche, K. U.; Lischka, H. Model study on sorption of polycyclic aromatic hydrocarbons to goethite. *J. Colloid Interface Sci.* **2009**, *330*, 244–249.
 73. Tunega, D.; Aquino, A. J. A.; Haberhauer, G.; Gerzabek, M. H.; Lischka, H. Hydrogen bonds and solvent effects in soil processes: a theoretical view. In *Solvation Effects on Molecules and Biomolecules*; Canuto, S., Ed. Springer: Berlin, **2008**, 1–27.
 74. Aquino, A. J. A.; Tunega, D.; Haberhauer, G.; Gerzabek, M. H.; Lischka, H. Interaction of the 2,4-dichlorophenoxyacetic acid herbicide with soil organic matter moieties: a theoretical study. *Eur. J. soil. Sci.* **2007**, *58*, 889–899.
 75. Aquino, A. J.; Tunega, D.; Pasalic, H.; Haberhauer, G.; Gerzabek, M. H.; Lischka, H. The thermodynamic stability of hydrogen bonded and cation bridged complexes of humic acid models-A theoretical study. *Chem. Phys.* **2008**, *349*, 69–76.
 76. Aquino, A. J. A.; Tunega, D.; Schaumann, G. E.; Haberhauer, G.; Gerzabek, M. H.; Lischka, H. Stabilizing Capacity of Water Bridges in Nanopore Segments of Humic Substances: A Theoretical Investigation. *J. Phys. Chem. C* **2009**, *113*, 16468–16475.
 77. Schulten, H. R.; Schnitzer, M. Three-dimensional models for humic acids and soil organic matter. *Naturwissenschaften* **1995**, *82*, 487–498.
 78. Schulten, H.-R.; Schnitzer, M. Chemical Model Structures for Soil Organic Matter and Soils. *Soil Sci.* **1997**, *162*, 115-130.
 79. Schulten, H.-R.; Leinweber, P. New insights into organic-mineral particles: composition, properties and models of molecular structure. *Biol. Fertil. Soils* **2000**, *30*, 399-432.
 80. Schulten, H.-R. New approaches to the molecular structure and properties of soil organic matter: Humic-, xenobiotic-, biological-, and mineral bonds. *Developments in Soil Science* **2002**, *28 A*, 351-381.
 81. Ahmed, A. A.; Kühn, O.; Leinweber, P. How Soil Organic Matter Controls Hexachlorobenzene-Soil Interactions: Adsorption Isotherms and Quantum Chemical Modelling. *Submitted*.
 82. Ahmed, A. A.; Kühn, O.; Leinweber, P. Controlled experimental soil organic matter modification for study of organic pollutant interactions in soil. *Sci. Total Environ.* **2012**, *441*, 151–158.
 83. Ahlrichs, A.; Bär, M.; Häser, M.; Horn, H.; Kölmel, C. Electronic structure calculations on workstation computers: The program system Turbomole. *Chem. Phys. Lett.* **1989**, *162*, 165-169.
 84. Lee, C.; Yang, W.; Parr, R. G. Development of the Colle-Salvetti correlation-energy formula into a functional of the electron density. *Phys. Rev. B* **1988**, *37*, 785–789.
 85. Vosko, S. H.; Wilk, L.; Nusair, M. Accurate spin-dependent electron liquid correlation energies for local spin density calculations: A critical analysis. *Can. J. Phys.* **1980**, *58*, 1200-1211.
 86. Yanai, T.; Tew, D.; Handy, N. A new hybrid exchange-correlation functional using the Coulomb-attenuating method (CAM-B3LYP). *Chem. Phys. Lett.* **2004**, *393*, 51-57.
 87. Feller, D. The role of databases in support of computational chemistry calculations. *J. Comp. Chem.* **1996**, *17*, 1571-1586.
-

-
88. Schuchardt, K.L.; Didier, B.T.; Elsethagen, T.; Sun, L.; Gurumoorthi, V.; Chase, J.; Li, J.; Windus, T.L. Basis Set Exchange: A Community Database for Computational Sciences. *J. Chem. Inf. Model.* **2007**, *47*, 1045-1052.
 89. Hehre, W.J.; Ditchfield, R.; Pople, J. A. Self-Consistent Molecular Orbital Methods. XII. Further Extensions of Gaussian-Type Basis Sets for Use in Molecular Orbital Studies of Organic Molecules. *J. Chem. Phys.* **1972**, *56*, 2257.
 90. Clark, T.; Chandrasekhar, J.; Spitznagel, G.W.; Schleyer, P.V.R. Efficient diffuse function augmented basis sets for anion calculations. III. The 3-21+G basis set for first-row elements, Li-F. *J. Comp. Chem.* **1983**, *4*, 294-301.
 91. Krishnan, R.; Binkley, J.S.; Seeger, R.; Pople, J.A. Self-consistent molecular orbital methods. XX. A basis set for correlated wave functions. *J. Chem. Phys.* **1980**, *72*, 650-654.
 92. Dunning, T. H. Gaussian basis sets for use in correlated molecular calculations. I. The atoms boron through neon and hydrogen. *J. Chem. Phys.* **1989**, *90*, 1007-1023.
 93. Head-Gordon, M.; Pople, J. A. MP2 energy evaluation by direct methods. *Chem. Phys. Lett.* **1988**, *153*, 503-506.
 94. Nantasenamat, C.; Isarankura-Na-Ayudhya, C.; Prachayasittikul, V. Advances in computational methods to predict the biological activity of compounds. *Expert Opin. Drug Discov.* **2010**, *5*, 633-654.
 95. Born, M.; Oppenheimer, R. Zur Quantentheorie der Molekeln. *Ann. Phys.* **1927**, *84*, 457-484.
 96. A. Szabo and N. S. Ostlund. *Modern Quantum Chemistry: Introduction to Advanced Electronic Structure Theory*. Macmillan, New York **1982**.
 97. <http://www.shodor.org/chemviz/basis/students/slater.html>
 98. Hartree, D. R. The wave mechanics of an atom with a non-coulomb central field. Part II-Results and discussion. *Proc. Cambridge Phil. Soc.* **1928**, *24*, 111-132.
 99. Roothan, C. C. J. New Developments in Molecular Orbital Theory. *Rev. Mod. Phys.* **1951**, *23*, 69-89.
 100. Löwdin, P. O. On the Non-Orthogonality Problem Connected with the Use of Atomic Wave Functions in the Theory of Molecules and Crystals. *J. Chem. Phys.* **1950**, *18*, 365-375.
 101. Møller, C.; Plesset, M. S. Note on an Approximation Treatment for Many-Electron Systems. *Phys. Rev.* **1934**, *46*, 618-622.
 102. Hohenberg, P.; Kohn, W. Inhomogenous Electron Gas. *Phys. Rev.* **1964**, *136*, B864-B871.
 103. Kohn, W.; Sham, L. J. Self-Consistent Equations Including Exchange and Correlation Effects. *Phys. Rev.* **1965**, *140*, A1133-A1138.
 104. Slater, J. C. *Quantum Theory of Molecules and Solids*, Vol. 4. MacGraw-Hill, New York **1974**.
 105. Becke, A. D. J. Density-functional exchange-energy approximation with correct asymptotic behavior. *Phys. Rev.* **1988**, *A38*, 3098-30100.
 106. Burke, K.; Perdew, J. P.; Wang, Y. *Electronic Density Functional Theory: Recent Progress and New Directions*. Plenum **1998**.
 107. Becke, A. D. J. Density-functional thermochemistry. III. The role of exact exchange. *Chem. Phys.* **1993**, *98*, 5648-5652.
-

-
108. Lee, C.; Yang W.; Parr, R. G. Development of the Colle-Salvetti correlation-energy formula into a functional of the electron density. *Phys. Rev.***1988**, *B37*, 785-789.
 109. Grimme, S. Accurate description of van der Waals complexes by density functional theory including empirical corrections. *J. Comput. Chem.***2004**, *25*, 1463-1473.
 110. Schäfer, A.; Klamt, A.; Sattel, D.; Lohrenz, J.; Eckert, F. COSMO Implementation in TURBOMOLE: Extension of an efficient quantum chemical code towards liquid systems. *Phys. Chem. Chem. Phys.***2000**, *2*, 2187-2193.
 111. Oostenbrink, C.; Villa, A.; Mark, A. E.; Van-Gunsteren, W. F. A Biomolecular Force Field Based on the Free Enthalpy of Hydration and Solvation: The GROMOS Force-Field Parameter Sets 53A5 and 53A6. *J. Comput. Chem.* **2004**, *25*, 1656-1676.
 112. Kühn, J. Das Versuchsfeld des landwirtschaftlichen Instituts der Universität Halle an der Saale. *Berichte Physiol. Labor- u, 15. Halle: Versuchsanstalt Landwirtschaftl. Institut, Univ.* **1901**, 169-189.
 113. Garz, J. 100-jähriges Bestehen des Versuches wiger Roggenbau Halle. *Arch Acker- u Pflanzenbau Bodenk* **1979**, *23*, 563-5671.
 114. Stumpe, H.; Garz, J.; Hagedorn, E. Die Dauerdüngungsversuche auf dem Versuchsfeld in Halle. In: Körschens, M.; Kundler, P. editors. *Dauerfeldversuche der DDR*. Berlin: Akad. Landw. Wiss **1984**, 25-66.
 115. Stumpe, H.; Garz, J.; Hagedorn, E. Die Dauerdüngungsversuche auf dem Versuchsfeld in Halle. In: Körschens, M. editor. *Dauerfeldversuche: Übersicht, Entwicklung und Ergebnisse von Feld- versuchen mit mehr als 20 Jahren Versuchsdauer*. 2nd ed. Berlin: Akad. Landw. Wiss **1990**, 25-71.
 116. Schmidt, L.; Warnstorff, K.; Dörfel, H.; Leinweber, P.; Lange, H.; Merbach, W. The influence of fertilization and rotation on soil organic matter and plant yields in the long-term eternal rye trial in Halle (Saale), Germany. *J. Plant Nutr. Soil Sci.***2000**, *163*, 639-48.
 117. Schulten, H.-R.; Leinweber, P. Characterization of humic and soil particles by analytical pyrolysis and computer modeling. *J. Appl. Anal. pyrolysis***1996**, *38*, 1-53.
 118. Leinweber, P.; Reuter, G. Influence of various fertilization on the mineralogical composition of clay fractions in long-term field experiments. *Z Pflanzenernähr Bodenkd***1989**, *152*, 373-377.
 119. Leinweber, P.; Schulten, H.-R.; Körschens, M. Hot water extracted organic matter: chemical composition and temporal variations in a long-term field experiment. *Biol Fertil Soils***1995**, *20*, 17-23.
 120. Landgraf, D.; Leinweber, P.; Makeschin, F. Cold and hot water-extractable organic matter as indicators of litter decomposition in forest soils. *J. Plant Nutr. Soil Sci.* **2006**, *169*, 76-82.
 121. Kiersch, K.; Kruse, J.; Eckhardt, K.-U.; Fendt, A.; Streibel, T.; Zimmermann, R.; Broll, G.; Leinweber, P. Impact of grassland burning on soil organic matter as revealed by a synchrotron- and pyrolysis-mass spectrometry-based multi-methodological approach. *Org. Geochem.***2012**, *44*, 8-20.
 122. Paterson, E. Importance of rhizodeposition in the coupling of plant and microbial productivity. *Eur. J. Soil Sci.***2003**, *54*, 741-50.
 123. Knicker, H.; González-Vila, F. J.; Polvillo, O.; González, J. A.; Almendros, G. Fire-induced transformation of C- and N-forms in different organic soil fractions from a dystric cambisol under a Mediterranean pine forest (*Pinus pinaster*). *Soil Biol. Biochem.* **2005**, *37*, 701-718.
-

-
124. Schulten, H.-R.; Leinweber, P. Thermal stability and composition of mineral-bound organic matter in density fractions of soil. *Eur. J. Soil Sci.* **1999**, *50*, 237–248.
 125. Schulten, H.-R. Analytical pyrolysis of humic substances and soils: geochemical, agricultural and ecological consequences. *J. Anal. Appl. Pyrolysis* **1993**, *25*, 97–122.
 126. Kim, J. S.; Ree, M.; Lee, S. W.; Oh, W.; Baek, S.; Lee, B.; Shin, T. J.; Kim, K. J.; Kim, B.; Luning, J. NEXAFS spectroscopy study of the surface properties of zinc glutarate and its reactivity with carbon dioxide and propylene oxide. *J. Catal.* **2003**, *218*, 386–95.
 127. Cooney, R. R.; Urquhart, S. G. Chemical trends in the near-edge X-ray absorption fine structure of monosubstituted and para-bisubstituted benzenes. *J. Phys. Chem. B* **2004**, *108*, 18185–18191.
 128. Hardie, A. G.; Dynes, J. J.; Kozak, L. M.; Huang, P. M. Influence of polyphenols on the integrated polyphenol-maillard reaction humification pathway as catalyzed by birnessite. *Ann. Environ. Sci.* **2007**, *1*, 91–110.
 129. Urquhart, S. G.; Ade, H. Trends in the carbonyl core (C 1s, O 1s) $\pi^*C=O$ transition in the near-edge X-ray absorption fine structure spectra of organic molecules. *J. Phys. Chem. B* **2002**, *106*, 8531–8538.
 130. Gillespie, A. W.; Walley, F. L.; Farrell, R. E.; Regier, T. Z.; Blyth, R. I. R. Calibration method at the N K-edge using interstitial nitrogen gas in solid-state nitrogen-containing inorganic compounds. *J. Synchrotron Radiat.* **2008**, *15*, 532–534.
 131. Stockholm Convention on Persistent Organic Pollutants website
<http://www.pops.int/documents/pops/>
 132. Canadian light source collaboration site. <http://exshare.lightsource.ca/sgm/Pages/Beamline.aspx>
 133. Kästner, J.; Carr, J. M.; Keal, T.W.; Thiel, W.; Wander, A.; Sherwood, P. DLFIN: An Open-Source Geometry Optimizer for Atomistic Simulations, *J. Phys. Chem. A* **2009**, *113*, 11856.
 134. Ufimtsev, I. S.; Martinez, T. J. Quantum Chemistry on Graphical Processing Units. 3. Analytical Energy Gradients and First Principles Molecular Dynamics. *J. Chem. Theory Comput.* **2009**, *5*, 2619.
 135. *TURBOMOLE V6.4 2012, a development of University of Karlsruhe and Forschungszentrum Karlsruhe GmbH, 1989-2007, TURBOMOLE GmbH, since 2007; available from <http://www.turbomole.com>.*
 136. van Gunsteren, W. F.; Billeter, S. R.; Eising, A. A.; Hünenberger, P. H.; Krüger, P.; Mark, A. E.; Scott, W. R. P.; Tironi, I. G. Biomolecular Simulation: The GROMOS96 Manual and User Guide; Vdf Hochschulverlag AG an der ETH Zürich: Zürich, **1996**.
 137. Cody, G. D.; Ade, H.; Wirick, S.; Mitchell, G. D.; Davis, A. Determination of chemical–structural changes in vitrinite accompanying luminescence alteration using C-NEXAFS analysis. *Org. Geochem.* **1998**, *28*, 441–455.
 138. Dhez, O.; Ade, H.; Urquhart, S. G. Calibrated NEXAFS spectra of some common polymers. *J. Electron Spectrosc. Relat. Phenom.* **2003**, *128*, 85–96.
 139. Hitchcock, A. P.; Mancini, D. C.; Gas phase core excitation database (online).
<http://unicorn.mcmaster.ca/corex/cedb-title.html>.
 140. Boese, J.; Osanna, A.; Jacobsen, C.; Kirz, J.; Jacobsen, C.; Kirz, J. Carbon edge XANES spectroscopy of amino acids and peptides. *J. Electron Spectrosc. Relat. Phenom.* **1997**, *85*, 9–15.
-

-
141. Samuel, N. T.; Lee, C.; Gamble, L. J.; Fischer, D. A.; Castner, D. G. NEXAFS characterization of DNA components and molecular-orientation of surface-bound DNA oligomers. *J. Electron Spectrosc. Relat. Phenom.* **2006**, *152*, 134–142.
 142. Ade, H.; Zhang, X.; Cameron, S.; Costello, C.; Kirz, J.; Williams, S. Chemical contrast in X-ray microscopy and spatially resolved XANES spectroscopy of organic specimens. *Science* **1992**, *258*, 972–975.
 143. Gordon, M. L.; Cooper, G.; Morin, C.; Araki, T.; Turci, C.; Kaznatcheev, K.; Hitchcock, A. P. Inner-shell excitation spectroscopy of the peptide bond: comparison of the C 1s, N 1s, and O 1s spectra of glycine, glycyl-glycine, and glycyl-glycyl-glycine. *J. Phys. Chem. A* **2003**, *107*, 6144–6159.
 144. Wan, J.; Tyliszczak, T.; Tokunaga, T. K. Organic carbon distribution, speciation, and elemental correlation within soil microaggregates: application of STXM and NEXAFS spectroscopy. *Geochim. Cosmochim. Acta* **2007**, *71*, 5439–5449.
 145. Kruse, J.; Schlichting, A.; Siemens, J.; Regier, T.; Leinweber, P. Pyrolysis-field ionization mass spectrometry and nitrogen K-edge XANES spectroscopy applied to bulk soil leachates—a case study. *Sci. Total Environ.* **2010**, *408*, 4910–4915.
 146. Kiersch, K.; Kruse, J.; Regier, T.; Leinweber, P. Temperature resolved conversion of soil organic matter under lab conditions as revealed by C and N XANES spectroscopy and Py-FIMS. *Thermochim. Acta* **2012**, *537*, 36–43.
 147. Gao, H.-J.; Jiang, X. Effect of initial concentration on adsorption-desorption characteristics and desorption hysteresis of hexachlorobenzene in soils. *Pedosphere* **2010**, *20*, 104–110.
 148. Caricasole, P.; Provenzano, M. R.; Hatcher, P. G.; Senesi, N. Chemical characteristics of dissolved organic matter during composting of different organic wastes assessed by C-13 CPMAS NMR spectroscopy. *Bioresour. Technol.* **2010**, *101*, 8232–8236.
 149. Hueso, S.; Brunetti, G.; Senesi, N.; Farrag, K.; Hernandez, T.; Garcia, C. Semiarid soils submitted to severe drought stress: influence on humic acid characteristics in organic amended soils. *J. Soils Sediment* **2012**, *12*, 503–512.
 150. Almendros, G.; Knicker, H.; González-Vila, F. J. Rearrangement of carbon and nitrogen forms in peat after progressive thermal oxidation as determined by solid-state ¹³C- and ¹⁵N NMR spectroscopy. *Org. Geochem.* **2003**, *34*, 1559–1568.
 151. Ketterings, Q. M.; Bigham, J. M.; Laperche, V. Changes in soil mineralogy and texture caused by the slash and burn fires in Sumatra, Indonesia. *Soil Sci. Soc. Am. J.* **2000**, *64*, 1108–1117.
 152. Karickhoff, S. W.; Brown, D. S.; Scott, T. A. Sorption of hydrophobic pollutants on natural sediments. *Water Res.* **1979**, *13*, 241–248.
 153. Schwarzenbach, R. P.; Westall, J. Transport of nonpolar organic compounds from surface water to groundwater. Laboratory sorption studies. *Environ. Sci. Technol.* **1981**, *15*, 1360–1367.
 154. Holmén, B. A.; Gschwend, P. M. Estimating Sorption Rates of Hydrophobic Organic Compounds in Iron Oxide- and Aluminosilicate Clay-Coated Aquifer Sands. *Environ. Sci. Technol.* **1996**, *31*, 105–113.
 155. Deane, G.; Chroneer, Z.; Lick, W. Diffusion and Sorption of Hexachlorobenzene in Sediments and Saturated Soils. *J. Environ. Eng.* **1999**, *125*, 689–696.
-

REFERENCES

156. Jodeh,S.; Jaradat, K.; Zatar, Z. Adsorption and Desorption Characteristics of Endosulfan Pesticide in Three soils in Palestine. *Department of Chemistry, Najah University*. **2009**.
157. Kumar, M.; Philip, L. Adsorption and desorption characteristics of hydrophobic pesticide endosulfan in four Indian soils. *Chemosphere***2006**,*62*, 1064–1077.
158. Toul, J.; Bezděk, J.; Kovářová, M.; Boháček, Z.; Hanák, J.; Milička, J.; Müller, P. Sorption of hydrophobic organic pollutants on soils and sediments. *Bull.Geosci.* **2003**, *78*, 205–223.
159. Jansen, H. B.; Ros, P. Non-empirical molecular orbital calculations on the protonation of carbon monoxide. *Chem. Phys. Lett.***1969**, *3*, 140-143.
160. Boys, S. F.; Bernardi, F.The calculation of small molecular interactions by the differences of separate total energies. Some procedures with reduced errors. *Mol. Phys.* **1970**, *19*, 553-556.

APPENDICES

Appendix 1. Effect of different basis sets such as 6-31G, 6-31++G, 6-311++G(d,p), and 6-311++G(2d,2p) using BLYP-D3 have been studied and shown in the following Figure

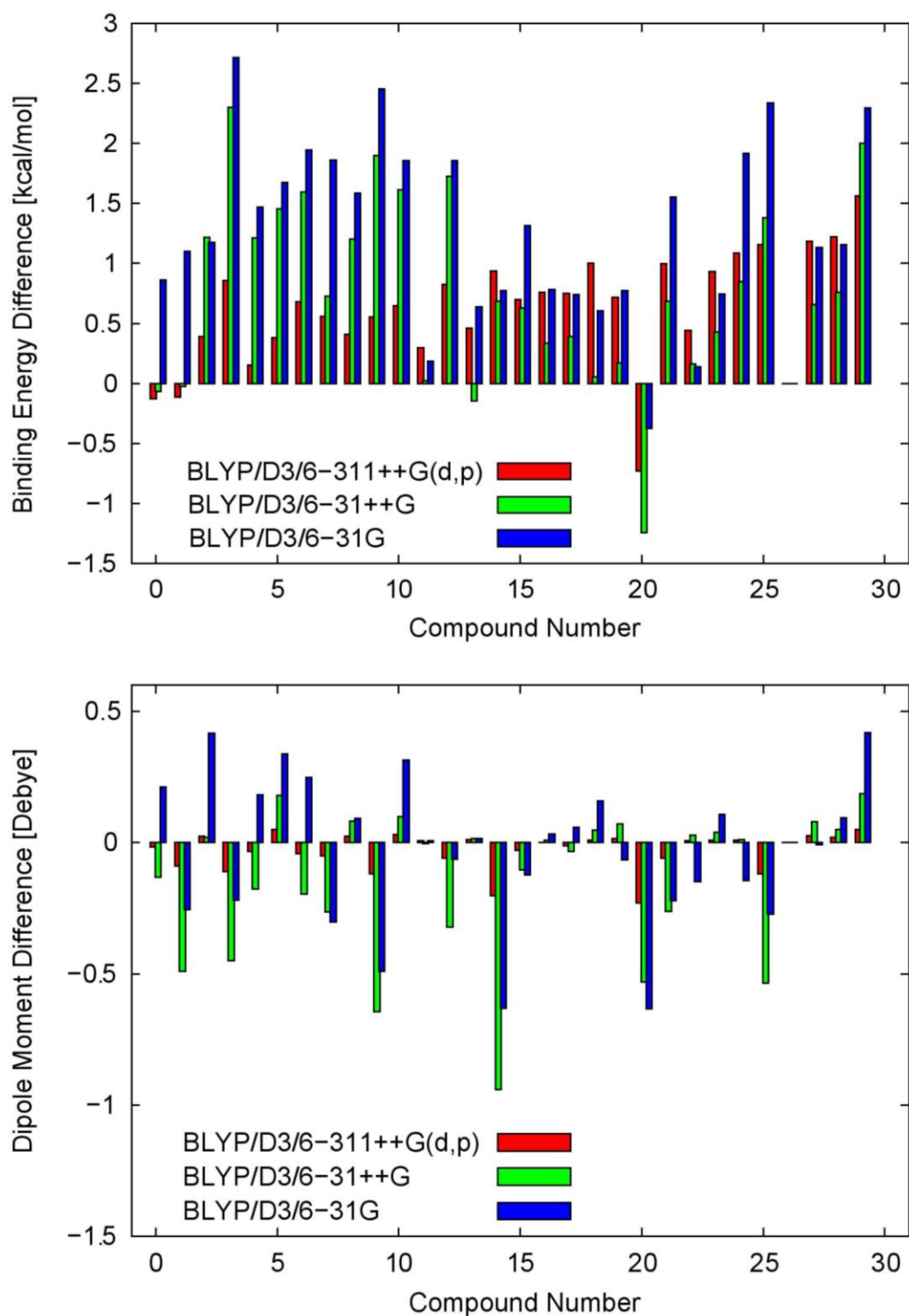


Figure 41. Binding energy differences of HCB with the SOM representative systems, dipole moment differences of the HCB-SOM complexes using BLYP-D3 at 6-31G, 6-31++G, 6-311++G(d,p) basis sets with respect to 6-311++G(2d,2p) basis set.

ACKNOWLEDGEMENTS

Before anything, I would like to start my acknowledgment with “العالمينز بالله الحمد”. This is Arabic sentence which means that I thank my God “ALLAH” and can be pronounced as Alhamdo le-llah rab al-alameen. So Alhamdo le-llah rab al-alameen not only for finishing my Ph.D. but for everything in my life.

With respect to the scientific issue, I didn't find people supported me like my supervisors Prof. Dr. Oliver Kühn and Prof. Dr. Peter Leinweber. It is my pleasure to thank them so much for giving me all scientific support and supervision. Again thanks for the patient guidance, encouragement and advice they provided throughout my time as a Ph.D. student. They planted inside me how to be independent person. They open the door to me to be involved in a new interdisciplinary scientific area combining chemistry, Physics, and soil science. Also they financially supported me in the last period after finishing of my scholarship to complete my Ph.D. thesis. Really thanks so much for my supervisors Prof. Dr. Oliver Kühn and Prof. Dr. Peter Leinweber.

I would like to introduce my acknowledgement to Prof. Dr. Ralf Ludwig for his supervision, helping and allowing me to be accepted in the Institute of Chemistry to make my defense there.

All thanks have to go to my supervisors in the master degree, Prof. Dr. Rifaat Hilal and Dr. Mohamed Shibl for what I learned from them, their guidance and encouragement, helping and supporting me till now.

I would like to thank all of my colleagues in both Prof. Dr. Oliver Kühn and Prof. Dr. Peter Leinweber groups.

I must express my gratitude to the dearest people to my heart, they are my mother and father. Whatever I introduce to them, absolutely I cannot return back their favors to me. In the same context, I'm unable to return back sacrifices of my wife for me, so thanks my beloved wife. Also I would like thank my children Mohammad and Ali, my sister, and my brothers. To all of my family members, I would like thank their continued support and encouragement to me.

I would like to thank the interdisciplinary faculty for its financial support to me through three years scholarship from 15.10.2009 to 14.10.2012.

PUBLISHED PAPERS

1. Ashour A. Ahmed, Oliver Kühn, Rifaat H. Hilal, Mohamed F. Shibl. Structure and Cooperativity of the Hydrogen Bonds in Sodium Dihydrogen Triacetate. International journal of Quantum chemistry 2013, 113, 1394-1400.
2. Ashour A. Ahmed, Oliver Kühn, Peter Leinweber. Controlled Experimental Soil Organic Matter Modification for Study of Organic Pollutant interactions in Soil. Science of the Total Environment 2012, 441, 151-158.
3. Rifaat H. Hilal, Shabaan A. K. Elroby, Ashour A. Ahmed. Conformational Preference and Mechanism of Decarboxylation of Levodopa. A Quantum Dynamics/Quantum Mechanics Study. International journal of Quantum chemistry (2013). doi: 10.1002/qua.24420
4. Ashour A. Ahmed, Rifaat H. Hilal, Mohamed F. Shibl. Cooperativity in Hydrogen Bonds of Sodium Dihydrogen Triacetate. (submitted)
5. Ashour A. Ahmed, Oliver Kühn, Peter Leinweber. How Soil Organic Matter Controls Hexachlorobenzene-Soil Interactions: Adsorption Isotherms and Quantum Chemical Modelling. (submitted)
6. Ashour A. Ahmed, Oliver Kühn, Peter Leinweber. A Computational Study of Hexachlorobenzene-Soil Organic Matter Interactions. Journal of Theoretical and Computational Chemistry (2013).

TALKS AND POSTERS**Talks**

1. Xenobiotics-soil interactions: Py-FIMS, XANES and theoretical modeling.
INF scholars meeting, University of Rostock, April 19, 2011.
2. Interaction of soil organic matter with xenobiotics: Pyrolysis field ionization mass spectrometry (Py-FIMS), X-ray absorption near-edge fine structure spectroscopy (XANES) and theoretical modeling.
Spectroscopy-Detective in Science, Rostock, Germany, June 17, 2011.
3. Molecular dynamics simulation: quantum dynamics course by O. Kühn.
Jeddah, Saudi Arabia, March 06, 2012.
4. Binding of chlorinated organic pollutants to soils.
76th annual meeting of the DPG and DPG spring meeting, Berlin, Germany, March 27, 2012.
5. Binding of chlorinated organic pollutants to soils.
Physics graduate seminar, Rostock, Germany, April 12, 2012.
6. Binding of hexachlorobenzene to soils: experimental measurement and theoretical modelling
DBG meeting, Rostock, Germany, September 11, 2013.

Posters

1. Binding of chlorinated environmentally active chemicals to soil surfaces: chromatographic measurements and molecular dynamics simulations.
2nd Interdisciplinary Scientific Seminar, Rostock-Warnemünde, March 25, 2010.
2. Binding of chlorinated organic pollutants to soils: experimental measurements and theoretical modeling.
Life, Light, Matter evaluation workshop, Rostock, May 3, 2012.
3. Binding of chlorinated organic pollutants to soils: experimental measurements and theoretical modeling.
Research camp, Rostock, June 20, 2012.
4. Binding of chlorinated organic pollutants to soils: experimental measurements and theoretical modeling.
Eurosoil 2012, Bari, Italy, July 2-6, 2012.
5. Binding of chlorinated organic pollutants to soils: experimental measurements and theoretical modeling.
STC 2012, Karlsruhe, Germany, September 23-27, 2012.
6. Binding of hexachlorobenzene to soils: experimental measurement and theoretical modelling
DBG meeting, Rostock, Germany, September 11, 2013.
7. How soil organic matter controls hexachlorobenzene-soil interactions: adsorption isotherms and quantum chemical modelling.
STC 2013, Erlangen, Germany, September 22-26, 2013.

CURRICULUM VITAE

Name: Ashour A. Ahmed

Date of birth: 14.11.1983

Nationality: Egyptian

Home address: Saft-Ellaban, Giza, Egypt

Current address: Maxim-Gorki straÙe 16, 18106, Rostock, Germany

Marital status: Married + two children

Email: ashour.ahmed@uni-rostock.de



Education

2001 High school, Giza, Egypt

May 2005 B.Sc, Chemistry, Grade: Excellent with honour, Chemistry Department, Faculty of Science, Cairo University, Egypt

August 2009 M.Sc., Physical Chemistry, Thesis entitled "Theoretical investigation of H-bond structure and dynamics in molecules of biological interest" Faculty of Science, Cairo University, Egypt

October 2009 Ph.D. Candidate, Institute of Physics, Rostock University, Germany

Supervisors: Prof. Dr. Oliver Kühn, Institute of Physics, Rostock University

Prof. Dr. Peter Leinweber, Institute of Land Use, Rostock University

Employment

2006-2009: Instructor, Chemistry Department, Faculty of Science, Cairo University, Egypt

Currently: Lecturer assistance, Chemistry Department, Faculty of Science, Cairo University, Egypt

ERKLÄRUNG

Ich versichere hiermit, die vorliegende Arbeit selbstständig angefertigt und ohne fremde Hilfe verfasst zu haben. Keine außer den von mir angegebenen Hilfsmitteln und Quellen wurden bei der Erstellung dieser Dissertation verwendet und die den benutzten Werken inhaltlich und wörtlich entnommenen Stellen wurden als solche kenntlich gemacht.

Rostock, Ashour A. Ahmed